The Igneous Rocks of the Western Margin of Lake Rotoroa, Nelson Lakes National Park

---

A Thesis

submitted in partial fulfillment

for the requirements of the Degree

of

MASTER OF SCIENCE IN GEOLOGY

at the

University of Canterbury.

by

Andrew Owen Cox

University of Canterbury

1994

FRONTISPIECE

View looking southwards towards the head of Lake Rotoroa
Nelson Lakes National Park.

ABSTRACT

The Rotoroa Complex located in NW Nelson, represents a remnant plutonic fragment of an extensive subduction system active between 140 - 130 Ma. The arc system has been subject to large scale transcurrent faulting during the Early Cretaceous. The result is a series of "*dismembered Mesozoic volcanic and plutonic arc associations that are sandwiched between terranes of the Western and Eastern Provinces*" (Kimbrough *et al* 1993). This association is collectively described as the Median Tectonic Zone (MTZ) by Bradshaw (1993), and Kimbrough *et al* (1993).

The rocks encompassed by the term Rotoroa Complex range from rare hornblendite through gabbro to diorite and quartz diorite, all typically rich in hornblende. The complex has been metamorphosed in part by the Early Cretaceous emplacement of the Separation Point Batholith, resulting in widespread felsic sheets and dikes of Separation Point Suite affinity being present throughout the Rotoroa Complex. Lamprophyre camptonite dikes of unknown age are also intruded throughout the complex, which has been subjected to brittle deformation due to movements on the Alpine Fault since Late Oligocene - Early Miocene times.

The Rotoroa Complex is broadly metaluminous, calc-alkaline, medium to high K in nature, and has island-arc subduction-related geochemical characteristics. The geochemical variation reflects primary igneous fractionation processes.

The Rotoroa Complex probably correlates with the Darran Complex of Fiordland, based on similarities in rock type, geochemistry, structural position and magnetic anomalies. The geochemical trends obtained from analyses of the Rotoroa Complex are sufficiently similar to those described in the Darran Complex to support this notion.

Acknowledgments

Firstly I would like to thank my mother and father for their patience and financial assistance over the last six years. Secondly I would like to thank the people who have lasted the distance and done a Masters, both for the good times and help I've had over the same period, especially Don and Georg.

A big thank you to my supervisors, Dr Steve Weaver and Dr Roddy Muir for their advice, prompt and patient critical reviews, and for allowing me the use of their (in press) paper and associated data from the Separation Point Batholith.

I would especially like to acknowledge Dr. Alva Challis for advice, provision of her 'in prep' map and notes on the Rotoroa Complex and geochemical analyses, which gave me a much needed framework to work from.

Thank you to Dr Andy Tulloch for comments and geochemical data.

A big thank you to all the people of L & M Mining Ltd who I have been involved with over the last two years, for the experience and financial opportunity.

Thank you to the Mason Trust Fund for a grant covering many of the numerous thesis related expenses.

Thanks to the Borcovsky family of Tutaki Valley for providing a base away from Lake Rotoroa.

Lastly thanks to all the miscellaneous people who have helped with this, Tod Waight for a wide range of things, Joss Campbell for structural thoughts, Rob Spiers for thin sections, Kerry Swanson for photographic assistance, the Browns for geochemical analyses, and little Bob Penter for computer assistance.

No thanks to the government.

TABLE OF CONTENTS.

LIST OF FIGURES

LIST OF TABLES:

Table **Page**

LIST OF APPENDICES

CHAPTER ONE: INTRODUCTION

1.1 Introduction

The Late Jurassic - Early Cretaceous Rotoroa Complex is "*a lithologically variable unit of mainly plutonic rock dominated by massive to weakly foliated dioritic rocks with hornblende - biotite - plagioclase - quartz assemblages*" (Kimbrough *et al* 1993). Mafic lamprophyre dikes of unknown age are found throughout the Complex. The effects of lower greenschist facies metamorphism, and metasomatism associated with the Early Cretaceous emplacement of the Separation Point Granite are widespread, as are late stage aplite and pegmatite dikes and sheets. Low temperature, high pressure brittle deformation features associated with the Cenozoic Alpine Fault, dominate outcrop throughout the Complex.

The Rotoroa Complex is located in NW Nelson, approximately 20 km east of Murchison **(Figure 1.1)**. It crops out over an area of ~ 18 x 35 km^2 and terminates to the SE where the Alpine Fault juxtaposes the Torlesse Supergroup rocks against it. To the SW, the Rotoroa Complex is in fault contact with the Glenroy Complex, and rocks of the Permian Brook Street Volcanics **(Figure 1.3)**. The northern boundary of the Rotoroa Complex is covered by Pliocene-Pleistocene gravels of the Moutere depression. Gravity and magnetic anomalies beneath the Moutere depression may be the northward extension of the Rotoroa Complex (Wellman 1973) and (Kimbrough *et al* 1993). To the West the Rotoroa Complex is fault bounded by the Murchison basin, which is being telescoped and compressed by a series of active imbricate thrusts within the Rotoroa Complex. In addition, these have trapped infaulted wedges of Tertiary sediments within the complex (Suggate 1984).

The Rotoroa Complex is considered to be part of the Median Tectonic Zone (MTZ). This is defined by Bradshaw (1993), and Kimbrough *et al* (1993), as a north-trending belt of disrupted Mesozoic volcano-plutonic and sedimentary terrane fragments lying between the Eastern and Western Provinces of the South Island.

1.2 Previous Work.

The complex was first described in publication by Fyfe (1928) .."*more basic plutonic rocks, consisting of diorite, quartz diorite, and basic granite, outcrop over much of the western part of Rotoroa Survey District*". The term Rotoroa Igneous Complex was first used by Henderson & Fyfe in 1935, while mapping an association of granitic and gabbroic to ultrabasic igneous rocks lying between Glenhope and Springs Junction.

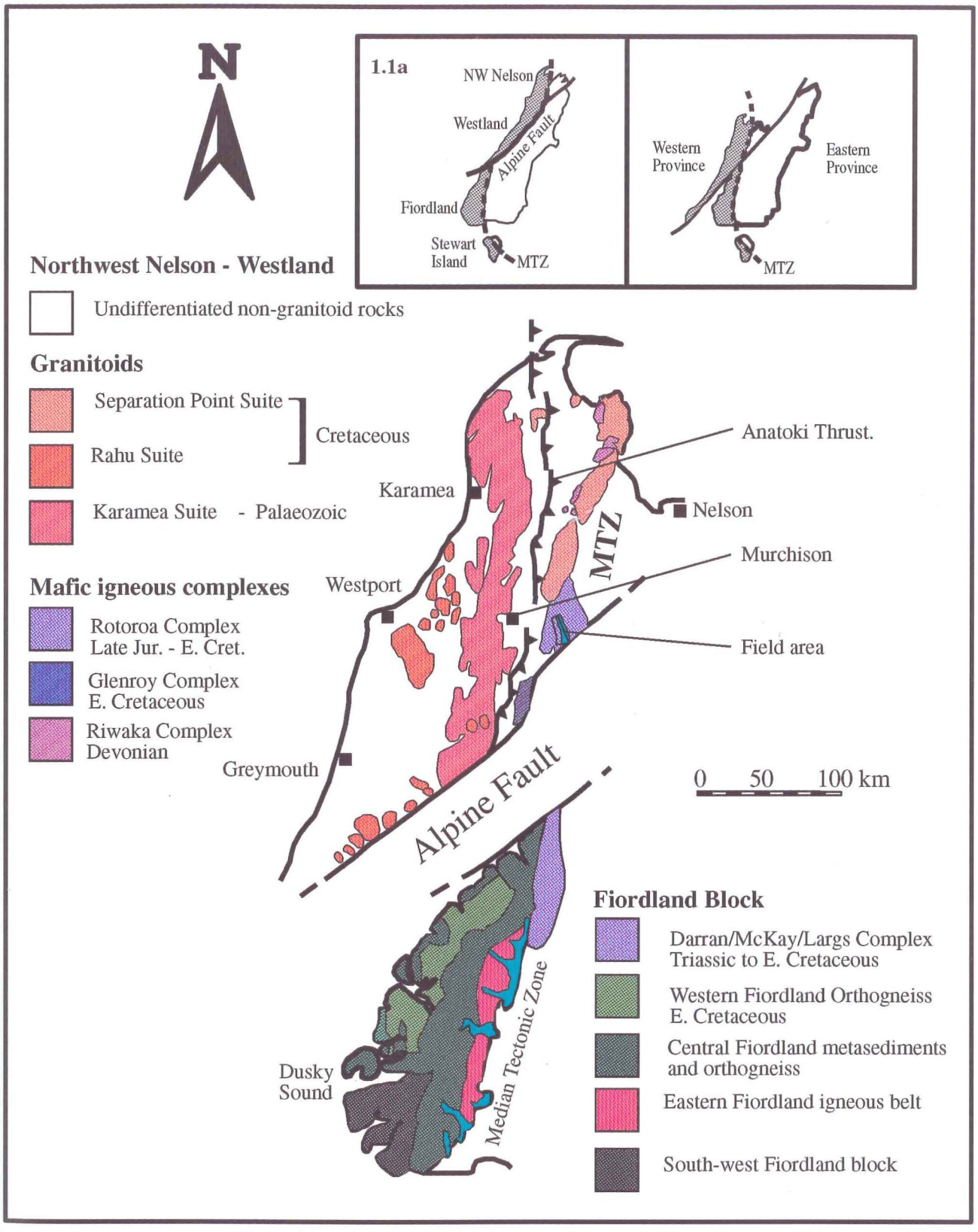

Figure 1.1 Simplified granitoid geology of Northwest Nelson and Fiordland after Muir et al (1994).
1.1a Configuration of the South Island, New Zealand before and after initiation of the Alpine Fault. (after Landis and Coombs 1967).

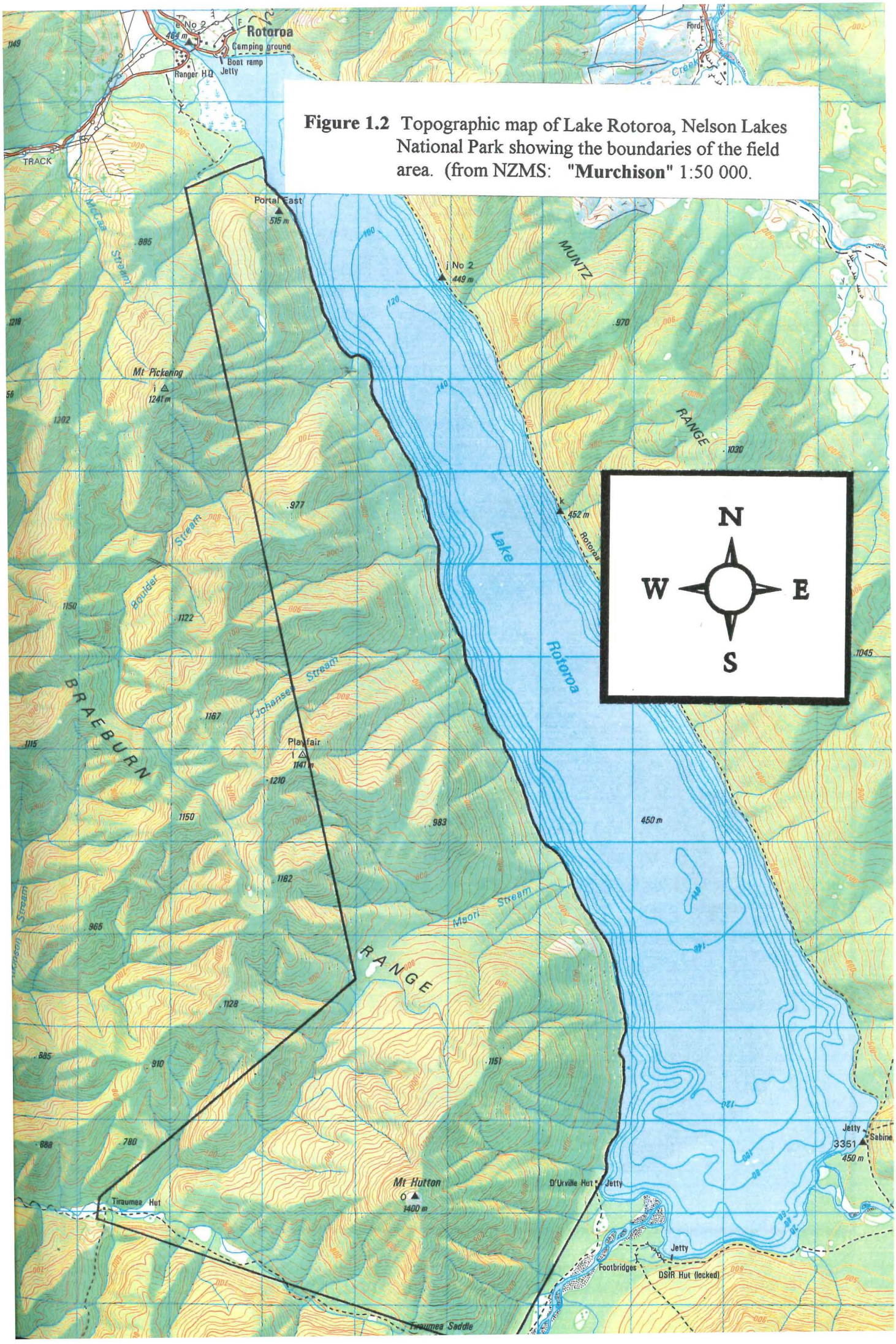

Figure 1.2 Topographic map of Lake Rotoroa, Nelson Lakes National Park showing the boundaries of the field area. (from NZMS: **"Murchison"** 1:50 000.

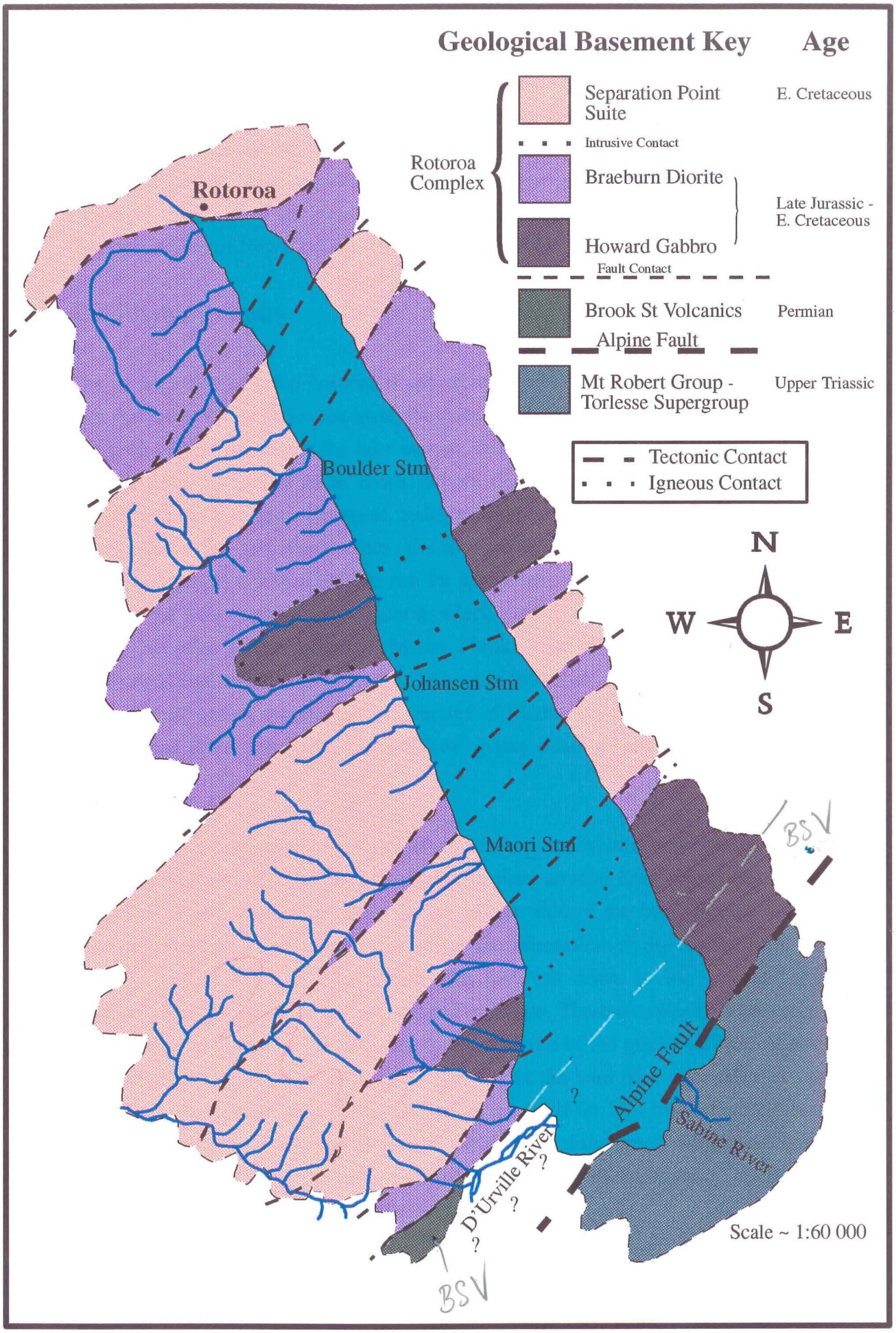

Figure 1.3 Schematic geology of Lake Rotoroa as mapped by Challis *et al* (in prep) NZGS 1:50 000 Sheet M29 BD "Lake Rotoroa".

This included the Glenroy Complex. The Rotoroa Igneous Complex at Lake Rotoroa is now known to be separate from the Early Cretaceous Glenroy Complex (Kimbrough *et al* 1993), but they were earlier grouped together by Bowen (1964), and Fyfe (1968). Reed (1968) recorded that "*granitic rocks comparable with the Mount Murchison Type* (then identified as Separation Point Granite) *are known within the Rotoroa Complex*". Currently Challis *et al* (in prep.) are about to release Sheet M29BD "**Lake Rotoroa**" Geological Map of New Zealand 1:50 000 **(Figure 1.3)**.

1.3 Physiography

The western side of Lake Rotoroa is approximately 14 km in length **(Figure 1.2)**. The lake surface is 450 m above sea level, the sides of which fall away rapidly to a maximum depth of 140 m. Bordering the lake margin, there is a narrow terrace of glacial debris ranging from 20 to 300 m in width. Where this occurs, it effectively obscures any exposure at the lake edge. However, bedrock is exposed along three sections of the lake shore. Above the shoreline terrace, the topography becomes much steeper, in some places as steep as a 600 m vertical rise for a kilometre horizontal distance. The highest point in the field area is Mount Hutton, which rises to a height of 1400 m above sea level. This joins to the NW with Mount Playfair and Mount Pickering to form the Braeburn Range which runs NW - SE. The entire field area is vegetated in mature native beech forest, except for the last few metres of Mount Hutton, which is a mixture of bedrock and alpine shrubbery, and a 300 m^2 grassy clearing behind Mt Hutton **(Figure 1.2).**

The drainage is dominated by a series of streams that are essentially perpendicular to the lake. The ridges which mark the catchments for these streams have a dominant NE - SW trend that is also present in ridges on the eastern side of the lake **(Figure 1.2)**. This dominant structural trend appears to mirror the orientation of the Alpine Fault at the southern end of the lake. The stream beds have cut down to the contact between basement and glacial cover and are stepped in nature. There is typically no outcrop for the first couple of hundred metres, due to the presence of the glacial terrace. Above the glacial terrace, the first outcrop occurs typically at the base of a waterfall that ranges from 5 - 30 m in height. Above this, the stream levels off for 50 - 100 m before returning to the glacial material customarily present in the walls of the creek, which then begin to gorge in anticipation of the next waterfall and outcrop of basement. This pattern is characteristic of creeks throughout the field area.

The wildlife in the field area is dominated by plagues of sandflies and wasps in summer time. These are largely absent during the colder months, which makes autumn a more attractive fieldwork prospect. Deer and trout are present in much debated abundance and

are responsible for a large number of the visitors to the area, as are popular tramping routes throughout the National Park area.

1.4 Aim of study

The aim of this study was to map and sample the field area to allow a more detailed petrographic and geochemical description of the Rotoroa Complex. These would then be used to determine the conditions and tectonic environment of emplacement of the Rotoroa Complex. These results on the Rotoroa Complex also permit correlation across the Alpine Fault, with the Darran Complex of Fiordland.

1.5 Methods

Five weeks of field work were completed in March - April 1993, and six days follow up work was completed in late November 1993. The D'Urville Hut was used as a base, with a boat for field transport and sample recovery. Field work included the mapping and sample collection of three stretches of exposure along the lake margin between (NZMS 260 M29 "Murchison" 1:50 000) 808244 and 803256, 800269 and 797267, 773328 and 772329, and all major creeks on the western margin of the lake. Maori stream through to the Tiraumea Hut via a creek that drains off the back of Mt Hutton, was also covered **(Figure 1.2)**. All mapping was done on a base map taken from a 1:25000 topoplot of NZMS 1:50000 series sheet M29 segment D.

Mapping proved very difficult for two reasons. Firstly, the amount of exposure was very limited. It was confined to sparse outcrops in creek beds, which often have difficult access and are usually badly weathered. Secondly, obtaining accurate locations when mapping in creeks surrounded by full grown beech forest was a problem.

Samples of the Separation Point, the Rotoroa Complex, the Brook Street Volcanics and the Mount Robert Subgroup of the Torlesse Supergroup were thin sectioned for petrographic analysis using Logitech equipment. All plutonic and dike rocks are classified following the recommendations of Le Maitre *et al* (1989). Point count data were obtained from samples by recording 1000 points per thin section. (see **Appendix # 2**). Their plagioclase compositions were determined using refractive index comparisons and Michel-Levy methods as described in Shelley (1985).

Geochemical samples (~ 1 kg) of the units described above were obtained for XRF major element analyses. These were prepared at the Geochemistry Lab, Geology Department, University of Canterbury to make fusion beads for major elements, following the general

methods of Norrish and Hutton (1969). XRF trace element analyses were obtained using 50 mm pressed powder pellets, prepared from powdered rock compressed with ~ 7 % aqueous polyvinyl alcohol. Analyses were procured using a Philips PW - 1400 X-Ray spectrometer combined with an on-line Hewlett Packard 300 computer (see **Appendix # 3**). Recalculated anhydrous major elements, CIPW norms, and geochemical diagrams were produced from Newpet92 software.

CHAPTER TWO: FIELD GEOLOGY AND STRUCTURE OF THE ROTOROA COMPLEX

2.1 Introduction to Field Geology

Remnant Tertiary sediments, and extensive glacial cover overlie much of the Rotoroa Complex. Within the field area, the Rotoroa Complex consists of three basic rock units: the Rotoroa Hornblendite, the Howard Gabbro, (subdivided into gabbro and metagabbro), and the Braeburn Diorite, (subdivided into diorites and quartz diorites). The Torlesse Supergroup and Brook Street Volcanics, both of which are in tectonic contact with the Rotoroa Complex also occur within the field area.
This chapter describes the range of rocks encountered and their field occurrence and relationship to the Rotoroa Complex. All six figure map references used in this chapter refer to NZMS 260 Sheet M29 "Murchison" 1:50 000. A fact map of field geology is enclosed in the map pocket at the back of this thesis.

2.2. Rotoroa Complex

2.2.1 Introduction

The Rotoroa Complex is located in NW Nelson to the east of Murchison **(Figure 1.1)**. It is a lithologically variable unit of "*mainly plutonic rock, dominated by massive to weakly foliated dioritic rocks, with hornblende - biotite - plagioclase - quartz assemblages*" (Kimbrough *et al* 1993). The local abundance of secondary amphibole and epidote reflect a metamorphic overprint, and the effects of pervasive metasomatism associated with the intrusion of the Separation Point Batholith are widespread throughout the complex (Challis *et al* in prep.). Felsic dikes of Separation Point affinity, and mafic lamprophyre dikes of unknown affinity intrude throughout the Rotoroa Complex.

Aronson (1968), obtained a Rb/Sr age of 115 Ma (Early Cretaceous) from a quartz diorite pegmatite from the Rotoroa Complex. This is now known to be approximately the age of the Separation Point Granite (Muir *et al* 1994). The age obtained by Aronson probably reflects resetting by the intrusion of the Separation Point Granite into the Rotoroa Complex, or the sample could be actual Separation Point Suite, which is likely considering that it is a pegmatite. A recent study by Kimbrough *et al* (1993), has dated a diorite in the Rotoroa Complex using U/Pb methods which give an age of 156 Ma . This is interpreted as a crystallisation age. Hornblende and biotite $^{40}Ar/^{39}Ar$ ages in the

range 140-130 Ma are believed to represent either emplacement ages, cooling ages or a metamorphic resetting event.

The precise relationships between the igneous rock types of the Rotoroa Complex are impossible to determine due to dense vegetation and the blanketing affect of glacial deposits, and accessibility problems which combine to obscure ~ 90 % of outcrop. No contacts between in-situ basement lithologies were observed during field work, other than those associated with minor intrusives.

2.2.2 Rotoroa Hornblendite

This unit is described in Challis *et al* (in prep.) but not named. For the sake of description I have labelled it the Rotoroa Hornblendite. It is a relatively rare component of the Rotoroa Complex and only occurs as small isolated lenses. It was noted in two locations, 770302, and 765323 and one other which was out of the mapped field area, at 773323. The rarity of the Rotoroa Hornblendite is consistent with the contention of Challis *et al* (in prep), that it represents fragments of an ultramafic rock body which underlies the Howard Gabbro as part of a layered intrusion. However in all three noted outcrops the hornblendite is associated with dioritic and even quartz-rich dioritic rocks.

In outcrop the hornblendite is very mafic and appears to resist weathering reasonably well compared with the surrounding host rock. When water worn and covered by moss, it can easily be mistaken for a mafic dike, and a fresh surface may be required for accurate identification.

In hand specimen the hornblendite comprises, coarse grained hornblende phenocrysts up to 2 cm in length which form a lattice enclosing laths of feldspar. Large euhedral pyrite crystals up to 3 mm are disseminated throughout the rock in some outcrops.

2.2.3 Howard Gabbro

In outcrop the Howard Gabbro is typically massive. The first impression is that the rock is very mafic, however on closer inspection, the rock typically has > 60 % feldspar, which is dark in appearance. The Howard Gabbro occurs throughout the field area, but is relatively rare in abundance when compared with the dioritic rocks. Much of the gabbro has been metamorphosed and altered to metagabbro, obviously they have a common geographical distribution. The metagabbro in outcrop is altered in appearance and has a green black colour. Fracturing and jointing are common which give the rock a blocky appearance.

In hand specimen, the gabbro is a pale grey, purple grey to black colour, holocrystalline, medium to coarse grained gabbro or gabbro diorite. Plagioclase is subhedral to euhedral and appears to exhibit a weak shape controlled fabric which is thought to represent a cumulus layering (Challis *et al* in prep.). This could also be a primary flow feature or a secondary metamorphic texture. The mafic phases are difficult to distinguish, with hornblende being both primary and secondary, replacing pyroxene, particularly in the metagabbros. In hand specimen the metagabbro is full of amphibole which gives it an overall green-black appearance. The amphibole, which is interstitial to the fabric formed by the plagioclase, gives the rock its speckled appearance.

2.2.4 The Braeburn Diorite

Due to the wide range of dioritic rocks covered by the term Braeburn Diorite, I have subdivided the diorites into a) the Braeburn Diorite, and the b) the Braeburn Quartz diorites, based on modal quartz content (**Chapter 3.3.3**).

a) Braeburn Diorite.

The Braeburn Diorite is widespread throughout the field area. The appearance of the Braeburn Diorite in outcrop is as variable as its many constituent rock types. The diorites range from melanocratic with a dark green hue, to leucocratic, sometimes containing up to 70 % leucocratic minerals. Jointing and fracturing are common features in outcrop, with dextral shear being dominant. Aligned mafic augen/xenoliths of hornfelsic material are present in the diorite but are more prominent in the quartz diorite. In hand specimen the diorite has a speckled appearance. This is due to the angular interwoven texture of the mafic and leucocratic phases. Feldspar dominates the diorites with interstitial hornblende, biotite and quartz being apparent.

b) The Braeburn Quartz Diorites.

The quartz diorite is more voluminous than the diorite. It occurs intermixed with the diorite, but is more prevalent as large domains. In the relatively undeformed samples, the outcrop is very similar to the speckled appearance of the diorites but has abundant free quartz and a higher percentage of leucocratic minerals, up to 90 %. In the really deformed samples like AC8C, a proto-mylonitic texture has developed with a good S - C fabric. This gives these rocks a gneissic protomylonitic appearance in outcrop (**Figure 3.4b**). Aligned mafic enclaves dominate most outcrops of the quartz diorite.

In hand specimen the less deformed diorites are equigranular, with leucocratic and mafic minerals still intermixed. A common orientation is however apparent in the constituent minerals, especially biotite. The more deformed sections are dominated by augen of feldspar, which have remained largely undeformed. Quartz ribbons have recrystallised, anastomosing around the feldspar to form a fabric. The quartz and feldspar form leucocratic layers which are distinct from mafic layers of biotite and rare hornblende. The biotites have accommodated much shearing and have grown in mafic layers around the rigid feldspar augen and quartz ribbons.

2.3 Brook Street Volcanics

The Permian Brook Street Volcanics (Thornton, 1985) occur in the SW corner of the field area, as an infaulted wedge in tectonic contact with the Rotoroa Complex **(Figure 1.3)**. Their true extent westwards is masked by the floodplain of the D'Urville River, however they have been mapped in tectonic contact with the Torlesse Supergroup further upstream by Bowen (1964). In outcrop they are very fractured and consist of intercalated, siliceous, fine grained, volcanic sediment and altered mafic igneous rock. Wherever outcrop is encountered it is characteristically dominated by medium to small scale brittle fractures.

2.4 Mount Robert Group of the Torlesse Supergroup

The Alpine Fault tectonically juxtaposes the Mount Robert Subgroup of the Torlesse Supergroup next to the Rotoroa Complex in the SE margin of Lake Rotoroa. Challis *et al* (in prep.), have inferred a Late Jurassic age for the Mount Robert Subgroup. The sandstone and mudstone mylonites **(Figures 2.6 and 3.8)**, are exposed in the SE corner of the lake where the fault passes through the head of the lake.

2.5 Separation Point Granite

The Separation Point Batholith is one of five batholiths which have intruded the Westland - West Nelson region and covers an area of ~ 650 km^2. (Tulloch, 1988),**(Figure 1.1)**. Separation Point in Golden Bay is the northern most outcrop. At its southern margin the Sepration Point Granite abuts against the Rotoroa Complex, separated by the Tutaki Fault. (Kimbrough *et al* 1993). The Separation Point Granite within the mapped area is described as being "*massive unfoliated tonalite, quartz diorite, and cross cutting dikes and sills of fine grained tonalite, aplite, and granite pegmatite*" (Challis *et al* in prep.),**(Figure 1.3)**. The Separation Point Granite has been U/Pb SHRIMP dated by Muir *et al* (1994) at 118 Ma.

Within the field of study there is only one occurrence of the Separation Point Granite which resembles the above description, but dikes and sheets of aplite and pegmatite are widespread throughout the Rotoroa Complex. A creek which drains into the Tiruamea River at 759229, exposes approximately 100 m of typical Separation Point Granite. In the field the notable point about this outcrop is that it is very leucocratic, > 90 %, which gives it a very white appearance with a pink hue. It appears to weather relatively easily and the creek has carved out a smooth face, which reveals that it is also very massive. The outcrop is very friable, and obtaining a fresh sample proved difficult. Two hundred metres upstream the granite is replaced by a quartz diorite which shows a good fabric and alignment of mafic enclaves **(Figure 2.16)**. The contact between the granite and the quartz diorite is obscured by alluvium from the creek bed. The quartz diorite is intruded by a zone of intense pegmatisation, spread over several hundred metres. Irregular intermediate to mafic intrusions are also widespread throughout this zone, but are not witnessed in the granite itself **(Figure 2.4)**. Challis *et al* (in prep.) note that the contact between the Separation Point Granite and the Braeburn Diorite may be marked by a zone of widespread pegmatites. The accompanying change in lithology is further evidence that this is a small apophysis or sheet of Separation Point Granite intruded into the Rotoroa Complex during emplacement of the main batholith.

In hand specimen the leucocratic, coarse, holocrystalline nature of the rock is apparent. Quartz, plagioclase and alkali feldspar are all distinguished by their colouration, being smoky grey, white and pink respectively. There is a noticeable paucity of mafic minerals, < 5 %, which comprise biotite and magnetite (**Figure 3.5 a - b** and **Table # 3.4**).

2.6 Brunner Coal Measures

One isolated outcrop of coal measures several hundred metres in length was mapped at 782247 and is pictured in **Figure 2.1**. The outcrop consists of quartzose sands and grit in a carbonaceous mudstone. A second outcrop of Tertiary coal measures is recorded by Bowen (1964) and Challis *et al* (in prep.), further south along the same fault structure at 768225, these are almost certainly the same infaulted block of Tertiary coal measures.

2.7 Glacial Cover

Pleistocene fluvio-glacial material has blanketed basement rocks throughout most of the field area **(Figure 2.2)**. On the western side of the lake these gravels all dip to the east, towards the lake at between 10 - 25°. They vary from poorly sorted, matrix supported boulder conglomerates with clasts up to 15 m across, to finely laminated green and light

Figure 2.1 The outcrop of the Tertiary Brunner Coal Measures in the clearing behind Mount Hutton (Deer prints in bank give approximate scale.)

Figure 2.2 The contact between the Rotoroa Complex and the Pleistocene-Pliocene glacial gravels.

Figure 2.3 Irregular mafic intrusions in the Braeburn Quartz Diorite near the contact with the Separation Point Granite

Figure 2.4 Typical example of a mafic to intermediate dike cutting the Braeburn Quartz Diorite, in this case on the lake edge.

brown sands and muds. Typically the creek bed reflects the slope of the contact between glacial cover and the Rotoroa Complex. The contact of which can be seen as high as 1000 m.

2.8 Dikes

Fined grained intermediate to mafic dikes are widespread throughout the Rotoroa Complex. Challis *et al* (in prep.) believe they also cut the Separation Point Granite, although I have not observed this. In the field the dikes are usually very obvious **(Figure 2.3)**. They are relatively mafic compared with the host rocks, and sometimes they weather out preferentially from their host rocks. In Maori stream at 800296, dikes have weathered out to form a series of weirs, 1 m - 2 m high and 5 - 10 m across, which pool the water behind them in a series of steps. The irregular mafic intrusions noted in the quartz diorite near the Separation Point Granite outcrop are also mafic dikes that have been complexly deformed **(Figure 2.4)**.

2.9 Structure

2.9.1 Introduction

On a local scale, numerous faults and fractures, dikes, joint sets, and foliations are widespread throughout the Rotoroa Complex. The evidence for brittle deformation throughout the field area is abundant. Small scale epidotised crush zones and macro to microscopic fractures, dominantly dextral, abound. The Alpine Fault provides a probable cause for this deformation.

2.9.2 Faults

The Alpine Fault is the largest and most dominant structural feature present in the field area. It enters the field area from the SW via Bull Creek and the Mole Tops **(Figure 2.5)**, and passes through the SE corner of the lake **(Figure 2.6)**. It re-emerges as it cuts a saddle through the Muntz Range, were it is visible as a series of fault traces, on its way to the Waiau Valley **(Figure 1.2)**. The fault zone is exposed over ~ 50 m of outcrop at 824216. Because of the proximity to the fault, the Torlesse sediments which make up the outcrop are mylonitic in texture, this is reflected in the outcrop which has a good foliation of ~ 200/70 E. **(Figures 2.6 and 2.15)**.

Figure 2.5 An outcrop of the Torlesse Supergroup in the vicinity of the Alpine Fault on the Mole Tops.

Figure 2.6 Part of the Alpine Fault exposure where it enters the lake, at the head of Lake Rotoroa.

The Alpine Fault is believed to have been active since the end of the Oligocene-Early Miocene times, (Cooper *et al* 1987), and has a total displacement of ~ 480 km. (Wellman and Willet, 1942). This has been modelled by Landis and Coombs (1967),**(See Figure 1.1a).** The emplacement of the Rotoroa Complex is dated at between 130 - 140 Ma. (Kimbrough *et al* 1993). This suggests that the Rotoroa Complex has been subject to ~ 25 Ma years of initial dextral strike slip deformation, with a more recent westward thrust component (Cooper *et al* 1987). It also indicates that any correlatives of the Mesozoic Rotoroa complex which occur on the Pacific side of the Alpine Fault will now be located 480 km south, in Fiordland.

A noticeable feature as you travel up the lake is a consistent NE to SW trend in the ridge-lines and streams that they bound. This is also apparent on a topographical map **(Figure 1.2)**. It is hardly a coincidence that the Alpine Fault, New Zealand's most significant and most active structural feature, which passes through the southern margin of the field area shares this orientation. It would almost certainly exert some structural control on the local geology. Challis *et al* (in prep.) have mapped sheets of Separation Point Suite rocks tectonically juxtaposed with, or intruded into sheets of Rotoroa Complex along this same orientation throughout the field area **(Figure 1.3)**. Two significant faults were noted in the field, the first was at 808248 **(Figures 2.7 and 2.15)**. This had a foliation of 216/85 W, approximately the orientation of the Alpine Fault. The outcrop was a mylonitic zone ~ 5 m in width exposed at the lake edge, very similar in appearance to the Alpine Fault exposure. On the northern side, the rocks were more quartz-rich diorites compared with the more mafic diorites on the southern side. However geochemically, both were Rotoroa complex. No sense of movement was discernible. The second was a large shear zone exposed by a slip at location 795215 **(Figure 2.8)**. The whole face is sheared and fractured and extremely weathered. The shear fabric ranges from 180/80 E to 240/80 W, but essentially mirrors the Alpine Fault **(Figure 2.15)**. Once again no shear sense indicators are apparent.

A third major fault structure, sympathetic to the Alpine Fault is clearly visible on air photographs and topographic maps passing through an area of Tertiary outcrop at 782247 **(Figure 2.2)**. The Rotoroa Complex is being telescoped over the Murchison basin to the west by a series of imbricate thrusts which accommodate shortening associated with oblique convergence on the Alpine Fault. These imbricate thrust sheets trap pockets of overlying Tertiary units in the complex (J.K. Campbell pers.comm.);(Suggate 1984),**(Figure 2.9)**. The rest of the Tertiary cover has been removed by uplift and erosion of the Rotoroa Complex

Figure 2.7 A major fault zone which crops out at the lake edge. This shares a similar orientation and is probably part of an active imbricate fault system associated with the Alpine Fault.

Figure 2.8 A second major shear zone exposed in a side creek. This also shares a similar orientation to the Alpine Fault.

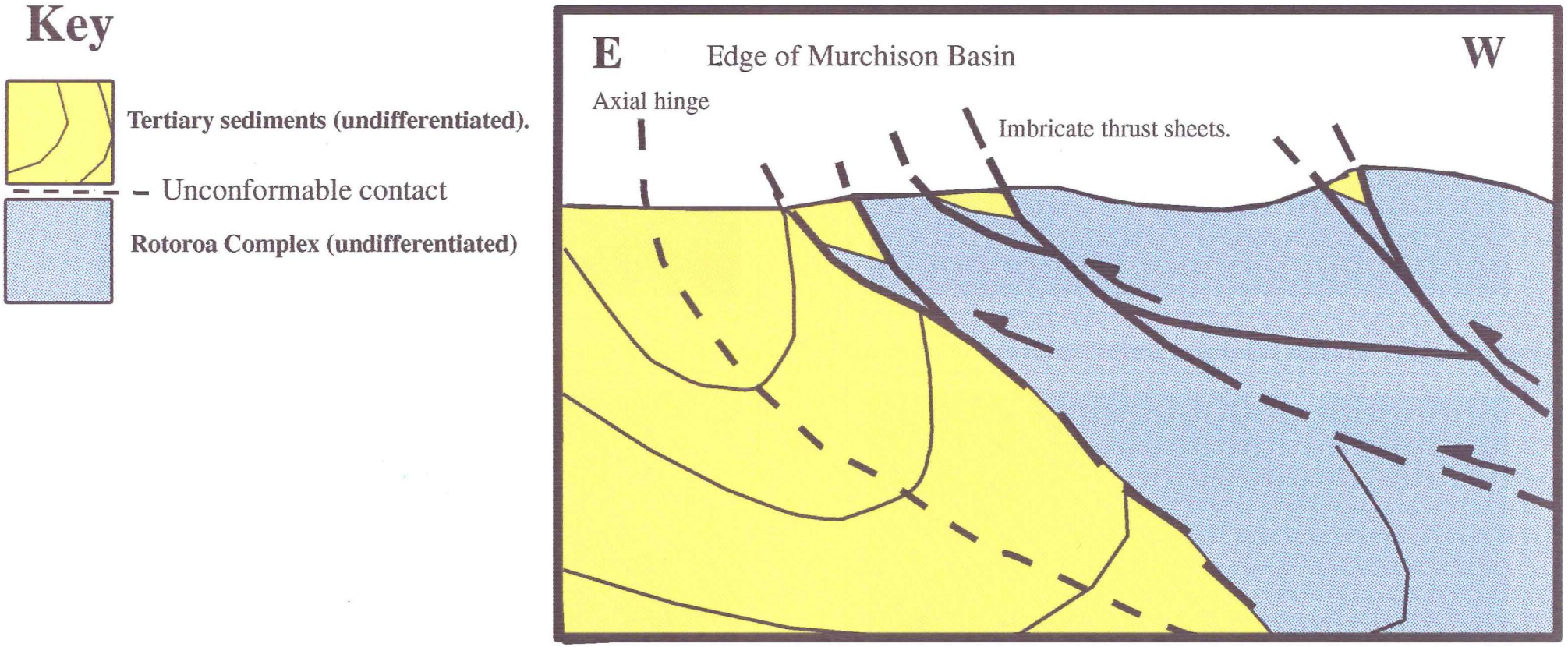

Figure 2.9 Schematic representation of imbricate fault development formed by telescoping of the Rotoroa Complex, showing how Brunner Coal Measures became infaulted into the complex.

a)

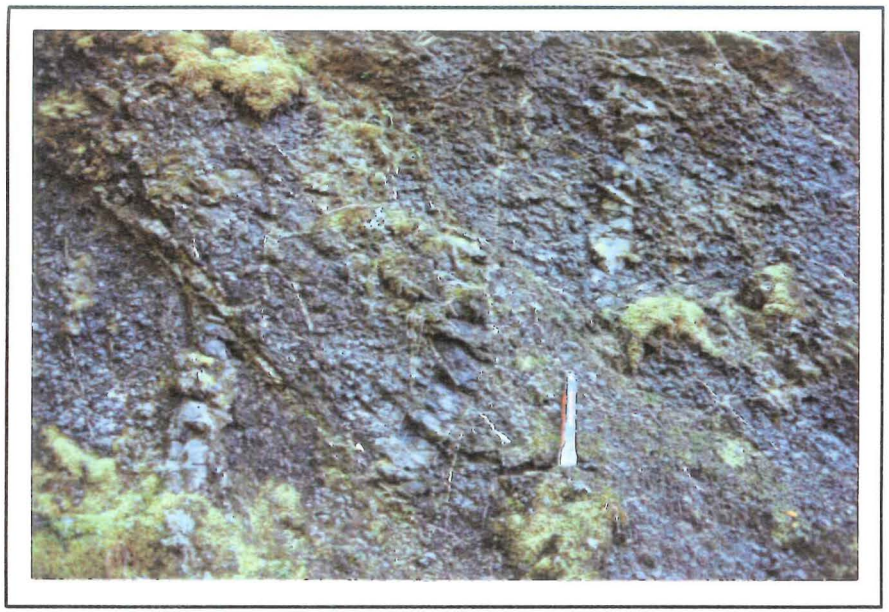

Figure 2.10a Mafic dike in shear zone, offset along two dextral fractures

b)

Figure 2.10b Two shears forming a sigmoidal augen in a pegmatite dike

c)

Figure 4.10c Sinistral offset in a dike. Note the foliation in the host rock.

d)

Figure 4.10d Multiple fracturing which is producing a crenulation effect.

Small scale faults, fractures and shears are ubiquitous throughout the Rotoroa Complex. Many dikes shear out to nothing along fractures, which have favoured the pre-existing weakness left by the dikes. As a result many of the shears share a similar orientation to the dikes. They range in offset from small faults of unknown displacement to centimetre scale offsets, all dominantly dextral. **Figure 2.10 (a - d)** illustrates examples of faults and fractures in the field. There are both dextral and sinistral shear senses in the smaller scale features, dextral offset appears to be dominant.

2.9.3 Dikes and Sheets

Both basaltic lamprophyre dikes and felsic dikes and sheets are intruded into the Rotoroa Complex. The felsic sheets i.e., aplites and pegmatites, are commonly sub-horizontal and in these cases should be strictly described as sills. In one outcrop, an aplite sheet is seen to crosscut a mafic dike and must postdate it **(Figure 2.11)**. Presuming the aplite was a late stage intrusion of the Separation Point Batholith, the mafic dike must predate the emplacement of the Separation Point Batholith. The mafic - intermediate dikes are of unknown age. Dikes have also accommodated much deformation and are sheared out, sometimes to nothing. Some have behaved more plastically than others, suggesting that the deformation may have occurred at a higher temperature than that responsible for the brittle effects, possibly during heating associated with the emplacement of the Separation Point Batholith.

Lamprophyre dike swarms have been mapped in the Hohonu and Alpine swarms by Cooper *et al* (1987), these have been dated at between 25 Ma to 90 Ma (Cooper *et al* 1987). Mafic dikes have also been described in the Victoria Range of the Karamea Batholith. Dr A. J. Tulloch (pers. comm.), has mapped Cretaceous lamprophyre dikes, and pre-Cretaceous "*so called composite dikes*" during mapping in the Victoria Range. Pirajno (1982), has also described these.

The orientations of the Hohonu and Alpine swarms are dominantly NNW - SSW. This trend is believed to be associated with a Cretaceous extensional tectonic regime during the opening of the Tasman Sea as the New Zealand and Australian continents were rifted apart. (Tulloch and Kimbrough, 1989). The dikes recorded in my field area are dominantly orientated at approximately ~ 050° **(Figure 2.12 & Figure 2.13)**. When poles to the dikes are plotted on a stereoplot projection **(Figure 2.13)**, it would appear that the dominant dike orientation is around 045° dipping from steeply east to steeply/moderately west. A secondary concentration occurs at 140° and dips range from vertical to steeply south, this may be a second generation.

Geochemically the Rotoroa lamprophyres are more evolved than an analyses provided by Dr A.J. Tulloch from the Victoria Range (**Appendix # 4**). Their orientation and cross-cutting relationships suggest an age greater than the 118 Ma age of the Separation Point Batholith (Muir *et al* 1994), for at least one generation of mafic - intermediate dikes at Lake Rotoroa, possibly similar to the "*pre-Cretaceous so called composite dikes*" described by Dr A.J. Tulloch (pers. comm.).

Figure 2.11 An aplite dikes which truncates a mafic - intermediate dike. Assuming that the aplite dike has a Separation Point Affinity, then the mafic dikes must predate emplacement of the Separation Point Batholith. The Mafic dike has accommodated post intrusive shearing at elevated temperatures as indicated by the plastic deformation of the aplite where it crosses the mafic dike.

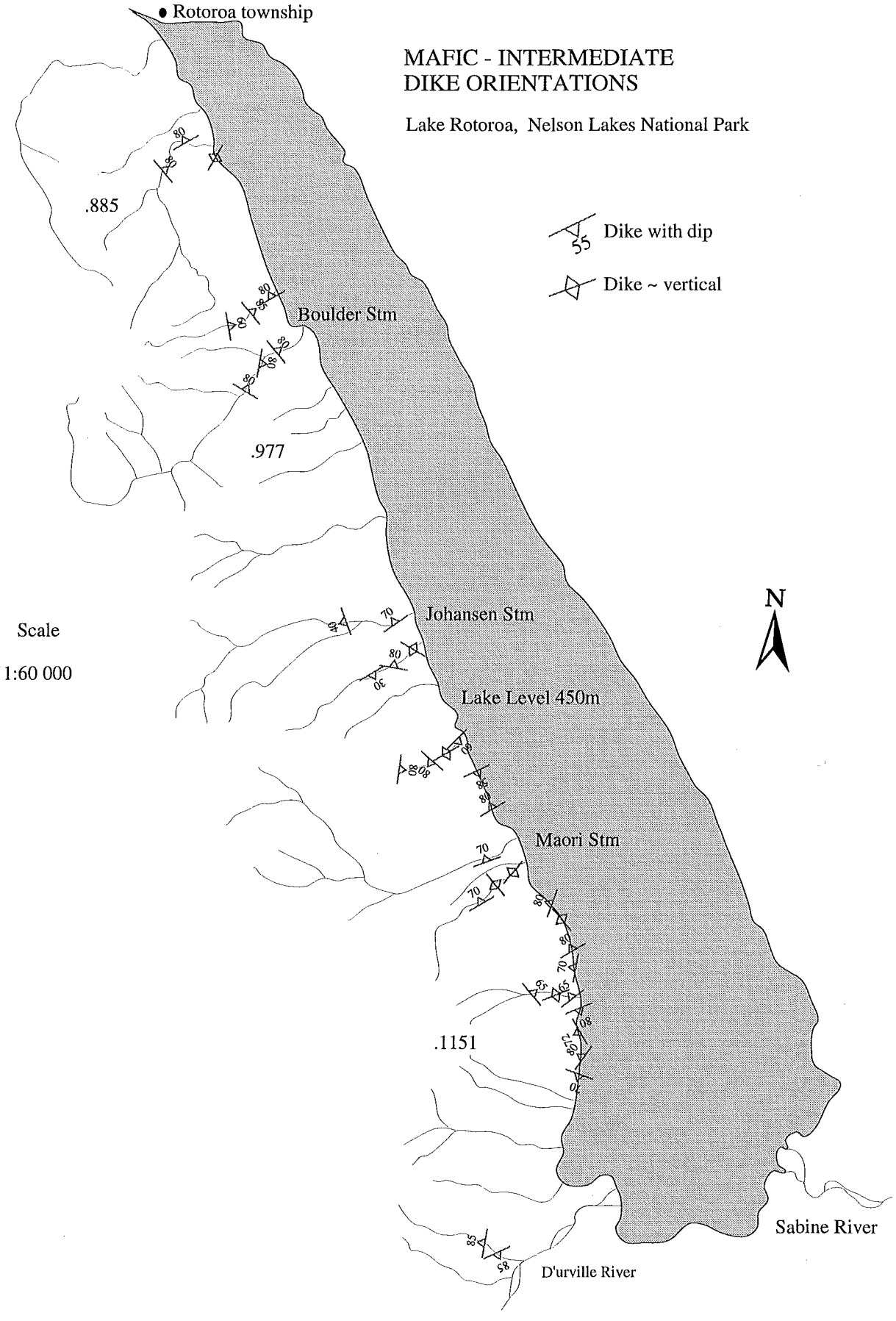

Figure 2.12 Representative mafic to intermediate dike orientations from the western margin of Lake Rotoroa

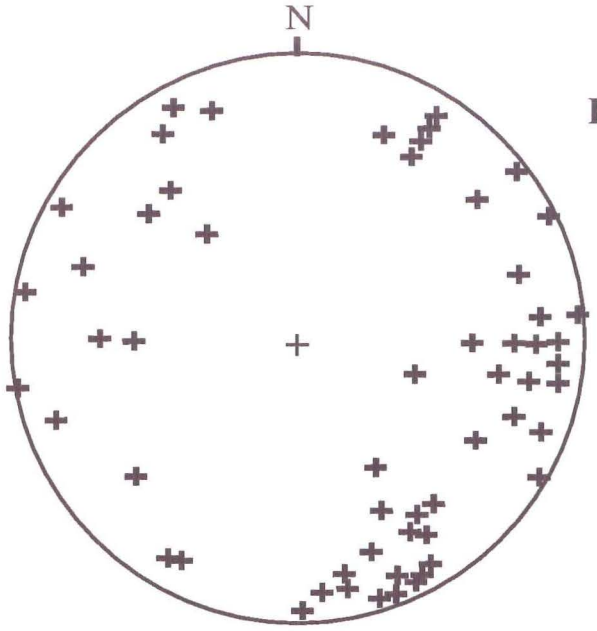

Figure 2.13 Schimdt projection stereoplot of poles to mafic- intermediate dikes.

No of sample points 57

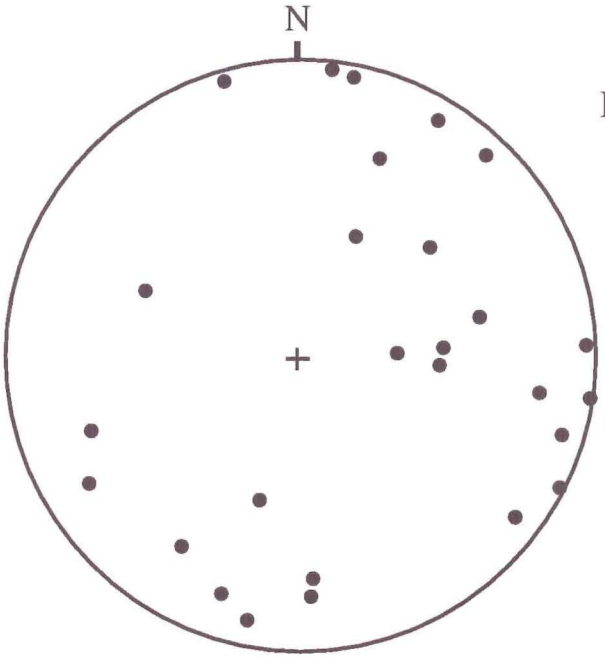

Figure 2.14 Schimdt projection stereoplot of poles to joints.

No of sample points 27

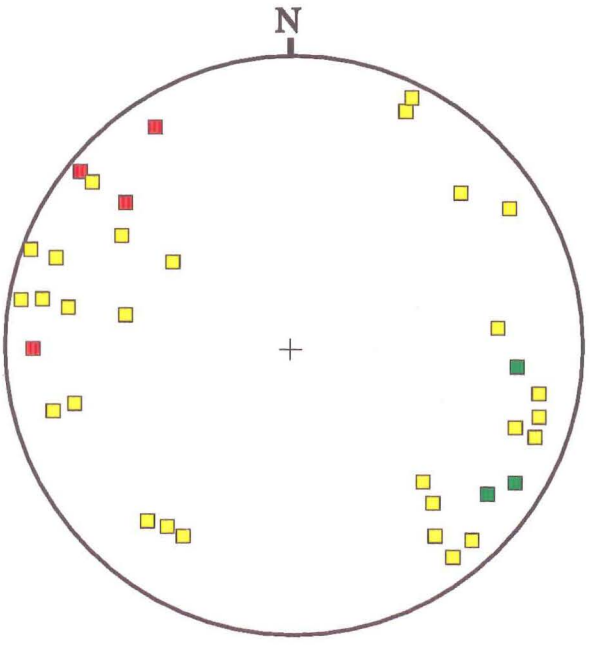

Figure 2.15 Schimdt projection stereoplot of poles to foliations.

No of sample points 35

Key:
- = Mineral fabric
- = Alpine Fault fabric
- = Major shear fabrics

Two possible explanations may explain this. The first is that a pre-Cretaceous generation of dikes was intruded into a NNE trending extensional structural regime prior to the emplacement of the Separation Point Batholith, possibly followed by a second ~ NW trending generation in the Upper Cretaceous. The second is that the dikes postdate the Separation Point Batholith, and may have been intruded in their present orientations, or sheared and rotated towards the plane of the Alpine Fault by either drag or rotation. However, this means that the aplite dikes cannot be of Separation Point Suite affinity.

2.9.4 Joints

The degree of joint development and orientation is extremely variable. In some surfaces there were up to five different orientations. The strike and dips are highly variable and do not appear to follow any strong definitive pattern. A plot of poles to joints is presented in **Figure 2.14**.

2.9.5 Foliations

Foliations in the Rotoroa Complex are present in the gabbro, diorites and quartz diorites of the Rotoroa Complex. There is a continuum of foliations ranging from a random alignment of constituent minerals through to gneissic proto-mylonites in the most deformed quartz diorite. The alignment of equigranular mafic and felsic minerals is a primary feature related to magma flow and cumulate texture in the parent magma during emplacement. The foliation formed by the alignment of minerals was recorded in several locations **(Figure 2.10c)** and is plotted as poles in **Figure 2.15**, showing an approximate N - S trend. This is however rather dilute and based on only 35 sample points. The zones of gneissic proto-mylonitic fabric with feldspar augen and quartz ribbons are more likely to be the result of high pressure - low temperature deformation associated with the Cenozoic Alpine fault and its major subfaults.

2.9.6 Mafic Enclaves

Aligned mafic enclaves are found throughout most of the Braeburn Quartz Diorite. They consist of mesocratic gabbro - dioritic enclaves enclosed in tonalite or quartz diorite of which aligned elongate lensoid enclave structures are predominant. These represent portions of a gabbro - dioritic magma which have become isolated in the quartz diorite magma (Marre 1986). They range in length from 2 cm **(Figure 2.16)**, to continuous sheets several metres in length **(Figure 2.17)**. The enclave structures are best exposed in

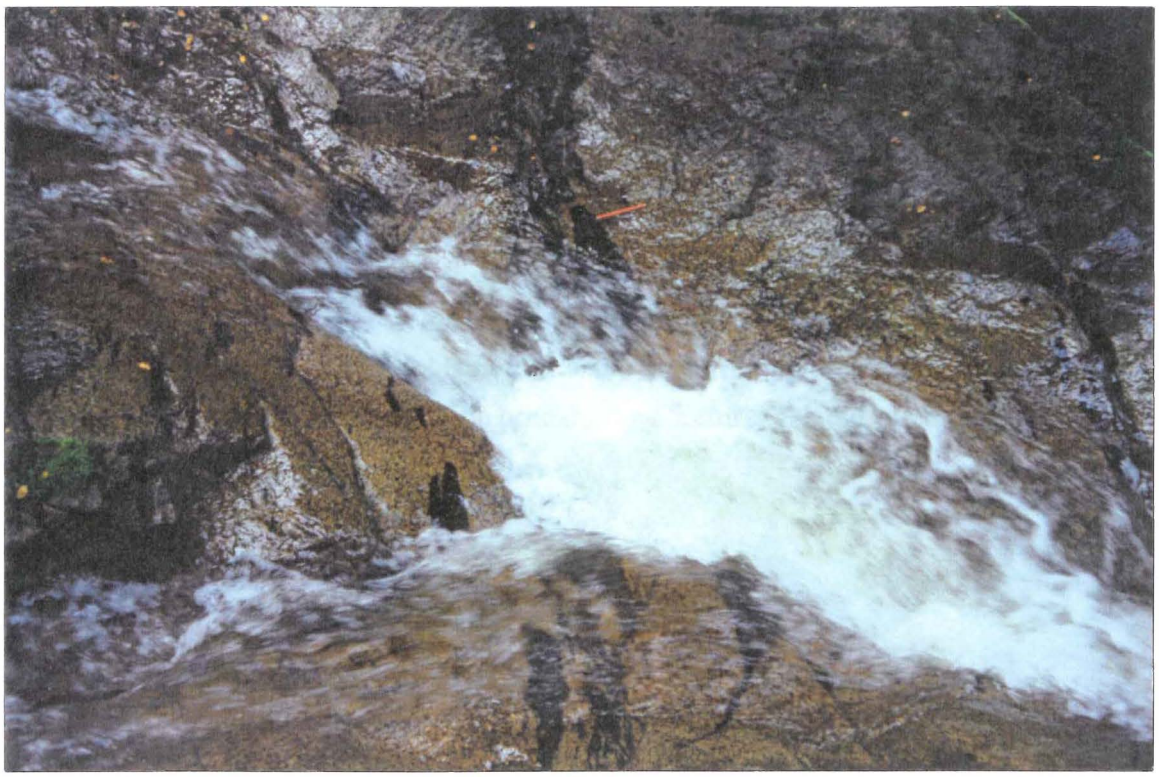

Figure 2.16 Singular aligned mafic enclaves in the Braeburn Quartz Diorite upstream of the Separation Point Granite exposure. (see text)

Figure 2.17 Multiple aligned mafic enclaves in the Braeburn Quartz Diorite (same locality)

Boulder stream, at 774306 and behind Mt Hutton at 758223. The density of the enclaves is also very variable. In some cases they are well rounded elongate ovals which are sparsely distributed **(Figure 2.16)**. In other situations they form a dense band of sub-angular to sub-rounded elongate enclaves which often inter-finger with the host quartz diorite.**(Figure 2.17)** In all cases the enclaves are aligned. This was produced by flow induced strain, during emplacement of the quartz diorite. The alignment is variable on a meso-scopic scale, and occurs as gentle swirls in the foliation of the enclaves. These could be interpreted as subtle folds which have occurred in a plastic state during metamorphism, but are more likely to be primary flow features related to emplacement of the magma.

CHAPTER THREE: PETROLOGY

3.1 Introduction.

The rocks of the Rotoroa complex range from mafic metamorphic amphibolites and rare lenses of hornblendite, to more common gabbros, diorites, and quartz diorites. Recently three new formations have been proposed as part of the Rotoroa Complex, (Challis *et al* in prep.), distinct from the Separation Point Suite as defined in Tulloch (1988). These include the Howard Gabbro, the Braeburn Diorite and the Kawatiri Amphibolite. The range of rock types within the Rotoroa Complex is believed to represent a "*gabbronorite - anorthosite - diorite - trondhjemite layered intrusion of Jurassic age.*" (Challis *et al* in prep.)

Extensive high temperature, low pressure metamorphism and metasomatism associated with the intrusion of the Early Cretaceous Separation Point Granite (Tulloch 1983), has altered much of the original Rotoroa Complex to metamorphic amphibolites. This often makes original lithological determination difficult. Mafic to intermediate lamprophyre dikes possibly intruded prior to emplacement of the Separation Point Batholith, and aplites and pegmatite veins intruded during and after emplacement, cut all Rotoroa Complex lithologies. These are most notable in the diorite and quartz diorites. The Alpine Fault which passes through the SE margin of the field area **(Figure 1.3)** is responsible for large imbricate subfaulting and ubiquitous small scale folding and faulting throughout the area.

For ease of field and microscope classification I have roughly followed the classification as set out by Challis *et al* (in prep), but subdivided the Braeburn Diorite into a) the Braeburn Diorite and b) the Braeburn Quartz Diorite, and named the hornblendite as the *Rotoroa Hornblendite.*

3.2 Petrogenetic Classification

All forty thin sections which were point counted **(Appendix # 1)**, are plotted according to the IUGS classification for igneous plutonic rocks. (Le Maitre *et al*, 1989). The results are presented in **Figure 3.1**. The rocks of the Rotoroa Complex define a strong calc-alkaline trend from gabbro - diorite in the Howard Gabbro through to granodiorites and granite in the Braeburn Quartz Diorites. The mineral assemblage present indicates lower greenschist facies metamorphism (Shelley 1993). Owing to this, some of the more deformed quartz diorites and metagabbros may not be properly classified, as metamorphism and deformation processes may have affected the relative abundances of

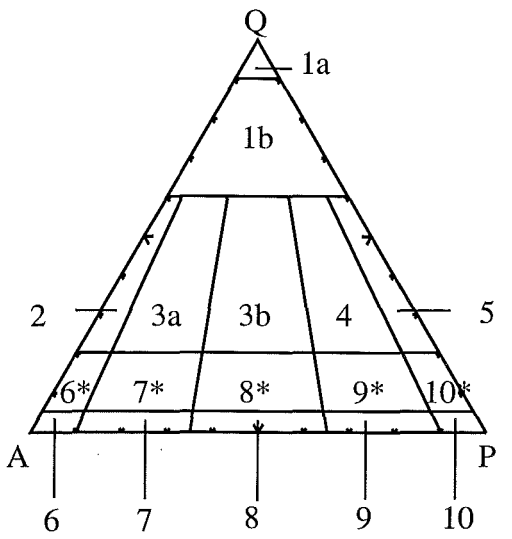

Key to fields:
1a quartzolite
1b quartz rich granitoid
2 alkali feldspar granite
3a syenogranite
3b monzogranite
4 granodiorite
5 tonalite
6* quartz alkali feldspar syenite
6 alkali feldspar syenite
7* quartz syenite
7 syenite
8* quartz monzogranite
8 monzonite
9* quartz monzodiorite/monzogabbro
9 monzodiorite/monzogabbro
10*quartz diorite/quartz gabbro/quartz anorthosite
10 diorite/gabbro/anorthosite

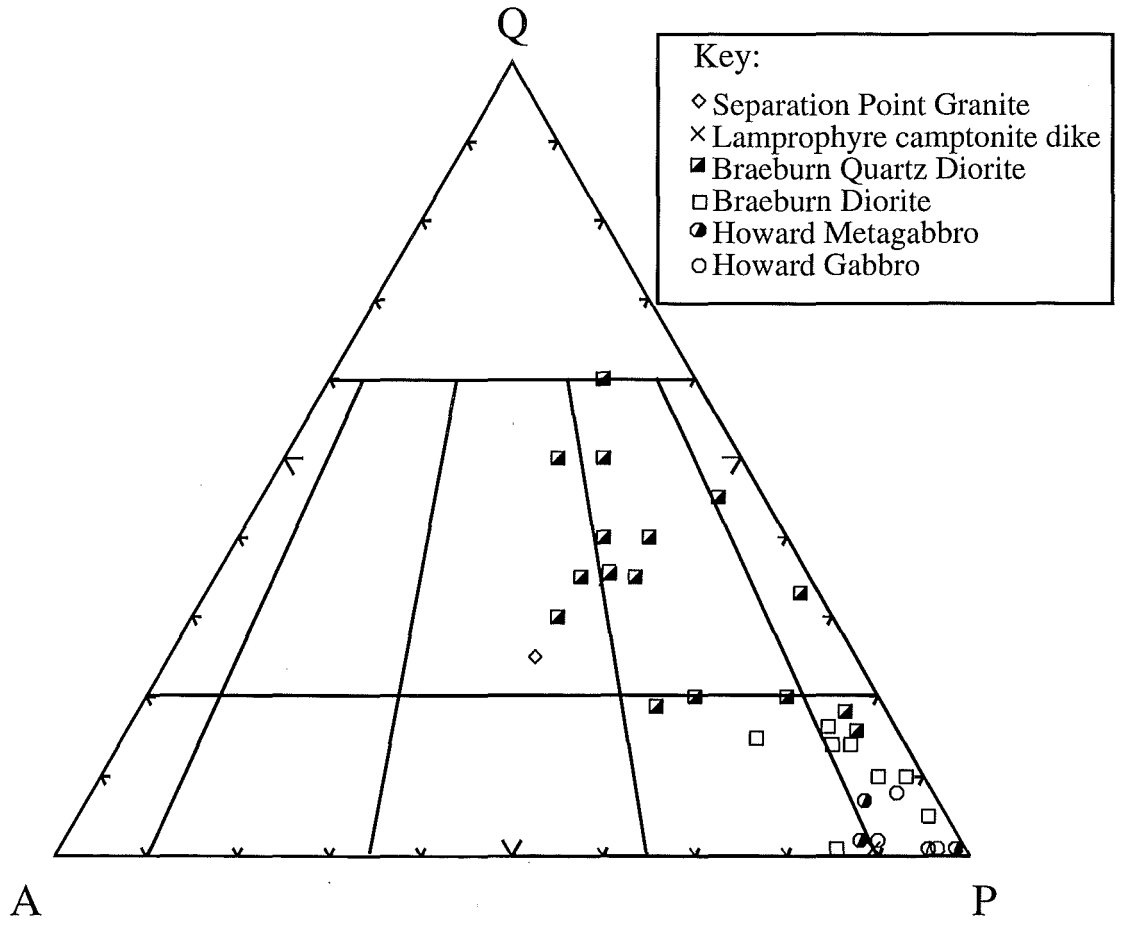

Figure 3.1 Modal Q-A-P diagram from thin sections of the Rotoroa Complex and other rocks within the field area. (after Le Maitre *et al* 1989). Point count results are presented in Appendix # 2.

quartz, plagioclase and alkali feldspar. Sample AC7A plots within the monzogranite field, consistent with it being part of the Separation Point Suite.

3.3 Rotoroa Complex

3.3.1 Rotoroa Hornblendite

The Rotoroa Hornblendite is exposed in rare occurrences as lenses and pods within the gabbro and diorites of the Rotoroa Complex. Challis *et al* (in prep.) believe that these represent fragments of ultramafic rock which underlie the gabbro as part of a layered intrusion.

In thin section the hornblendite is holocrystalline, fine to coarse grained and has a inequigranular blasto-porphyritic texture **(Figure 3.2)**. Using the classification for ultramafic rocks (M>90%) of Le Maitre *et al* (1989), slide AC8D falls within the hornblendite field. In AC8D the large phenocrysts of pleochroic green-dark green subhedral hornblende are up to 1 cm in diameter, and make up 85 % of the slide. Some sections show characteristic 54^{o} cleavage, twinning is common and inclusions of biotite are widespread. Remnant phenocrysts of very altered plagioclase of similar size are still apparent but saussuritization has largely obscured existing albite twinning. Refractive Index (RI) determination using Becke lines as described in Shelley (1985), suggest albite composition.

Biotite is widespread throughout the slide, commonly as inclusions in the hornblende. Yellow to yellow/brown biotite typically occurs as fine grained flakes around 0.1 - .5 mm, however larger flakes up to 1 cm do occur.

The finer groundmass is made up of pleochroic pale to dark green fibrous amphibole, finer grained feldspar combined with secondary granular epidote and sericite.

Accessory minerals include apatite and titanite. Opaque minerals are conspicuously absent in AC8D although pyrite is visible in hand specimen in other samples e.g. AC27F.

Figure 3.2a Typical texture of Rotoroa Hornblendite in plane polarised light. The field of view across the length of the photograph is 7mm.

Figure 3.2b The Rotoroa Hornblendite in cross polarised light. The scale is the same as the photograph above.

3.3.2 a) Howard Gabbro

This unit crops out at several points along the shore of Lake Rotoroa and also occurs in several of the side creeks. (See Map). The Howard Gabbro can be identified by a distinctive purple colouration of the plagioclase feldspar on fresh surfaces.

Several thin sections of the Howard Gabbro were made and examined AC3E, AC3F, AC9C, AC23B, **(See Appendix # 1. for locality)**. The point count results when classified according to Le Maitre *et al* (1989), **(Figure. 3.1)** typically fall in the field 10, diorite, gabbro, and anorthosite. Using the Plagioclase, Pyroxene, and Hornblende triplot (Le Matire *et al* 1989) the gabbro can be further classified as gabbronorite. The metagabbros plot in the hornblende gabbro and pyroxene hornblende gabbro fields.

Table # 3.1 Typical modes of Howard Gabbro and Metagabbro.

	Gabbro		Metagabbro	
Sample No:	AC3E	AC23B	AC3F	AC9C
Quartz	1.3	3.8	1.0	0.5
Plagioclase	63.9	64.5	56.6	53.2
K-feldspar	3.8	1.9	1.8	1.3
Pyroxene	15.1	16.0	0.9	0.0
Hornblende	1.0	4.0	37.9	40.8
Biotite	10.3	1.0	1.0	2.2
Magnetite	4.6	8.8	0.8	2.0
Total:	100.0	100.0	100.0	100.0

The typical Howard Gabbro is holocrystalline, medium grained, with a texture that varies between hypidiomorphic granular to intergranular/trachytic. The laths of feldspar which define the intergranular texture also show a crude alignment which gives the trachytic texture. Challis *et al* (in prep.) attribute this texture to being in the plane of layering cumulus. This could also be interpreted as a primary flow feature formed during emplacement as is seen in the quartz diorites. **Figure 3.3a** shows AC3E, a typical example of the Howard Gabbro in both cross polarised light.

Plagioclase which appears purple in hand specimen is subhedral to euhedral in thin section and ranges from 1 mm up to 4 or 5 mm long. The purple colouration appears to be due to alteration products within the feldspar. Challis *et al* (in prep.) attribute the

colouration to "*heating of original black feldspar during the intrusion of the Separation Point Granite.*" Epidote is a common replacement product indicating saussuritization; sericitization also occurs. Albite and carlsbad twinning in the feldspars are still visible, as is zoning in the crystals. Challis *et al* (in prep.) note reverse zoning, with labradorite (An_{60-70}) in the core zoned to andesine in the rims. Evidence of brittle deformation is apparent with small fractures commonly offsetting twin planes and grain boundaries, undulose extinction is also common.

Pyroxene is pale pink in plane polarised light, typical of the clinopyroxene augite. It ranges from 0.2 to 3 mm in diameter. A range of crystal forms can be observed, from anhedral to octahedral euhedral grains exhibiting classic 90° cleavage. Often only remnant crystals are discernible due to alteration and growth of secondary amphibole. In some slides, AC12E for example, the pyroxene is mixed with opaques in a myrmekite like texture. This is explained as "*blebs and needles of dark brown to opaque Fe/Ti oxides.*" (Challis *et al* in prep.). In more altered or metamorphosed samples the pyroxene is altered at its margins. Small green to pale blue pleochroic grains of hornblende became more common as it starts to replace the pyroxene. AC3E is a particularly fresh gabbro and virtually no hornblende is present.

Hornblende is apparent in two generations, which combined may make up to 40 % of the constituent minerals in metagabbros. Primary hornblende exists as fibrous rims around pyroxene crystals and independent crystals which may be up to 4 mm in size. Primary hornblende is distinguishable by being pleochroic straw yellow to green. Secondary pleochroic pale green to darker green fibrous actinolite aggregates containing numerous 1 - 2 mm crystals, and grows as a alteration product replacing clinopyroxene. It is commonly widespread throughout the slide in both dense concentrations where large pyroxenes have existed, and in a sparse disseminated distribution throughout the slide as a alteration product.

The amount of biotite in the gabbro is very variable **(Table # 3.1)**. The size of the biotite ranges from small flakes around ~ 0.2 mm, up to 3 mm sheets. The crinkly extinction is the best way of identifying the biotite, as the pleochroic colours may be yellow, green, brown to red brown. The grains are often poikilitic, enclosing pyroxene, plagioclase and opaques. There is some evidence of deformation in some slides, which has caused crenulations to develop in the cleavage of the biotite. The biotite is commonly associated with the opaque minerals.

Quartz is present but rare. It occurs as isolated interstitial anhedral grains between 0.1 - 1.0 mm. Undulating extinction is an ubiquitous feature of these grains.

The opaque mineral present is thought to be magnetite due to its relatively euhedral nature, although ilmenite is probably also present. The percentage of opaques is very variable, and may range from <1 % to 10 % **(Table # 3.1)**. Accessory minerals include epidote, apatite and rare titanite.

The amount of secondary hornblende and alteration mineralisation e.g. epidote, sericite and development of metamorphic textures show that the Mid to Late Jurassic Howard Gabbro (Kimbrough *et al* 1993), has undergone subsequent metamorphism. The source of the metamorphism is likely to be heating and deformation associated with the intrusion of the younger Separation Point Granite in the Early Cretaceous. The evidence of brittle deformation contained in many of the slides may be associated with this event , but is perhaps more likely the result of relatively recent deformation associated with the adjacent Alpine Fault. Field evidence for abundant shearing and brittle fracturing sympathetic to the Alpine Fault throughout the field area would support this.

3.3.2 b) The Metagabbro

The typical metagabbro is a holocrystalline, medium to fine grained rock. It still has remnants of the gabbroic intergranular and trachytic textures preserved in the feldspars, however the growth of aggregates of amphibole in the pyroxene and throughout the slide as fibrous growths has partially obscured them **(Figure 3.3b)**.

The plagioclase is mostly subhedral, although the occasional euhedral grain occurs. The phenocrysts range from 2 - 4 mm in size. Albite twins and carlsbad twins can be recognised in the less altered slides. Refractive Index using Becke lines methods (Shelley 1985), indicates that the feldspar is albite. Alteration is a common feature and varies from slide to slide, some are almost totally saussuritized to epidote whereas others have mild sericitization of their cores. Brittle fracturing offsetting twins and grain boundaries can be observed in some sections. Rare grains of microcline and sometimes perthite do occur.

Hornblende dominates the metagabbros **(See Table # 3.1.)**. Primary pleochroic pale blue - green fibrous tremolite grains ~ 0.1mm, are common as reaction rims/coronas around what were originally pyroxene phenocrysts. Some remnant pyroxene is still present in the cores of less altered slides. In the more altered slides, secondary darker green - green pleochroic grains of actinolite, 0.1 - 0.5 mm, pseudomorph the pyroxene.

Figure 3.3a Typical texture of the Howard Gabbro in cross-polarised light. The field of view covered by the length of the Photograph is 3mm.

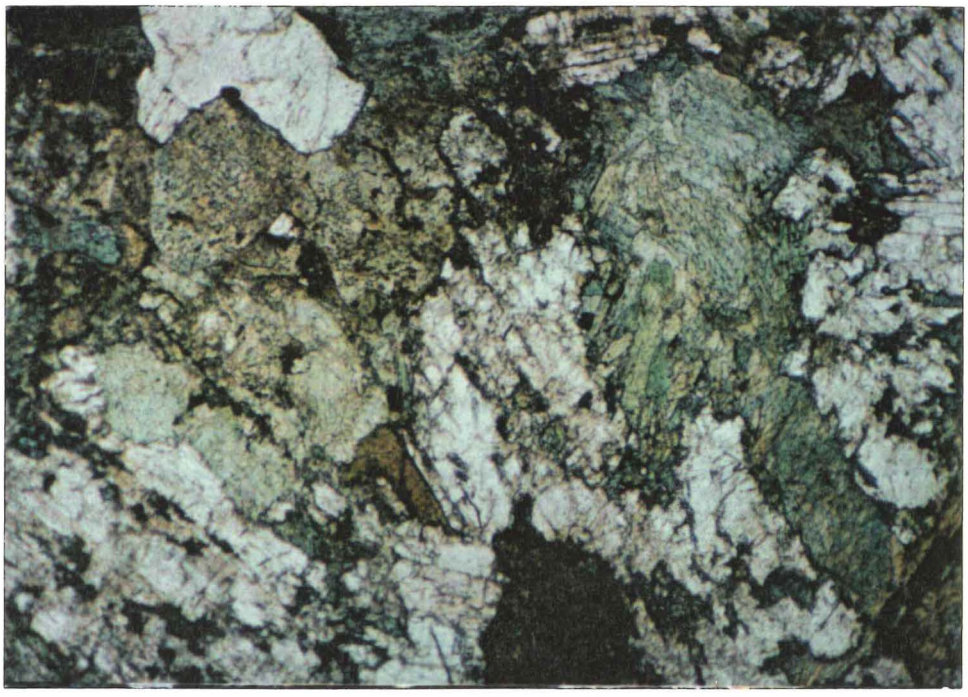

Figure 3.3b The Howard Metagabbro, an metamorphosed version of the Howard Gabbro. Note growth of secondary amphibole. The field of view covered by the length of the photograph is also 3 mm.

These exist as aggregates of up to 4 - 5 mm in size. The secondary hornblende has also grown throughout the rock as disseminated flakes.

Biotite is present as pleochroic light brown to dark brown flakes, ranging from 0.2 - 2.0 mm. It often occurs with hornblende rimming remnant pyroxene phenocrysts. Curvature of some of the cleavage indicate that the biotite has been deformed. The biotite is associated with the opaque minerals, as in the gabbro.

Like the Howard Gabbro, the metagabbo has small quantities of interstitial quartz present. Other accessories include epidote, apatite, haematite, ilmenite and magnetite.

3.3.3 Braeburn Diorite

The Braeburn Diorite is the most common rock type in the field area. The range of rocks encompassed within the Braeburn Diorite includes "*diorite, melanodiorite, quartz diorite, trondhjemite, migmatite and intrusion breccia.*" (Challis *et al* in prep.). I have subdivided these into two groups, on the basis of an arbitrary 15 % modal quartz content. This is because there are two distinct groupings, one with modal quartz < 15 %, and another where modal quartz is >25 %. The result is, a) the Braeburn Diorites, and b) the Braeburn Quartz Diorites.

a) The Braeburn Diorite

Several slides of diorite were examined including AC3G, AC11B, AC16K and AC17E. On the Q-A-P classification diagram (Le Maitre *et al* 1989) they fall in Field 10. diorite, Field 9. quartz monzodiorite and the lower half of Field 4. granodiorite. **(Figure 3.1)**. Point count results are contained in **Appendix # 1**.

Table # 3.2 Typical modal composition of the Braeburn Diorite.

Sample No:	AC16K	AC3G	AC11B	AC17E
Quartz	2.6	8.5	8.8	14.0
Plagioclase	39.5	58.7	50.6	25.8
K-feldspar	3.2	6.7	8.2	11.4
Hornblende	36.6	10.5	24.4	37.7
Biotite	15.0	12.7	6.4	4.8
Magnetite	3.1	2.9	1.6	6.3
Total	100.0	100.0	100.00	100.0

The typical diorite is a holocrystalline, medium to fine grained hypidiomorphic granular textured rock. The rock has a rather uniform crystal size of 2 - 3 mm. There is also a weak fabric caused by the alignment of the constituent minerals **(Figure 3.4a)**.

Plagioclase feldspar is euhedral to subhedral in shape and ranges in length from 1 - 4 mm. Albite twins and carlsbad twins are abundant but in some cases they are highly altered. The alteration is mostly sericitization of the cores of the phenocrysts, epidote is relatively rare, saussuritization is a secondary process. An values are varied, and in most cases the Michel-Levy method of determination as described in Shelley (1985), cannot be used. Comparison of refractive indices between quartz and feldspar, (Shelley 1985), gives values ranging from K-spar/Albite to Oligoclase /Andesine in the fresher samples. There is remnant zoning in many of the feldspars however it is very weak. There is evidence of recrystallisation occurring along the grain boundaries of plagioclase grains with myrmekitic intergrowths of quartz invading the plagioclase.

Alkali feldspar occurs as subhedral grains of microcline up to 4 mm (but usually smaller), which often exhibit perthitic texture and cross hatch-twinning. The phenocrysts are usually poikilitic enclosing plagioclase, biotite and opaques.

Quartz occurs as both subhedral - anhedral singular interstitial grains and interstitial mosaics within a framework of plagioclase, hornblende and biotite. The individual grains are up to 1 mm in size, whereas the mosaics vary in size in different sections from 0.5 - 3 mm, as do the constituent subgrains from 0.1 to 0.5mm. Almost all quartz shows evidence of deformation in possessing strong undulose extinction indicating lattice strain. Recrystallisation at the margins of plagioclase and quartz grains has formed very coarse myrmekitic growths.

Hornblende is present in two generations. Primary tremolite is fibrous and is light brown to blue - green pleochroic. This occurs in the centre of clumps or aggregates of hornblende, which have probably replaced pyroxenes. The secondary hornblende is light green - dark green pleochroic actinolite, and ranges in size from small fibrous flakes to larger skeletal clumps up to 3 mm in diameter.

Biotite is widespread throughout the diorite. It is typically pale brown to brown green pleochroic, and exists as small skeletal flakes and ~ 2 mm anhedral sheets with good cleavage. The cleavage is sometimes warped indicating deformation.

Accessory minerals are dominated by titanite which may constitute up to 1 % of the rock in some cases. Opaques are another accessory mineral which may be as high as 10 % in

some sections and include magnetite, ilmenite, and probably pyrite. Trace accessories are apatite and secondary epidote.

b) The Braeburn Quartz Diorites.

The quartz diorites contain > 15 % modal quartz, and often exhibit granitic textures. The more silica-rich samples are true granodiorites, e.g. AC5I. Accompanying the increase in leucocratic minerals is a decrease in the mafic phases. Hence biotite and hornblende are not as common as in the diorites. The fabric which is weakly developed in the diorites, is much stronger in the quartz diorites. When the point count results were plotted according to Le Maitre *et al* (1989), **(Figure 3.1)**, the quartz diorites plotted in Field 4. granodiorite, and Field 3B. monzogranite.

Table # 3.3 Typical modal composition of the Braeburn Quartz Diorites.

Sample No:	AC16N	AC5I	AC8C	AC20M
Quartz	25.9	31.3	34.7	37.0
Plagioclase	37.1	52.0	33.7	42.8
K-feldspar	8.8	3.9	5.3	12.2
Biotite	23.8	5.5	24.3	2.6
Hornblende	1.5	6.4	1.6	4.6
Magnetite	2.9	0.9	0.4	0.8
Total	100.0	100.0	100.0	100.0

The textures and grain size vary relative to the amount of deformation shown in the section. The typical texture in the least deformed diorites is holocrystalline, medium to fine grained, hypidiomorphic granular. The more deformed quartz diorites exhibit a bimodal grainsize. Larger porphyroclasts of feldspar typically 2 - 5 mm in diameter, are contained in a < 1 - 2 mm sized groundmass of quartz, biotite and hornblende. This gives the most deformed examples a gneissic - protomylonitic texture **(Figure 3.4b)**.

Quartz occurs in the less deformed quartz diorites as small anhedral mosaics and single anhedral grains. The largest single grain or aggregate that occurs is ~ 2 mm. The subgrains in the aggregate/mosaics are < 0.5 mm. All have varying degrees of undulose extinction. In some cases these form simple myrmekitic intergrowths with feldspar. In the deformed rocks the quartz occurs as mosaics and ribbons.

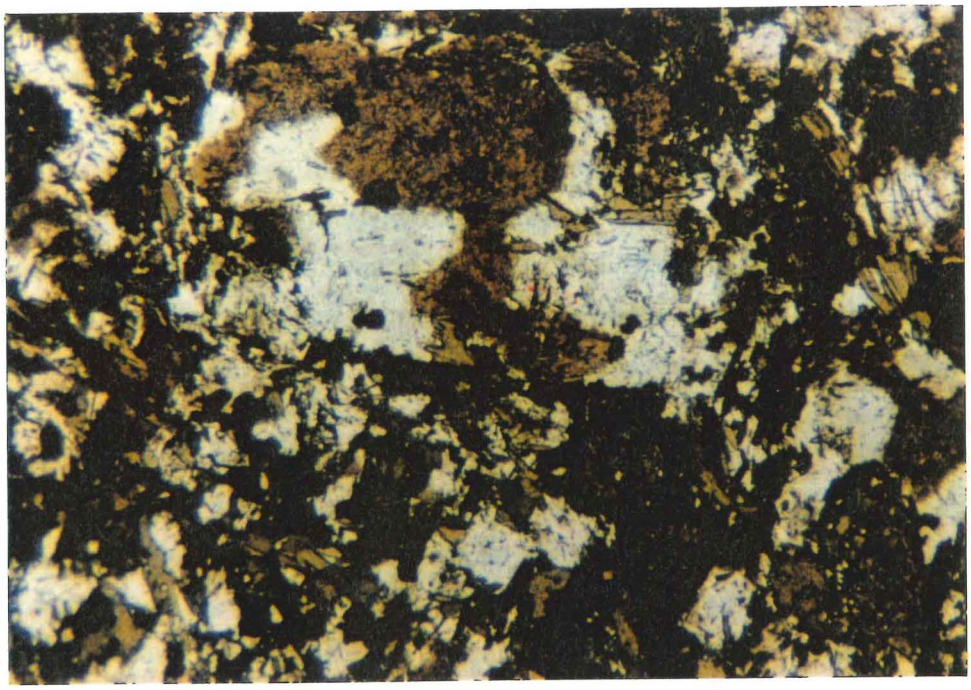

Figure 3.4a Typical example of the Braeburn Diorite. The field of view covered by the length of the photograph is 3 mm.

Figure 3.4b An example of the protomylonitic-gneissic texture in a more deformed sample of the Braeburn Quartz Diorite. The field of view covered by the length of the photograph is 7 mm.

The presence of ribbons indicates that ductile or plastic behaviour has occurred and therefore some degree of metamorphism and associated heating has occurred. These are finer grained than the less deformed diorite. The ribbons are as long as 8 mm but consist of numerous subhedral subgrains < 0.2 mm in size, this constitutes some sort of grainsize reduction. The ribbons help to define the foliation, and have grown around the less ductile feldspar grains like the biotite. Undulose extinction in the quartz ribbons is not as strong as in the less deformed quartz diorites, this indicates recrystallisation has occurred. The quartz ribbons often form coarse intergrowths with the plagioclase at the contacts.

The plagioclase phenocrysts are subhedral to euhedral and range in size from 1 - 5 mm. Both albite and carlsbad twins are present and there is a very weak concentric zoning present in the plagioclase. A composition of (An_{27} to An_{30}) oligoclase was determined using the Michel-Levy method (Shelley, 1985). This was supported by comparison of quartz and plagioclase refractive indices.(Shelley, 1985). In the less deformed quartz diorites, mild sericitization of the cores is a standard feature of most grains, with the occasional granule of epidote present especially in the more deformed samples. In the undeformed samples the plagioclase shows little evidence of deformation. In the protomylonites, plagioclase porphyroclasts show brittle fracturing infilled with quartz, rounded corners on grains and more intense saussuritization of the cores. Rough myrmekitic growths are more common at the margins of plagioclase porphyroclasts than in the undeformed diorites.

Alkali feldspar is more common in the quartz diorites than the diorites. It is present both as microcline with cross hatch twinning, perthitic texture, and compositional zoning. The phenocrysts are subhedral to anhedral, 1 - 4 mm, and commonly poikilitic, particularly in the perthitic grains. Along the margin of alkali feldspar in more deformed examples, fine grained quartz and feldspar < 0.1 mm has recrystallised.

Biotite is the most dominant mafic phase in the quartz diorites. It is green - brown to yellow - brown pleochroic, with a good cleavage and mottled extinction. In the less deformed samples biotite ranges being small flakes, 0.3 mm up to large 4.0 mm sheets e.g. AC8E. Although these share a common length orientation they do not join up to form layers. In the protomylonitic slides e.g. AC8C, the biotite defines a pronounced foliation **(Figure 3.4b)**. This fabric in the biotite is made up of larger 3 mm flakes and lenticular aggregates which combine to form elongate lenes, that flank the quartz ribbons and anastomose around feldspar porphyroclasts. The biotite appears to have recrystallised in the plane of the foliation as its long axis is parallel to the foliation, and shows little evidence of strain. The biotite is commonly observed with titanite, small flakes of muscovite and opaque minerals.

Hornblende seems to be variable in both size and quantity in the quartz diorite. In one undeformed sample AC8E, it is bimodal. Both are light green - dark green pleochroic, the smaller fibrous flakes are < 1 mm, and are spread throughout the slide with no preferred orientation. The larger grains are subhedral to euhedral and 2 - 3 mm in size. These larger grains have a rough long-axis preferred orientation, which is shared by the biotite. In the more deformed gneissic quartz diorites, hornblende is relatively rare. It does occur as small < 1 mm flakes within the biotite and shares the same pronounced orientation. This may be the result of the increased leucocratic component of the rock, or some aspect of the deformation process **(Figure 3.4b)**.

Titanite is ubiquitous throughout the quartz diorites. Epidote is rare in the less deformed quartz diorites outside of the cores of plagioclase grains. In the more deformed rock it can constitute up to 5 %, most of which is secondary. In AC8C the granules of epidote, around 0.1 mm - 0.3 mm, have grown within the biotite-rich zones where the shearing has been concentrated, indicating it is a product of deformation.

3.4 THE SEPARATION POINT GRANITE.

The only sample of Separation Point Granite found during field work is represented by thin section AC7A. In thin section the rock is very obviously holocrystalline, and exhibits a coarse grained granitic - allotriomorphic texture.

Table # 3.4 Modal Composition of Separation Point Granite AC7A.

Sample No:	AC7A
Quartz	23.5
Plagioclase	47.4
K-feldspar	24.6
Biotite	3.4
Muscovite	.7
Magnetite	.4
Total:	100.0

Quartz occurs as large 1 - 2 cm single grains and mosaics/aggregates of the same size, made up of subgrains of around 2 - 3 mm. The grains are subhedral to anhedral. Undulose extinction is variable. In some grains the extinction is clean, whereas others

exhibit a weak mottled extinction. Dust rims are visible in most of the subgrains. There are a few examples of simple quartz intergrowths intruding into feldspar grain boundaries, however they are not common.

Plagioclase laths are up to 1cm long are present but 4 mm is average. They range from subhedral to euhedral in habit. They show strong oscillatory zoning often highlighted by dust rims They are albite (An_{13}) in composition at their outer margin. Carlsbad twinning dominates the phenocrysts, but albite twinning is present. There is a weak sericitization in the cores of all of the plagioclase phenocrysts suggesting a more calcic composition. Inclusions of euhedral biotite and muscovite are common in the plagioclase.

The alkali felspar occurs as large poikilitic microcline megacrysts of up to 1 cm diameter. Perthitic texture dominates the alkali feldspar **(Figure 3.5)**. Inclusions of plagioclase, biotite, and small muscovite flakes are present

Biotite is the most conspicuous mafic mineral. Phenocrysts of 2 - 3 mm are common, and exhibit light brown to dark brown pleochroism. Often green - brown pleochroic streaks are evident in the biotite as is the occasional flake of muscovite.

Accessory minerals including muscovite, magnetite, allanite, titanite, epidote and apatite are all present in minute quantities.

3.5 INTERMEDIATE TO MAFIC DIKES.

Two samples of dikes were made into thin sections. These were AC5G and AC15B. Both of these were classified as camptonite lamprophyres according to Le Maitre *et al* (1989) and Rock (1991).

Plagioclase is > orthoclase, feldspars are > foids. Predominant mafic minerals include biotite and characteristic panidiomorphic red - brown hornblende which indicate that they are best described as the alkali lamprophyre camptonite.

The dikes are holocrystalline - hypocrystalline, and slide AC15B contains the occasional spherulite. Large phenocrysts up to 2 mm of plagioclase and hornblende are set in a fine grained intergranular to trachytic groundmass < 0.1 mm. The groundmass consists of fine grained plagioclase and hornblende and occasional biotite **(Figures 3.6a and 3.6b).**

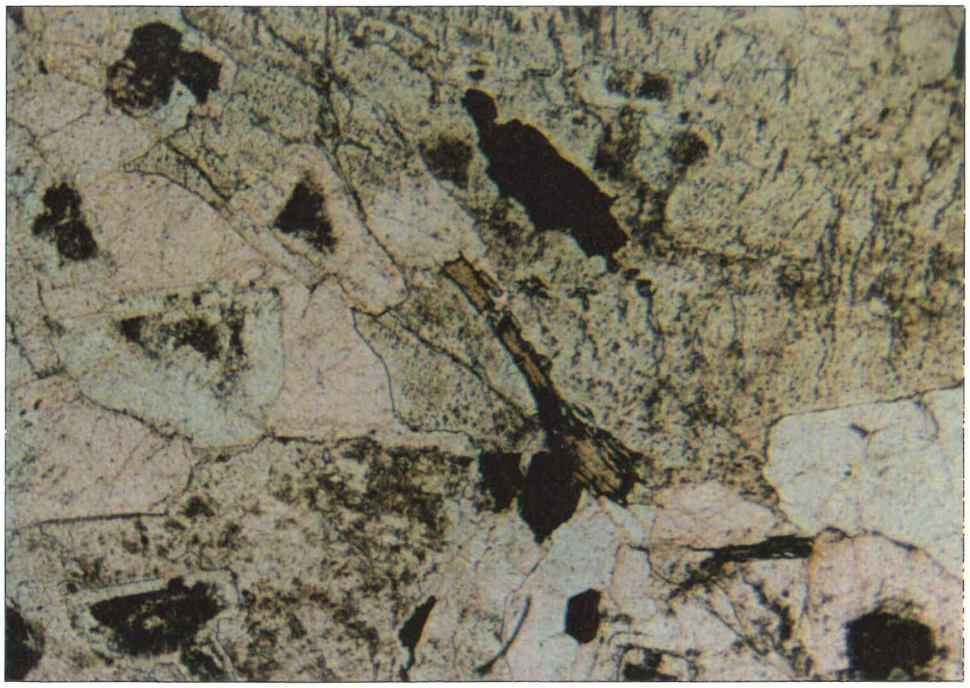

Figure 3.5a The texture of the one sample of Separation Point Granite AC7A, in plane polarised light. The field of view covered by the photograph is 7 mm in length

Figure 3.5b The same slide in cross-polarised light, which shows cross hatch twinning and perthitic texture in the alkali-feldspar. The scale is the same as above.

Table # 3.5 Typical modal composition of two mafic - intermediate lamprophyre dikes.

Sample No:	AC5G	AC15B
Quartz	0.8	0.0
Plagioclase	47.3	48.0
K-feldspar	1.8	1.0
Hornblende	41.5	41.3
Biotite	2.7	8.1
Magnetite	5.9	1.6
Total:	100.0	100.0

The plagioclase which occurs as ~ 2 mm phenocrysts is very sericitized, and appears as a ghostly outline of the original phenocryst. In some less altered samples carlsbad twins can still be made out. The groundmass plagioclase is much smaller, < 0.2 mm and is also altered. Refractive index comparisons between quartz and feldspar using Becke lines as described in Shelley (1985), indicate that the plagioclase is albite - oligoclase.

The hornblende phenocrysts are light brown to dark brown pleochroic, and range between 0.5 - 2 mm in length. Some phenocrysts are embayed and enclose the groundmass. The hornblende is euhedral and may show twinning. Good 54^{o} cleavage is still apparent in some euhedral sections. The groundmass contains green to green - brown pleochroic secondary hornblende, usually < 0.2 mm which is probably replacing primary hornblende. This is interstitial to the groundmass plagiocase. Accessory minerals include rare flakes of biotite in the groundmass, granular titanite, and epidote.

3.6 The Brook Street Volcanics

The Permian Brook Street Volcanics (Thornton, 1985) occur in the SW corner of the field area, as an infaulted wedge in tectonic contact with the Rotoroa Complex **(Figure 1.3)**. In outcrop they are very fractured and broken and consist of intercalated siliceous fine grained volcanic sediment and mafic igneous rock. Two slides were made, AC1A and AC1B. AC1A is a extremely altered, silicified, fine grained volcanogenic sedimentary rock which is too fine to resolve individual minerals under the microscope. Brittle fractures and quartz veins cut the rock and are picked out by iron staining. AC1B is an altered basaltic rock **(Figure 3.7)**, the fine grained nature of which also makes point counting impossible.

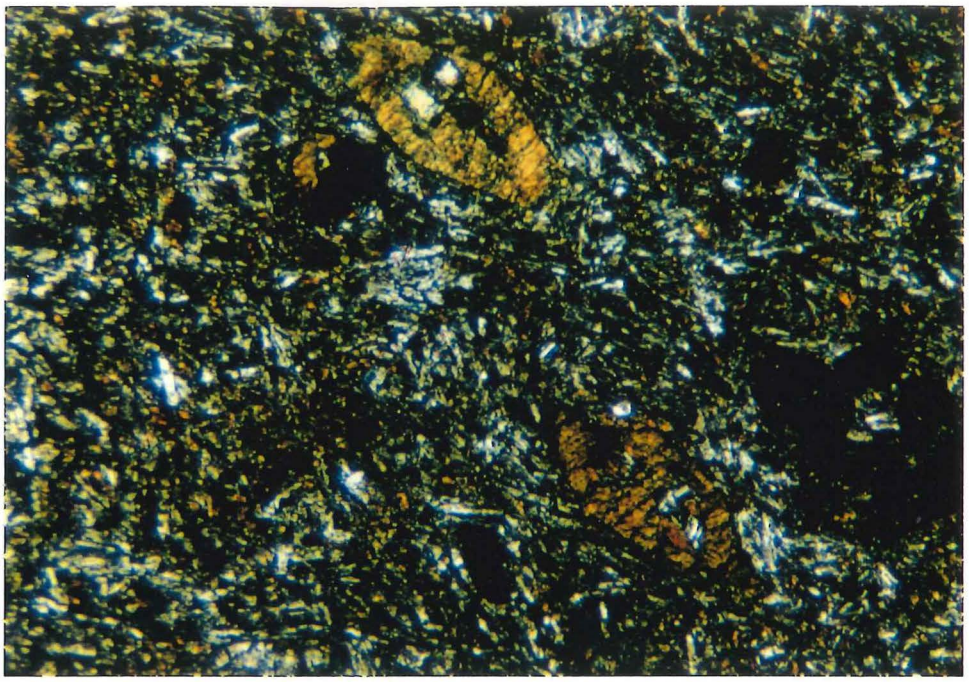

Figure 3.6a Porphyritic texture in a mafic-intermediate lamprophyre camptonite dike. The field of view covered by the length of the photograph is 7 mm.

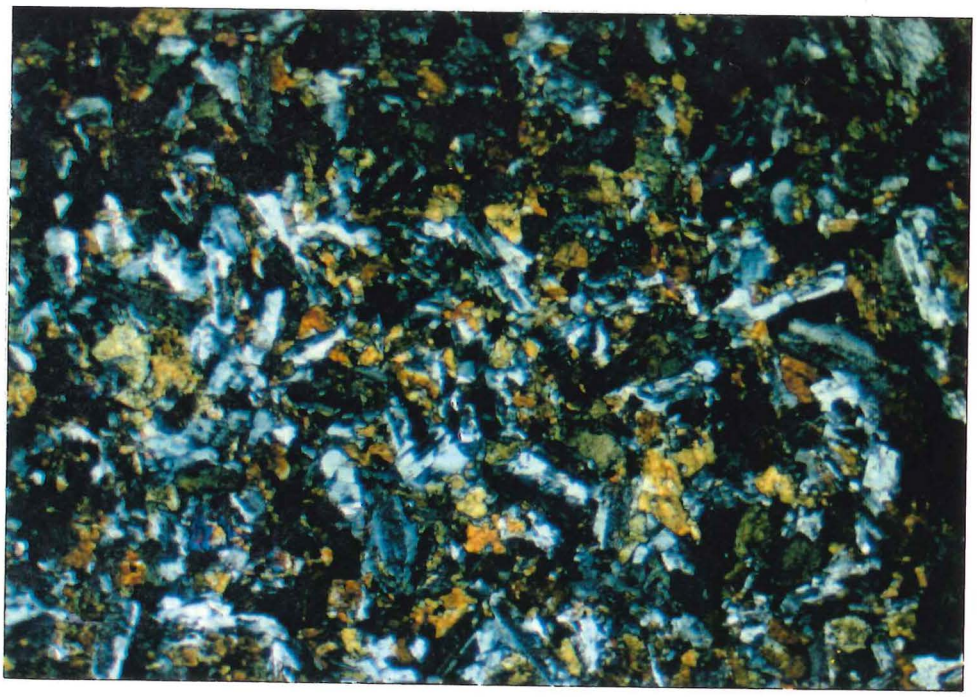

Figure 3.6b Intergranular texture in a mafic-intermediate lamprophyre camptonite dike. The field of view covered by the length of the Photograph is 3 mm.

The texture of AC1B is hypocrystalline, medium to fine grained, with phenocrysts of augite clinopyroxene and plagioclase feldspar set in a glassy groundmass.

The plagioclase is totally altered to carbonate and sericite. The remnant shapes indicate that crystals were 1 mm - 2 mm, euhedral laths. An % could not be obtained. Clinopyroxenes range from 0.1 mm to 4 mm, are mostly euhedral, some show good 90^{o} cleavages. The presence of iddingsite pseudomorphs suggest the occurrence of olivine. The dominant accessory mineral is finely disseminated magnetite <0.1 mm, which may make up as much as 10 % of the rock. Secondary epidote is widespread throughout the shear zones in the rock, The basalt has been fractured and veined with quartz like AC1A (note the offset in the pyroxene in **Figure 3.7**). The presence of the Alpine Fault nearby is almost certainly the cause for this.

3.7 The Torlesse Supergroup.

The Torlesse Supergroup has been brought into tectonic contact with rocks of the Rotoroa Complex by the Alpine Fault in the SE corner of the field area. One thin section of the Torlesse mylonite was made, cut parallel to the foliation and in the plane of the lineation, AC22A. **(Figure 3.8)**. The rock is dominated by quartz and occasional feldspar augen up to 1 mm, in a fine grained matrix that includes carbonate, muscovite, epidote, and apatite. The matrix has a very strong fabric and shape preferred orientation, which anastomoses around the augen. The quartz forms very small ribbons of two to five subgrains but occurs mostly as single grains probably of sedimentary origin. Undulose extinction is a feature of all quartz grains to varying degrees.

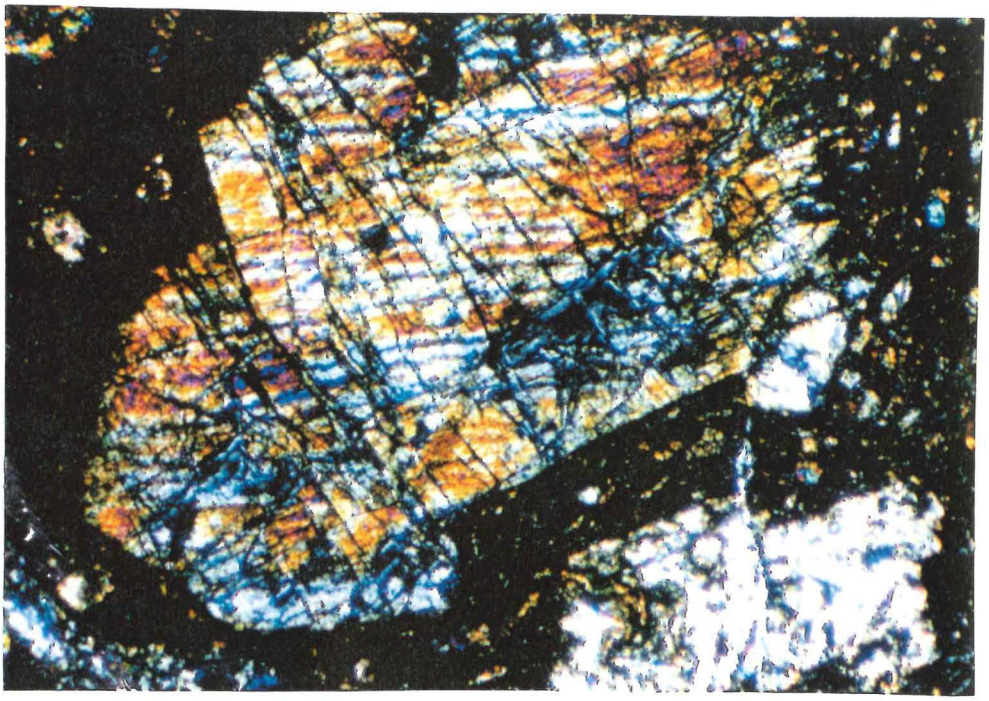

Figure 3.7 Texture of an altered basaltic rock from the Brook Street Volcanics. Note the brittle fracturing offsetting the large pyroxene phenocryst. The field of view covered by the length of the photograph is 3 mm.

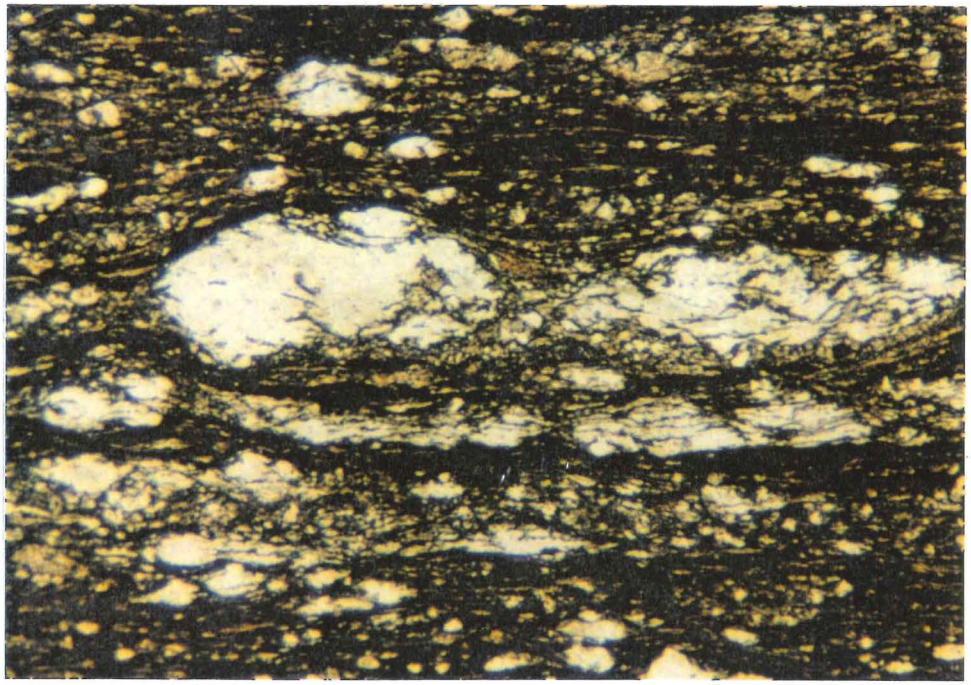

Figure 3.8 Mylonitic texture in the Mount Robert Subgroup of the Torlesse Supergroup, which marks the exposure of the Alpine Fault. The field of view covered by the length of the photograph is 7 mm.

CHAPTER FOUR: GEOCHEMISTRY

4.1 Introduction

The rocks of the Rotoroa Complex are geochemically distinct from the rocks of the Separation Point Batholith. This was highlighted by plotting my geochemical data against a Separation Point dataset compiled by Muir *et al* (in press). Additional analyses of Rotoroa Complex and the Separation Point rocks, provided by Dr. Alva Challis, helped to more closely define the geochemical trends. It should however be noted that none of these analyses was taken from within my immediate field area.

XRF major oxide and trace element geochemical analyses were obtained for 51 samples. **(These are presented in Appendix # 3)**. These include one sample designated Separation Point Granite, seven felsic dikes, and five samples of intermediate to basic dikes. The remaining 38 samples are considered to be the Rotoroa Complex rocks.

4.2 Rotoroa Complex

Major oxide and trace element analyses of 38 samples of the Rotoroa Complex show that the SiO_2 values of the Rotoroa Complex rocks, range from ~ 43 wt % in the Rotoroa Hornblendite to ~ 74 wt % in the Braeburn Quartz Diorites. The major elements exhibit generally continuous trends; TiO_2, Al_2O_3, Fe_2O_3, MgO, CaO and P_2O_5 all decrease with increasing SiO_2. Na_2O and K_2O increase at first, and decrease during later fractionation. Rotoroa Complex rocks have characteristically low Sr which shows a very gentle decrease with increasing fractionation. The Sr values remain relatively low decreasing from ~ 1000 ppm at 43 wt % SiO_2 to ~ 400 ppm at ~ 75 wt % SiO_2. Rb values are more scattered, but increase with increasing SiO_2 from 5 ppm to 120 ppm in the most SiO_2 rich samples. Ba like Rb, is also scattered suggesting mobility, but shows a trend from 20 ppm at 43 wt % SiO_2 increasing to ~1000 ppm at 75 wt % SiO_2. High Ni and Cr values are typical of the Rotoroa Complex, particularly in the more mafic samples (e.g. the Rotoroa Hornblendite).

4.2.1 Classification

The Rotoroa Complex rocks show a strong calc-alkaline differentiation trend from the hornblendite through to the quartz diorites. This is exhibited on the geochemical AFM diagram of Irving and Barager (1971) in **Figure 4.1**. A plot devised by Peacock (1931)

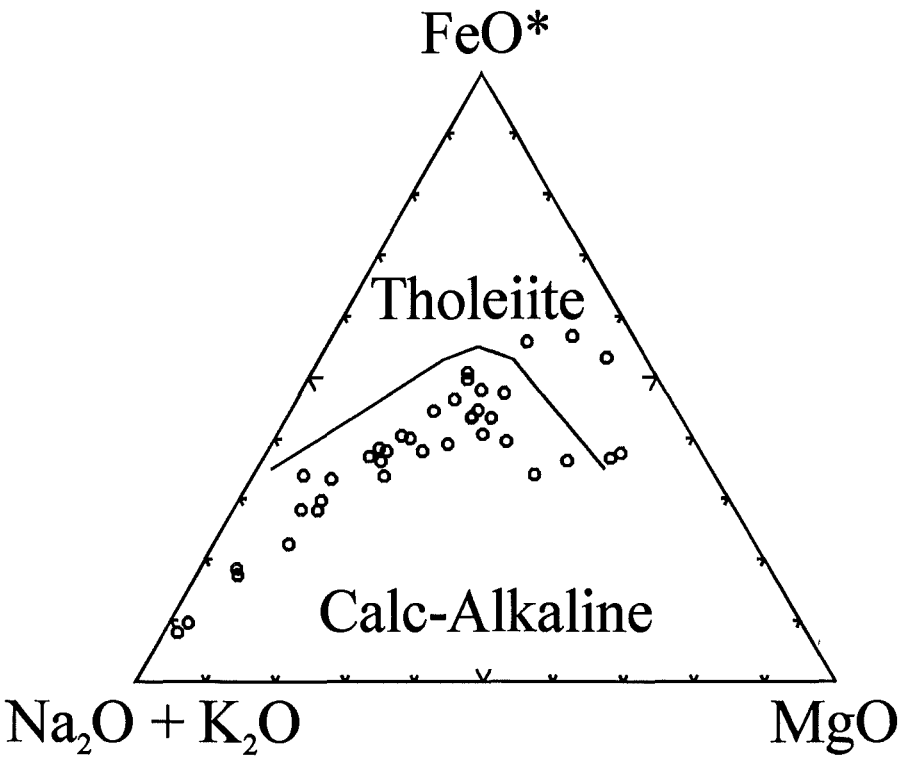

Figure 4.1 The AFM diagram of Irvine and Barager (1971), which highlights the strong calc-alkaline trend in the Rotoroa Complex rocks, represented as unfilled circles.

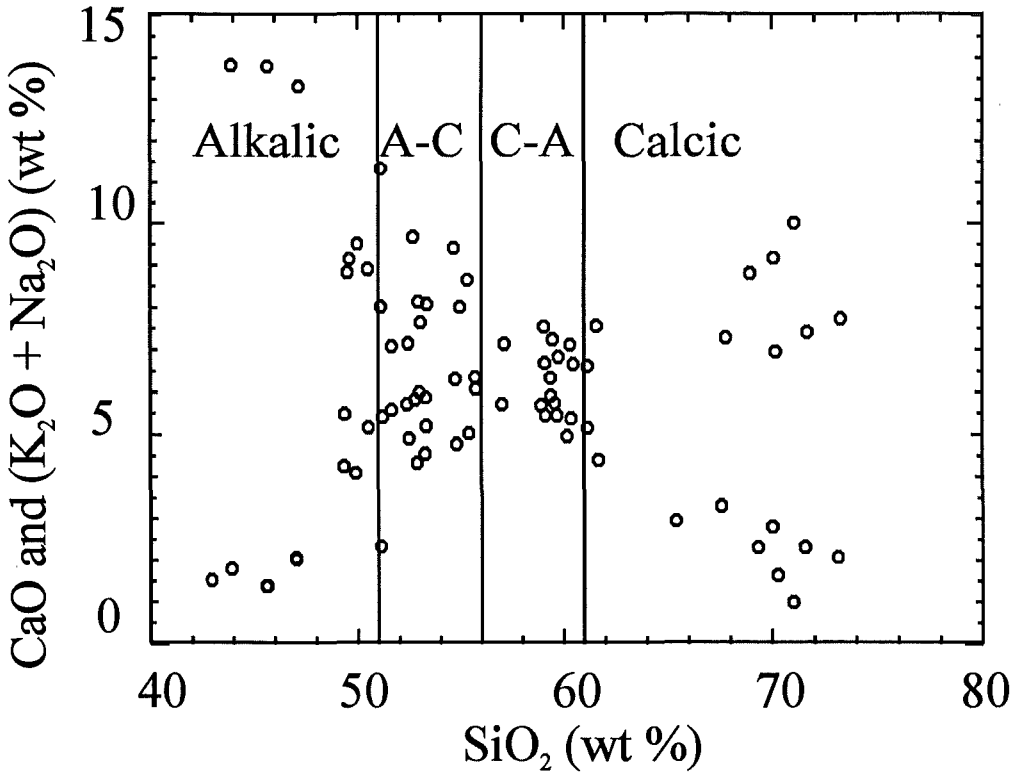

Figure 4.2 The Alkali diagram of Peacock (1931). The field where the trends cross each marks the character of the rocks as a whole, in this case calc-alkaline.

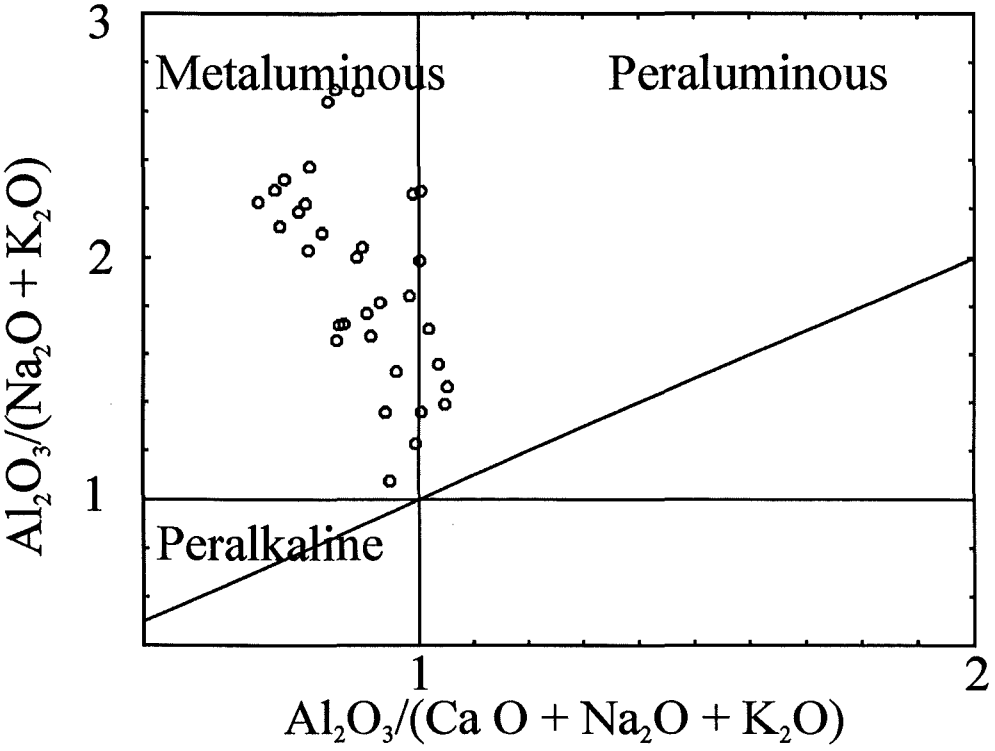

Figure 4.3 The plot of Maniar and Piccoli (1989), which shows the dominant metaluminous to weakly peraluminous nature of the Rotoroa Complex

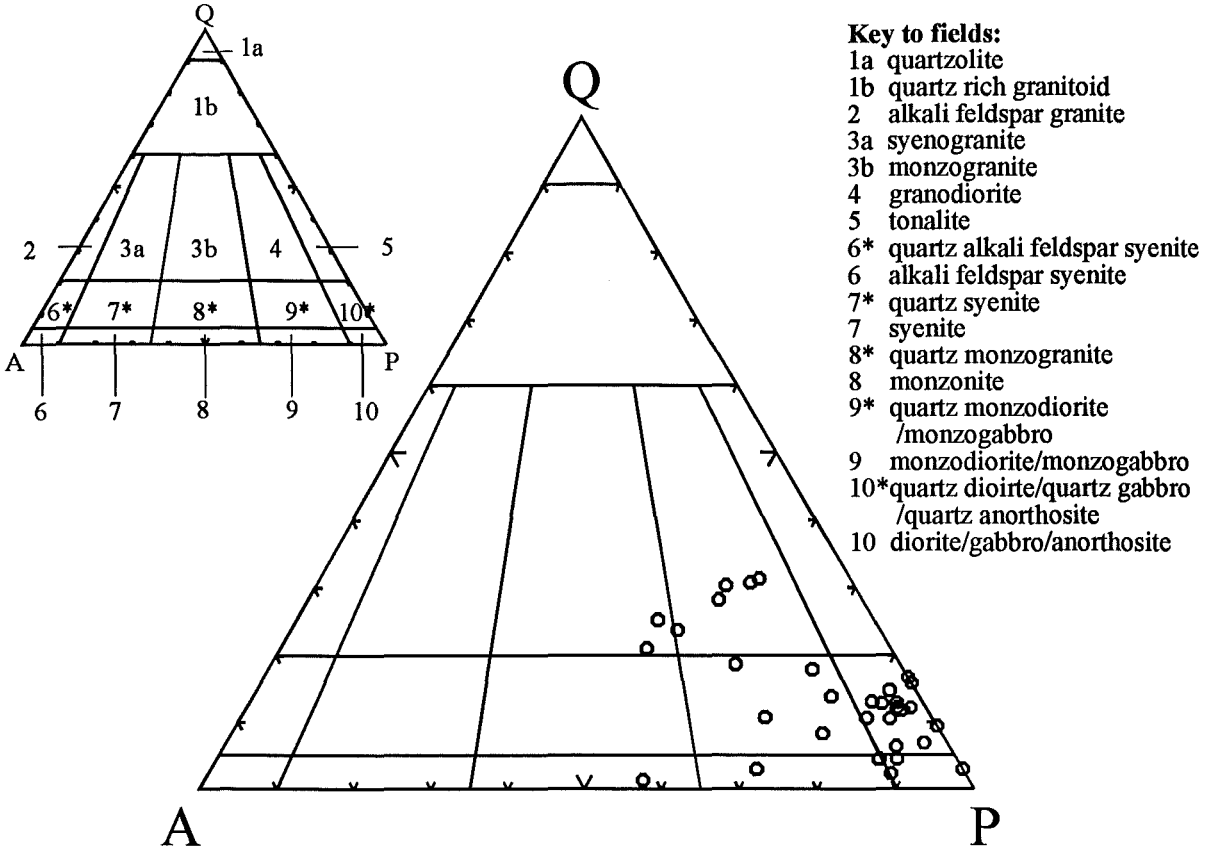

Figure 4.4 Mesonormative Q-A-P classification of the Rotoroa Complex rocks. (after Le Maitre *et al* 1989)

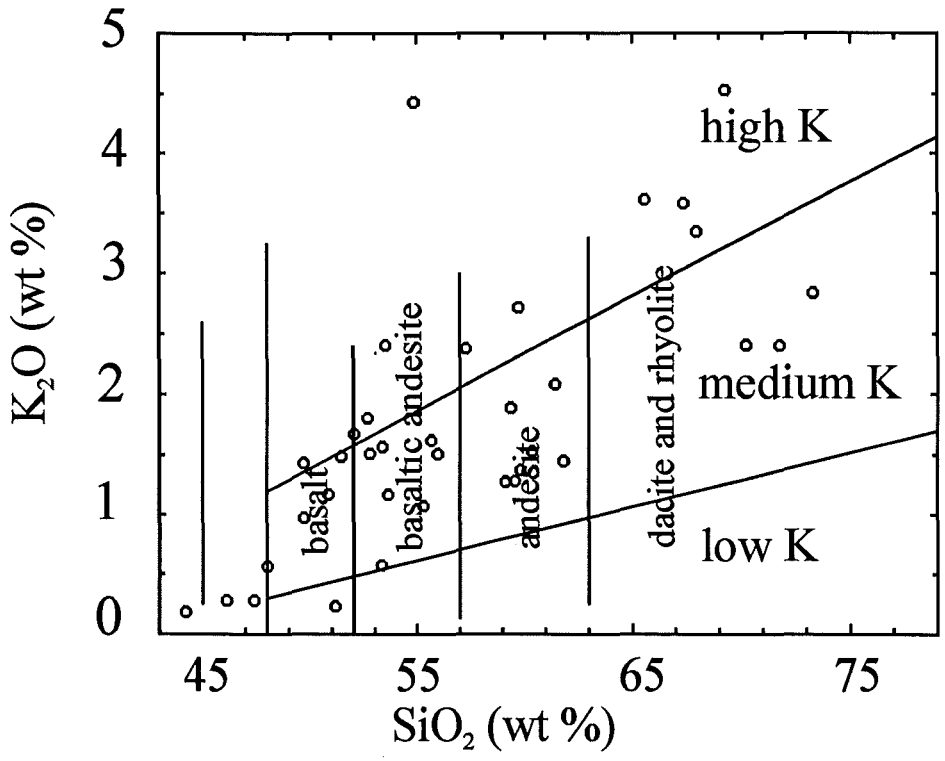

Figure 4.5 Plot of SiO2 (wt %) vs K2O (wt %) for the Rotoroa Complex. The constituent rocks range from sub-basaltic to dacite-rhyolites which are transitional between medium and high K in nature.(after Le Maitre *et al* 1989)

which plots total alkalis against silica also illustrates the calc-alkaline nature of the complex (**Figure 4.2**). The Aluminium Saturation Index (ASI) of samples from the Rotoroa Complex varies from (0.32) metaluminous in the Rotoroa Hornblendite to (1.05) slightly peraluminous in some of the quartz diorites. Of the Rotoroa Complex rocks, ~ 75 % are metaluminous. This is illustrated in **Figure 4.3** by the plot of Maniar and Piccoli (1989). The high content of hornblende in many of the rocks correlates with the high calcium content of the samples, which contributes to their metaluminous nature The quartz diorites which make up the other 25 % are weakly peraluminous, but these are relatively poor in hornblende. An average (A.S.I.) value of all Rotoroa Complex rocks sampled = 0.88.

The rocks encompassed in the Rotoroa Complex range mesonormatively from gabbros to monzogranites (**Figure 4.4**). They are dominantly subalkaline and can be geochemically described as medium to high K basalts - dacite rhyolites with a broad calc-alkaline character (**Figure 4.5**). Challis *et al* (in prep) label them M- type Granites based on major and trace element data. These are described by Pitcher (in Hsu 1982) as granites whose parental magma is derived directly from the mantle or subducted oceanic crust. These are typical of an oceanic island arc geological environment. This is consistent with the subalkaline medium to high K calc-alkaline nature of the Rotoroa Complex and its subduction-related trace element signature.

4.2.2 Fractionation

A fractionation trend is apparent in the Rotoroa Complex from the mafic hornblendite through to the felsic quartz diorites and is attributed to primary magmatic processes. Metamorphism has clearly dispersed more mobile elements, judged by the scattered nature of many of the geochemical plots. Harker plots of major oxides versus SiO_2 from 38 samples of the Rotoroa Complex are presented in **Figure 4.6 a - h**.

a) Major elements

Most major oxides show an approximate linear decrease with SiO_2 except Na_2O and K_2O, which increase up to ~ 65 wt % SiO_2 before decreasing owing to feldspar fractionation. In most of the plots, particularly Fe_2O_3 (**Figure 4.6c**), there is a distinct subtrend, which is consistently the same samples. These lack any apparent geographical control. This shows there is a series of lines of liquid descent occurring. Polybaric fractionation, or fractionation at different pressures is a powerful effect and will fractionate different trends from the same primary composition. This is understandable as the Rotoroa Complex is plutonic complex as opposed to a single magma chamber. The elements CaO and Al_2O_3 decrease with increasing fractionation. This could represent

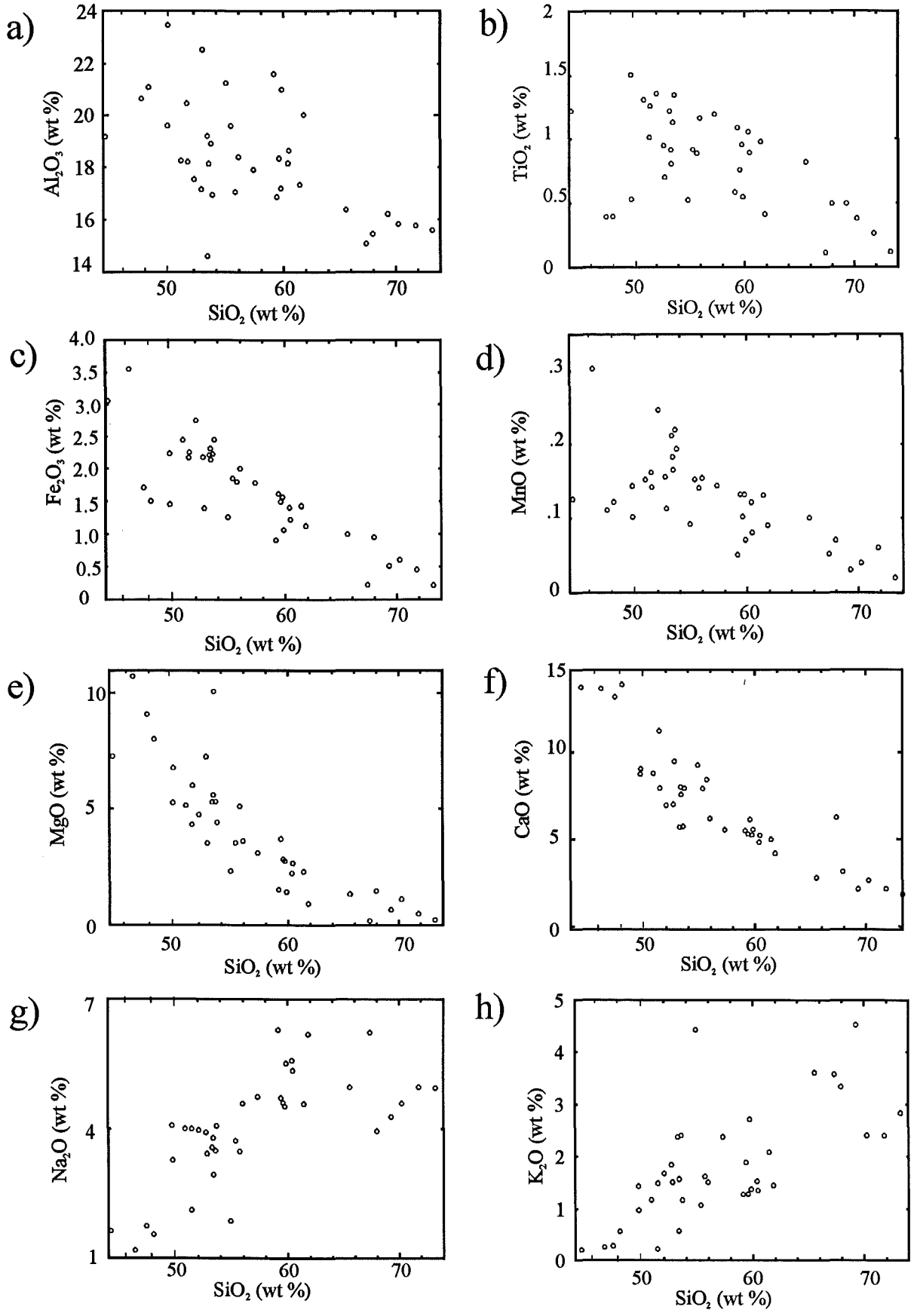

Figure 4.6 Major element oxide trends from the Rotoroa Complex, plotted against SiO_2. The Rotoroa Complex is represented by unfilled circles.

the crystallisation of plagioclase feldspar, however Sr (**Figure 4.7a**), which should also decrease, remains relatively level. The decrease in CaO may in fact be related to the crystallisation of hornblende, which is present throughout the Rotoroa Complex. The increase and then late decrease in K_2O suggests the crystallisation of K-spar in the late stage quartz diorites. Ba which is also removed by the crystallisation of K-spar shows similar behaviour to K_2O. The Ba versus SiO_2 diagram (**Figure 4.7d**) has a degree of scatter which indicates that Ba has been mobile. Ti decreases with increasing SiO_2. This is attributed to the crystallisation of biotite. Petrographically biotite is more abundant with increasing SiO_2, especially in the quartz diorites, which would remove Ti during late stage crystallisation. The decrease in Fe_2O_3 and MgO is attributed to the crystallisation of olivine, pyroxene, and amphibole, particularly in the early stages of fractionation. P_2O_5 shows two trends, the dominant trend appears to decrease with fractionation. A second trend increases then begins to decrease at ~ 60 wt % SiO_2. The primary trend indicates that apatite or monazite has crystallised.

b) Trace elements

Harker plots of trace element versus SiO_2 are presented in **Figure 4.7a - h**. Crystallisation of biotite is also responsible for the reduction of Zn and Nb with fractionation. Plagioclase crystallisation as indicated by removal of Sr, is more intense during the late stages of fractionation. Zr increases in concentration until the crystallisation of zircon occurs at 65 - 70 wt % SiO_2, causing it to decrease. Part of this reduction may be achieved by Zr substituting for Ti in titanite in the diorites and quartz diorites. Crystallisation of magnetite during ongoing fractionation has removed Ti and V from the parent magma. Cr and Ni are both relatively constant until ~ 50 wt % SiO_2 then decrease with increasing fractionation. The crystallisation of clinopyroxene and olivine respectively would explain this. Both phases are apparent in the gabbros but not the hornblendites, which may explain the initial behaviour. The element Y is low and appears to remain static with fractionation but the plot is too scattered for confident interpretation. Crystallisation of titanite may be offsetting the incompatible behaviour of this element by holding it's relative concentration in the parent source static. The incompatible element Rb increases in concentration as would be expected with increasing fractionation.

4.2.3 Spidergrams

Two spidergrams of 5 selected analyses of the Rotoroa Complex are presented in **Figure 4.8 (a & b)**. The plot was normalised to PRIM and created as recommended by McDonough *et al* (1992).(Normative values used are given in **Appendix # 3**). **Figure**

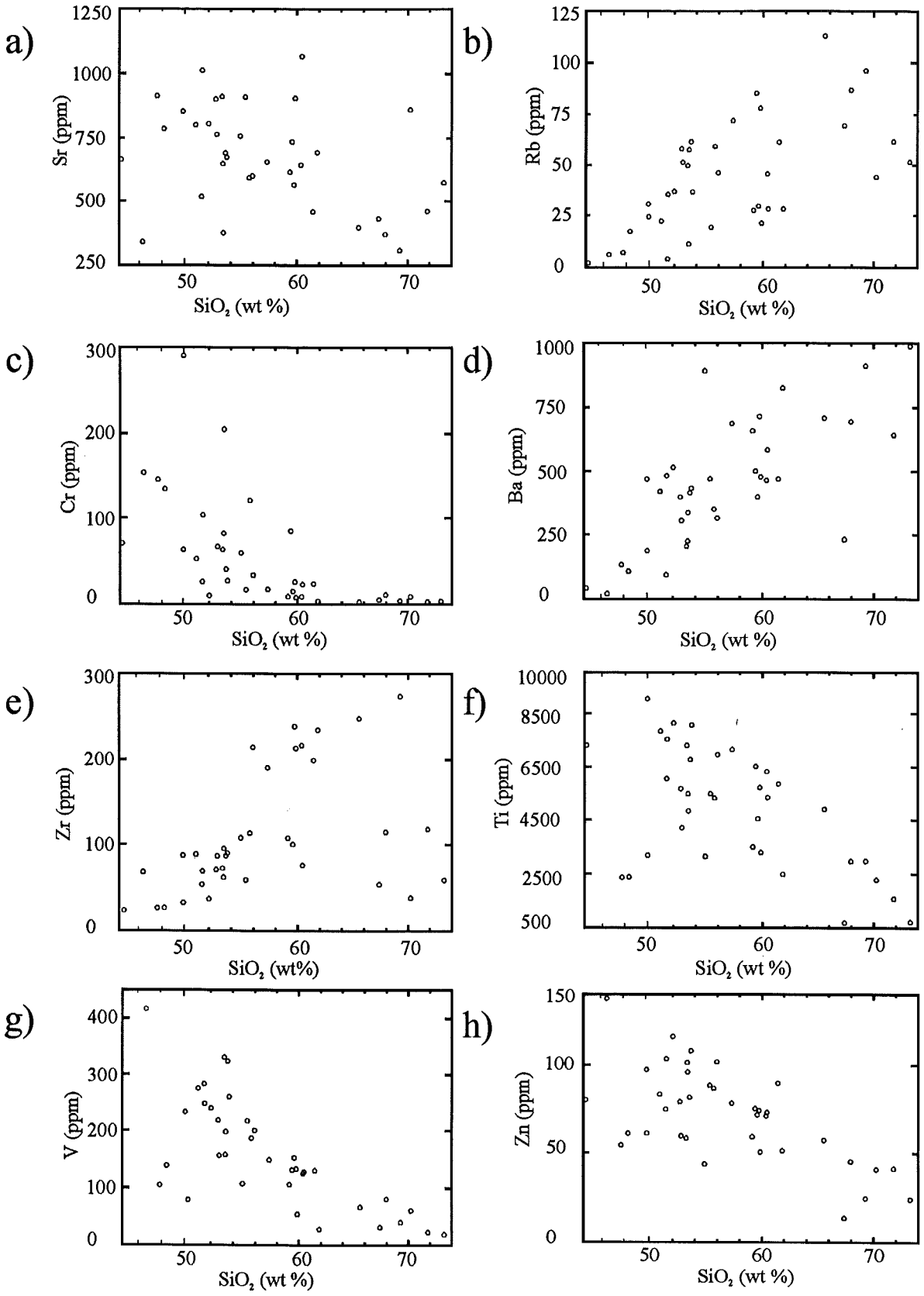

Figure 4.7 Trace elements of the Rotoroa Complex plotted against SiO_2. The Rotoroa Complex is represented by unfilled circles.

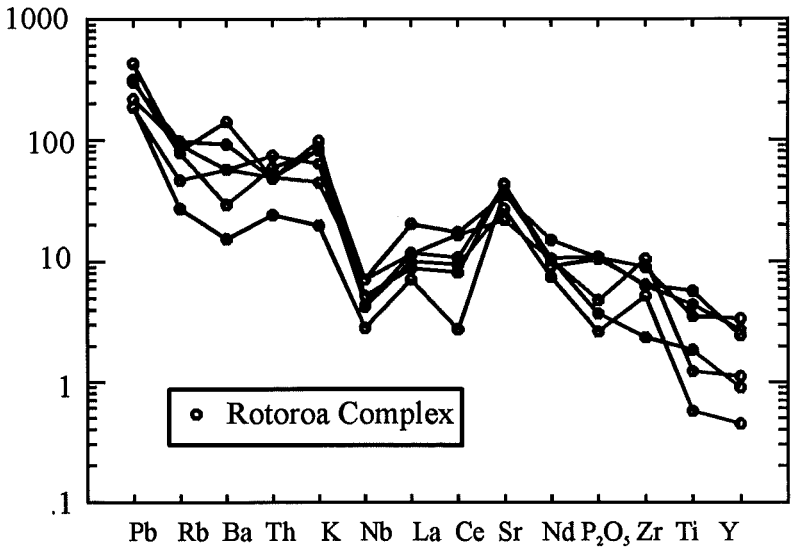

Figure 4.8a PRIM normalised spider diagram showing the primary trend of LILE enrichment and HFS element depletion in the Rotoroa Complex.

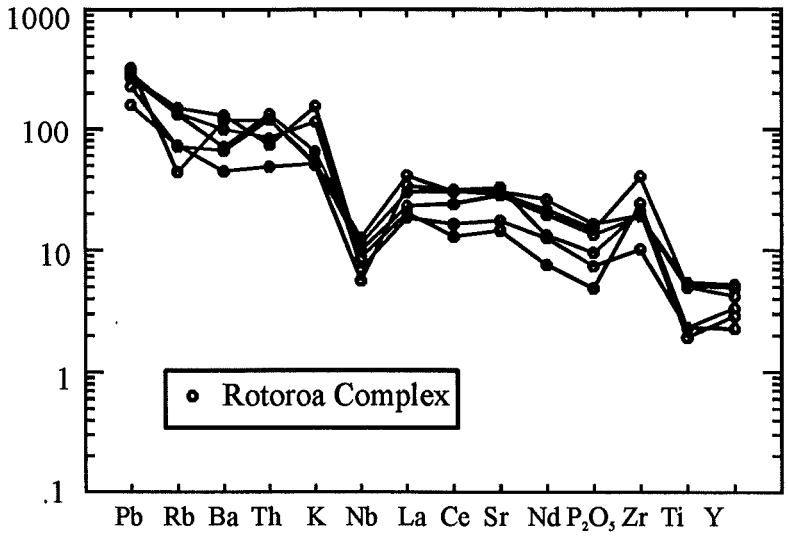

Figure 4.8a PRIM normalised spidergram showing secondary trend in the Rotoroa Complex, believed to be an evolved equivalent of the primary trend above in **Figure 4.8a**.

4.8 (a & b) illustrates the two distinct REE trends which occur within the Rotoroa Complex. The dominant trend **(Figure 4.8a),** is characterised by a Sr peak and relatively low zirconium. The second, but less common trend is typified by a flat Sr pattern and a positive Zr spike **(Figure 4.8b)**. There appears to be no geographic control on the location of these groups. A common feature of the second group is that they are mostly elevated in SiO_2 relative to the range of values within the Rotoroa Complex. The dominant group with a Sr peak is attributed to a source with no plagioclase in the residue e.g, melting of plagioclase free hornblende +/- garnet peridotite in the mantle wedge. This must occur at a depth where plagioclase is becoming unstable i.e the amphibolite - eclogite or plag-peridotite - garnet-peridotite transition at 80 - 100 km. The second group without a Sr peak must have a source with Sr removed by crystallisation of plagioclase. This suggests that they might be a more evolved group than the primary group. They are elevated in Zr and Th which build up as incompatibles, and are characteristically high in silica relative to the 38 samples overall. Both groups have a steep pattern defined by the enrichment of LILE's, typical of subduction-related suites of rocks. The result is a spidergram with a spiked pattern with peaks at Rb, Th, K, Sr and a marked trough at Nb. This is attributed to metasomatism of the mantle source by fluids released from the subducted slab. (Wilson 1989). The relative depletion in the high ionic potential elements has been variably attributed to higher degrees of partial melting and to stability of residual mantle phases. A notable feature is that the Rotoroa Complex appears to be a low Y suite. This suggests the suite is derived from a garnet bearing protolith from a considerable depth. Once again this implies a very thick continental crust or an ultimate origin in the mantle wedge at depths > 80 - 100 km.

4.2.4 Tectonic Environment

The analyses of the Rotoroa Complex are plotted in a series of tectonic discrimination plots designed to determine the environment of emplacement. In the Rb versus Y+Nb plot for granitoid rocks of Pearce *et al* (1984), presented in **Figure 4.9**, the diorites and quartz diorites of the Rotoroa Complex plot within the VAG (Volcanic Arc Granite) field. The Rotoroa analyses are also plotted on a triangular diagram by Pearce *et al* (1977). This determines tectonic environment for rocks with 51 - 56 wt % SiO_2. The analyses all fall in the orogenic field **(Figure 4.10)**. Both of these diagrams are consistent with the subduction related environment indicated by the REE spiderplot.

Pearce and Cann (1973) have devised two triangular diagrams using Ti, Zr and Y or Sr to determine tectonic setting of basic volcanic rocks **(Figures 4.11 & 4.12)**. It should be noted that these diagrams were intended for use with unaltered fine grained basaltic

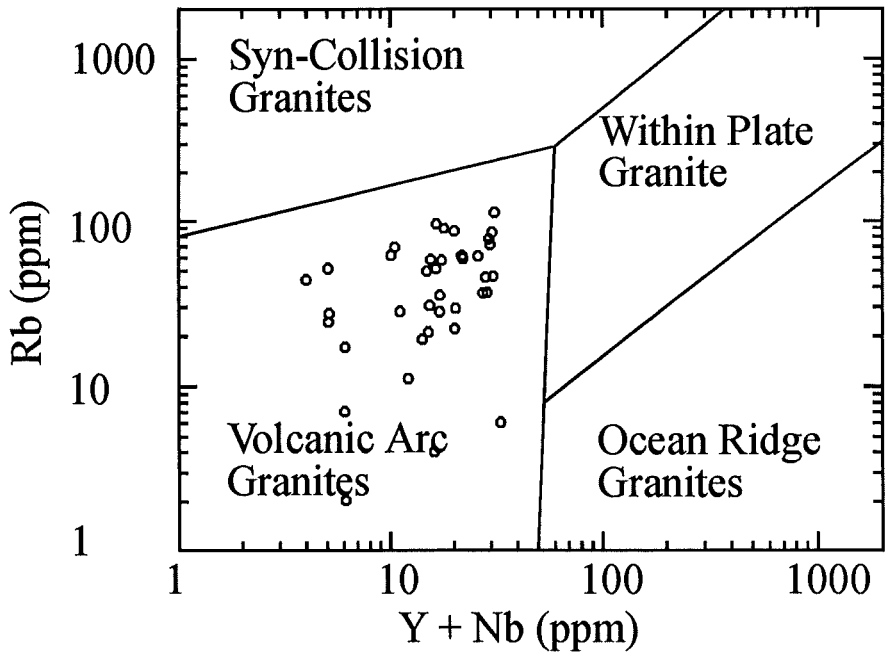

Figure 4.9 The Rotoroa Complex analyses all fall within the Volcanic Arc Granite field of Pearce *et al* (1984).

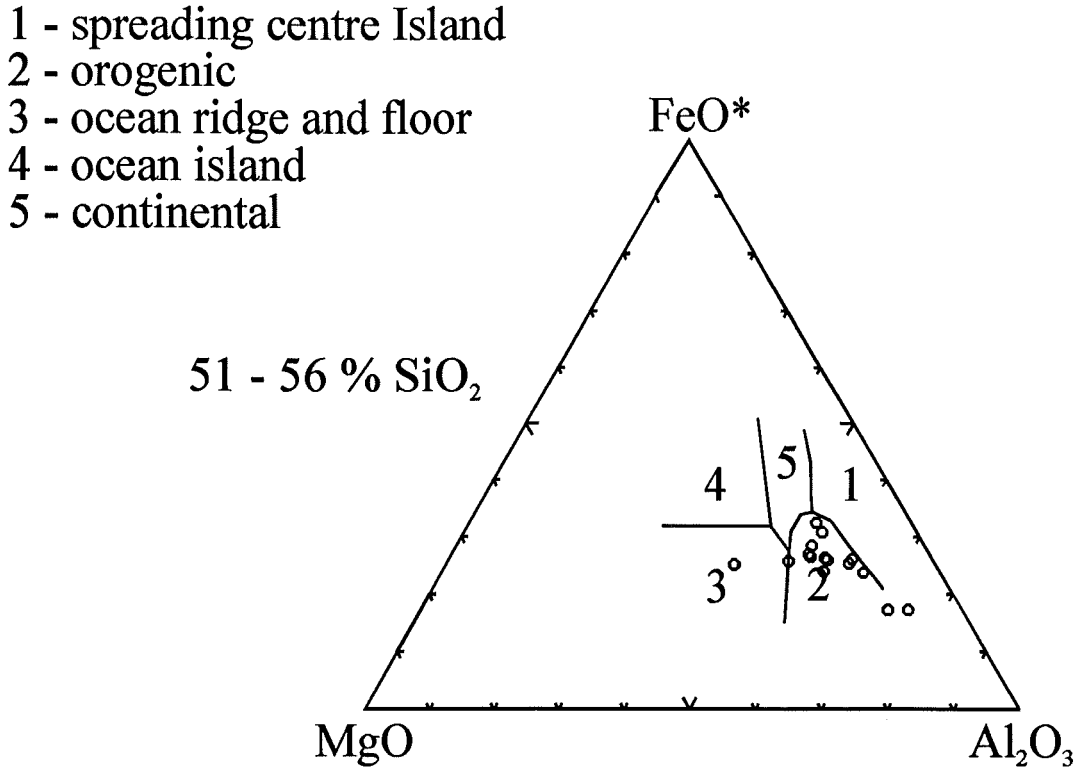

Figure 4.10 Rocks from the Rotoroa Complex with between 51 - 56 % SiO_2 plot within the Orogenic field of Pearce *et al* (1977).

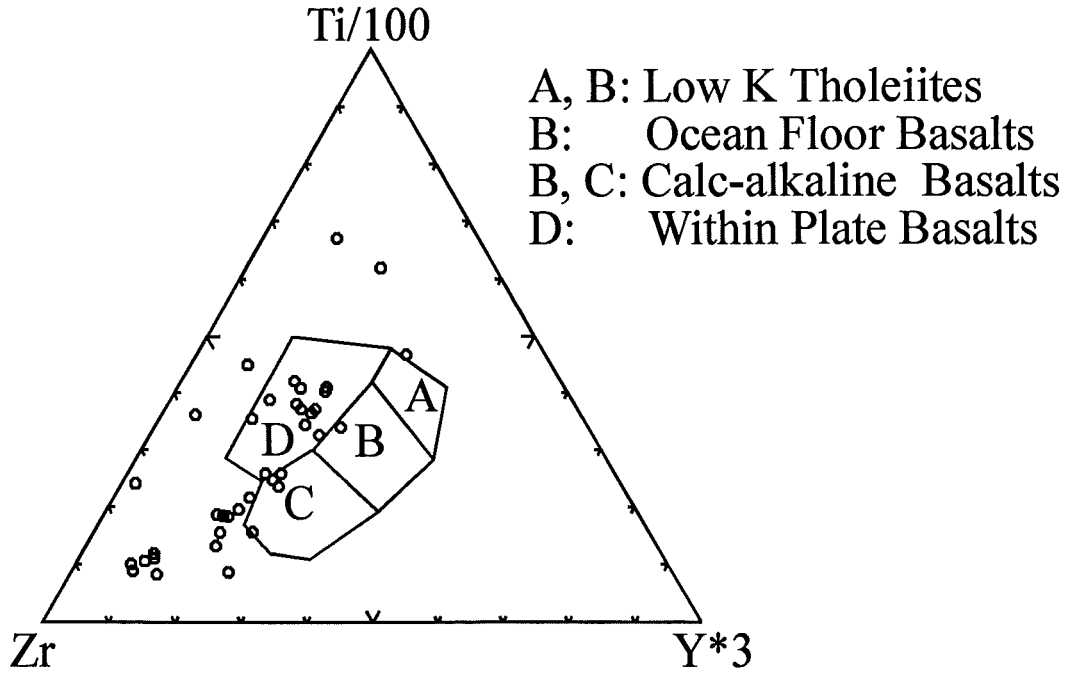

Figure 4.11 Tectonic discrimination diagram of Pearce and Cann (1973). The Rotoroa Complex rocks plot off the A-B-C calc-alkaline trend due to anomalously low Y.

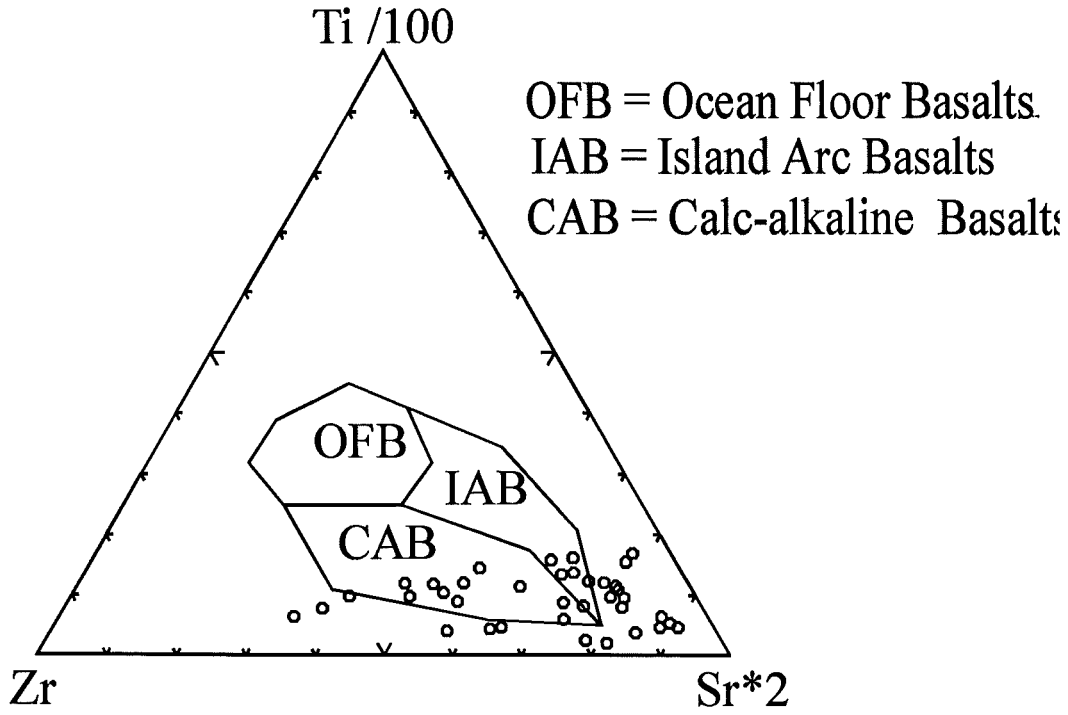

Figure 4.12 A second tectonic discrimination diagram by Pearce and Cann (1973), illustrating that the Rotoroa Complex is from a calc-alkaline basalt forming environment.

rocks. **Figure 4.12** is anomalous in showing that the Rotoroa Complex has the characteristics of Within Plate Basalts (WPB), all other plots show that they are calc-alkaline basalts. This is caused by the low Y content of the Rotoroa Complex which suggests a high pressure garnet bearing source. The Rotoroa Complex represents a calc-alkaline fractionated igneous suite emplaced into an island arc subduction environment. The tectonic discrimination plots are all consistent with the description of Kimbrough *et al* (1993), that the Rotoroa Complex was "*part of a series of dismembered Mesozoic volcanic-plutonic arc associations*" which make up the Median Tectonic Zone.

4.3 Separation Point Granite

One sample from within the field area fits the geochemical characteristics of a Separation Point Suite rock. Sample AC7A is a monzogranite and the only outcrop of Separation Point Granite noted during fieldwork.

4.3.1 Classification

The Separation Point Granite sample is high in SiO_2 containing ~ 73 wt %, and has $Na_2O > K_2O$. It is characterised by comparatively high Sr and Rb relative to the Rotoroa Complex, however the highly fractionated end members of the Separation Point suite are depleted in Sr (Muir *et al* in press). This occurs to a lesser extent in the more silicic Rotoroa Complex rocks. **(Figures 4.16a & 4.7a)**. The granite sample has a Alumina Saturation Index (A.S.I.) value of 1.05, which indicates a weakly peraluminous composition characteristic of an evolved I-type granite. (Tulloch, 1988). Normative corundum is 0.76, which also supports a peraluminous character for the Separation Point Granite. Their dominantly peraluminous nature is shown in the diagram of Maniar and Piccoli (1989),**(Figure. 4.13)**. The Separation Point Suite is described in more detail in Muir *et al* (in press).

4.3.2 Fractionation

The major oxides and trace elements of the Separation Point Granite sample, five pegmatite dikes and two aplite dikes are presented in **Figure 4.15 a - h** and **Figure 4.16 a - d**. Aronson (1968) dated a quartz diorite pegmatite at 115 Ma using the Rb-Sr method. This is consistent with the age of the Separation Point emplacement recorded by Kimbrough *et al* (1993) and Muir *et al* (1994). In one instance an aplite dike cuts a mafic dike **(Figure 2.11).** The aplite dikes which are minor bodies associated with granitic magnetism must postdate the Rotoroa Complex and the mafic dikes. It is unlikely that the aplites are not related to the Separation Point Suite, and they are assumed as such in

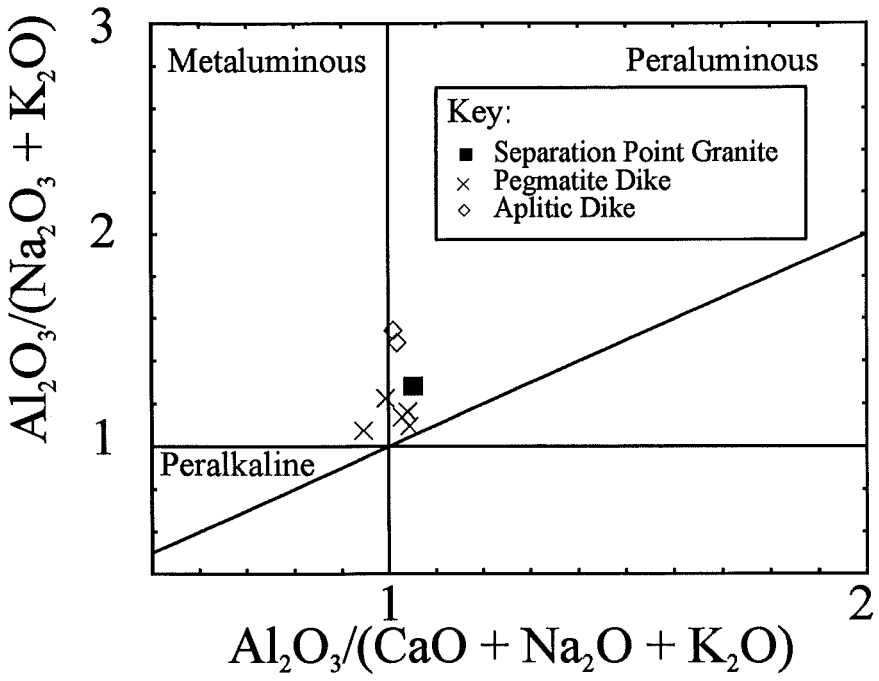

Figure 4.13 The diagram of Maniar and Piccoli (1989), which shows that the granite sample and most of the felsic dikes are weakly peralumminous. Two of the pegmatites are weakly metalumious.

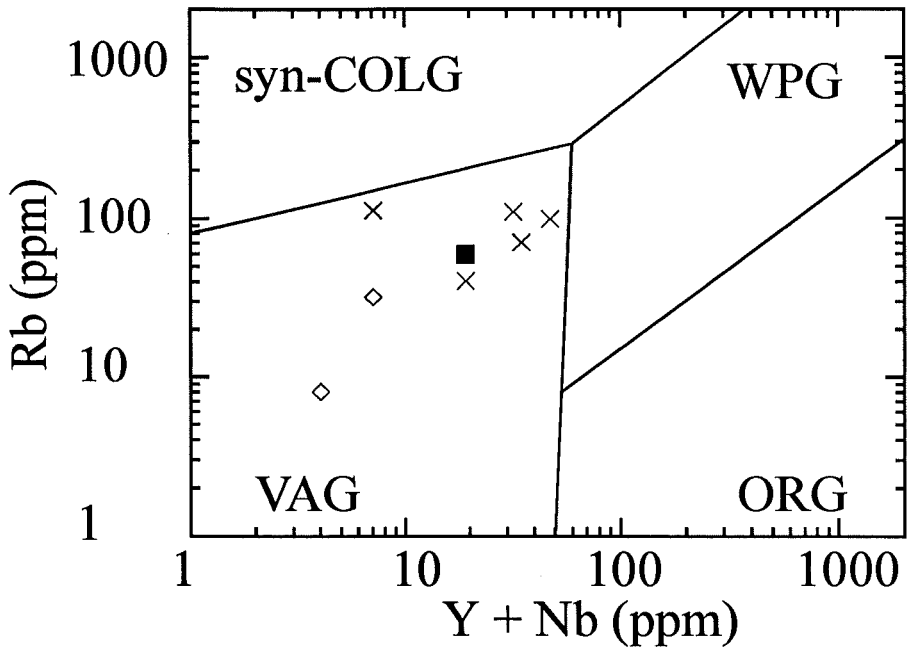

Figure 4.14 Tectonic discrimination Diagram of Pearce et al (1984). The sample of granite and felsic dikes all fall in the field V.A.G (Volcanic Arc Granite).

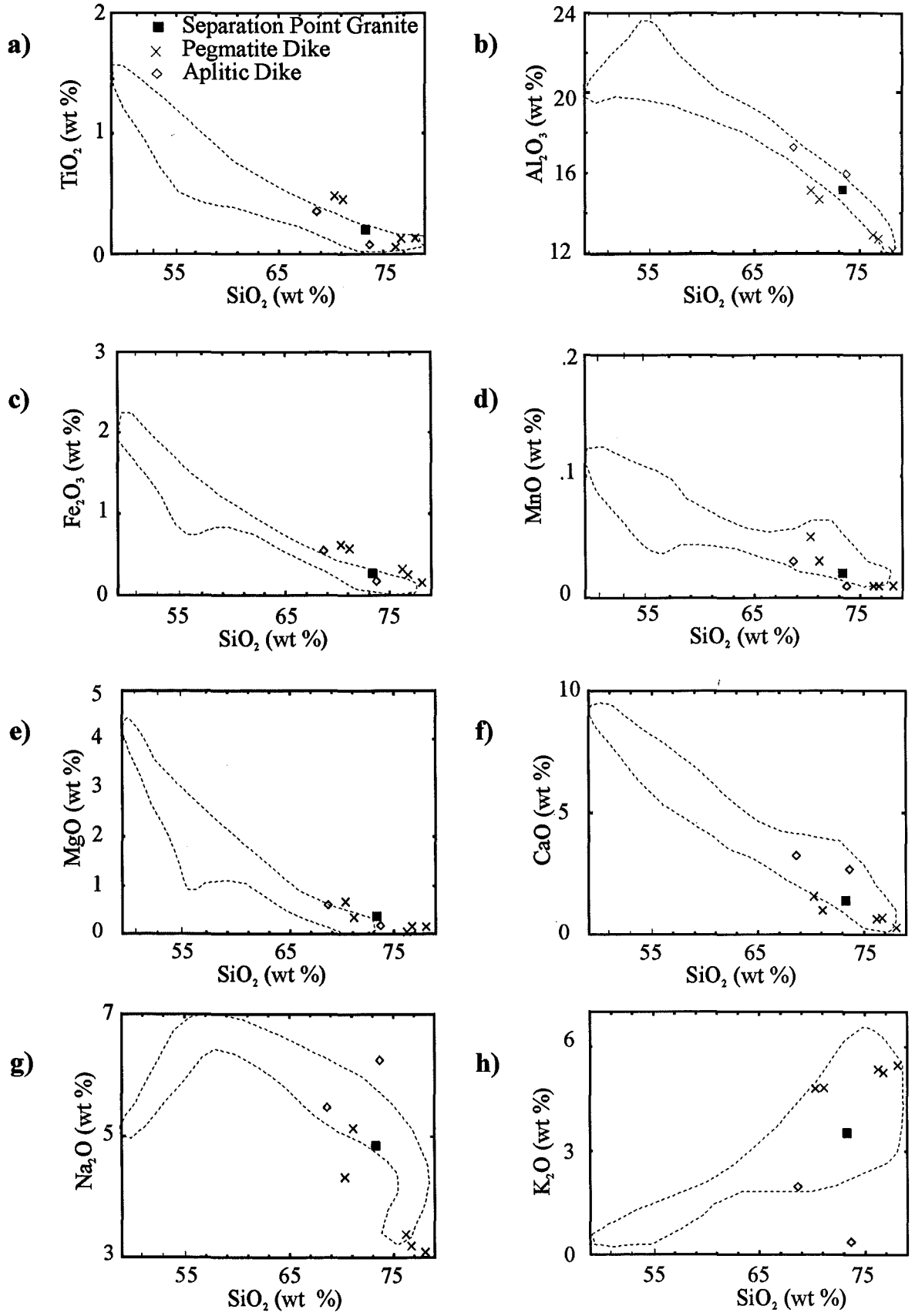

Figure 4.15 Major element oxides of the one sample of Separation Point, five pegmatite dikes and two aplite dikes. The dashed field represents the Separation point Batholith dataset of Muir (*et al* in prep.)

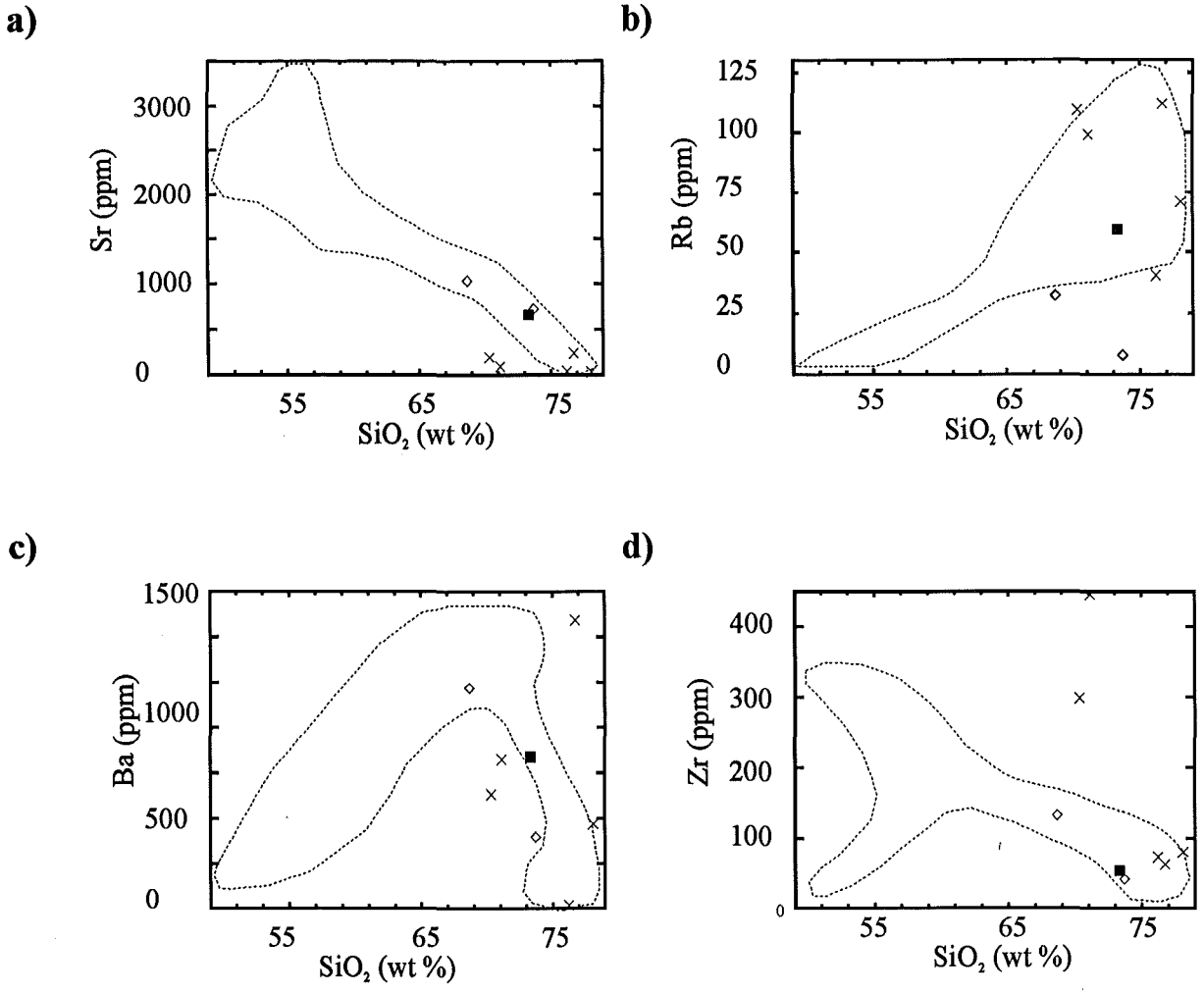

Figure 4.16 Selected trace element of one sample of Separation Point Granite, five pegmatite dikes and two aplite dikes. The dashed field represents the Separation Point Batholith dataset of Muir *et al* (in prep.).

Key:
- ■ Separation Point Granite
- × Pegmatite Dike
- ◇ Aplitic Dike

the following classification. This suggests that the mafic - intermediate dikes might predate the ~118 Ma Separation Point Batholith. (Muir *et al* 1994).

a) Major elements

The major oxide CaO decreases in the Separation Point dataset (Muir *et al* in press), throughout fractionation with the crystallisation of plagioclase. This is also seen in the Separation Point Batholith sample and felsic dikes which lie on Separation Point Batholith trends **(Figure 4.15)**. Al_2O_3 and Sr, which is also an indicator of plagioclase crystallisation fall very rapidly in the late stages of fractionation. Because sample AC7A is relatively high in SiO_2, Sr is very low which is consistent with the dataset of Muir *et al* (in press). K has been removed by the crystallisation of K-feldspar and is very low. The similar behaviour of Ba would support this. The reduction of TiO_2 from the parent source in the very late stages of fractionation was achieved by the crystallisation of biotite, the only mafic phase in the Separation Point Granite sample. The low Fe_2O_3 and MgO is consistent with the mineralogy of the samples **(see Appendix # 2)**. The ferro-magnesian mafic phases have removed these elements during earlier fractionation.

b) Trace elements

Harker plots of selected trace elements are presented in **Figure 4.16 (a-d)**. In the granite and felsic dikes Rb appears to have been mobile and plots are badly scattered. Zr and Th behave as incompatible elements and the pegmatites are all elevated in both these elements and depleted in Cr and Ni. The granite and felsic dike are all extremely poor in Ti due to removal by crystallisation of biotite and titanite.

4.3.3 Spidergrams

The spidergram of sample AC7A and the felsic dikes is presented in **Figure 4.17**. The granite sample shows many features of the subduction related pattern described in the Rotoroa Complex, although these are not as marked. Besides an enrichment in the LILE's, there is a noticeable Sr peak, accompanying a Nb and Ti trough. In the pegmatites there is a Sr trough indicative of feldspar crystallisation during very late stage fractionation.

4.3.4 Tectonic Environment

The sample of Separation Point Suite and felsic dikes are plotted on the Rb versus Y + Nb plot of Pearce *et al* (1984), in **Figure 4.14**. They plot within the VAG (Volcanic Arc Granite) field.

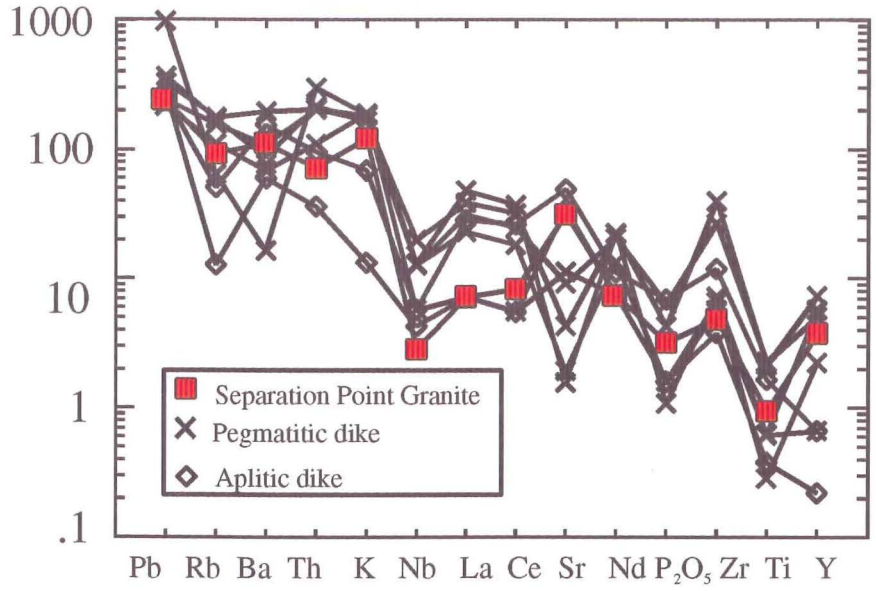

Figure 4.17 PRIM normalised spidergram showing trace element trends in the Separation Point Granite sample and felsic dikes from Lake Rotoroa.

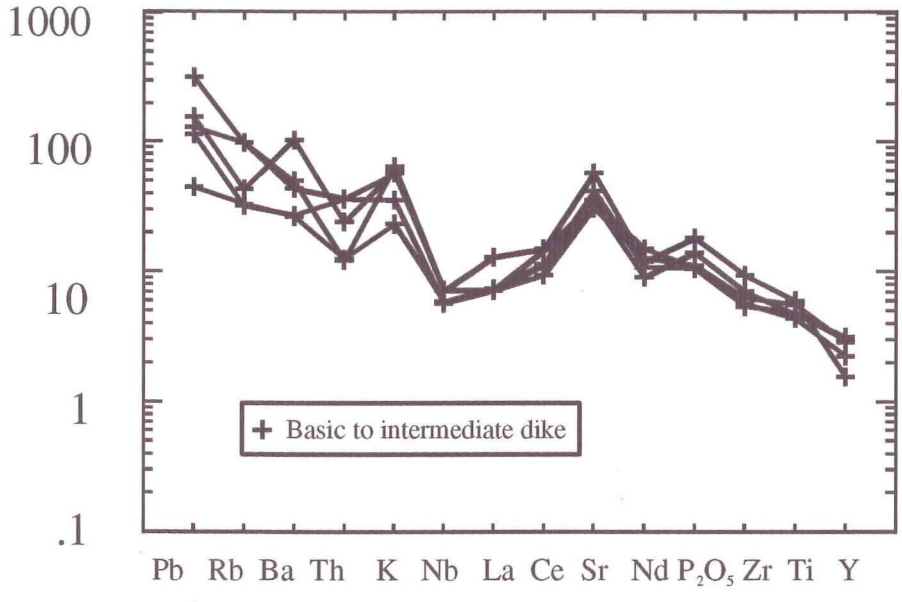

Figure 4.18 PRIM normalised spidergram of trace element abundances from mafic to intermediate lamprophyre dikes from Lake Rotoroa.

The geological setting of the Separation Point Pluton indicates a within-continent emplacement related to subduction processes. This is consistent with the calc-alkaline weakly peraluminous I-type classification and REE pattern. This is also in agreement with the inferred subduction environment of emplacement (Tulloch 1988).

4.4 Lamprophyre Dikes

Five samples of intermediate to mafic alkali lamprophyre camptonite dikes were sampled and geochemically analysed. They are classified according to Le Maitre *et al* (1989) in **Figure 4.19**. Three of the dikes which are presented as crosses plot within the basalt field. The remaining two plot within the basaltic-trachy-andesite field. Because they are sodic and have Na_2O - 2.0 > K_20 they are classed as mugearites. Geochemically the dikes are elevated in K_2O, P_2O_5 and Ba compared with similar rocks of the Rotoroa Complex. They are also notable for their low La and Ce content relative to the rocks of the Rotoroa Complex. A spidergram of the dikes is presented in **Figure 4.18**.

4.4.1 Classification

The Dikes are essentially basaltic in composition, with evidence of an alkalic trend. They have the characteristics of the alkali lamprophyre camptonite (Rock 1991).

4.4.2 Tectonic Environment

In the tectonic discrimination plot of Pearce and Cann (1973), four of the dikes plot in the WPB (Within Plate Basalt) field **(Figure 4.20)**. The fifth sample plots just outside due to it's lower Y content. This is consistent with their geological setting.

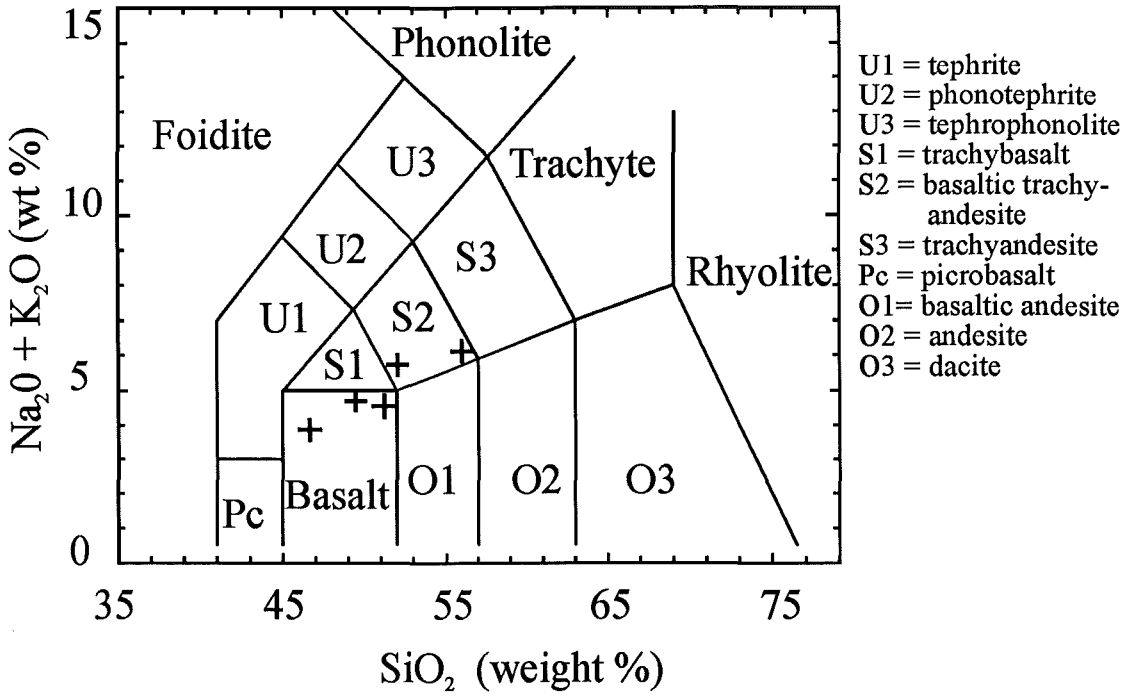

Figure 4.19 Geochemical classification of the lamprophyre dikes from Lake Rotoroa. (after Le Maitre *et al* 1989).

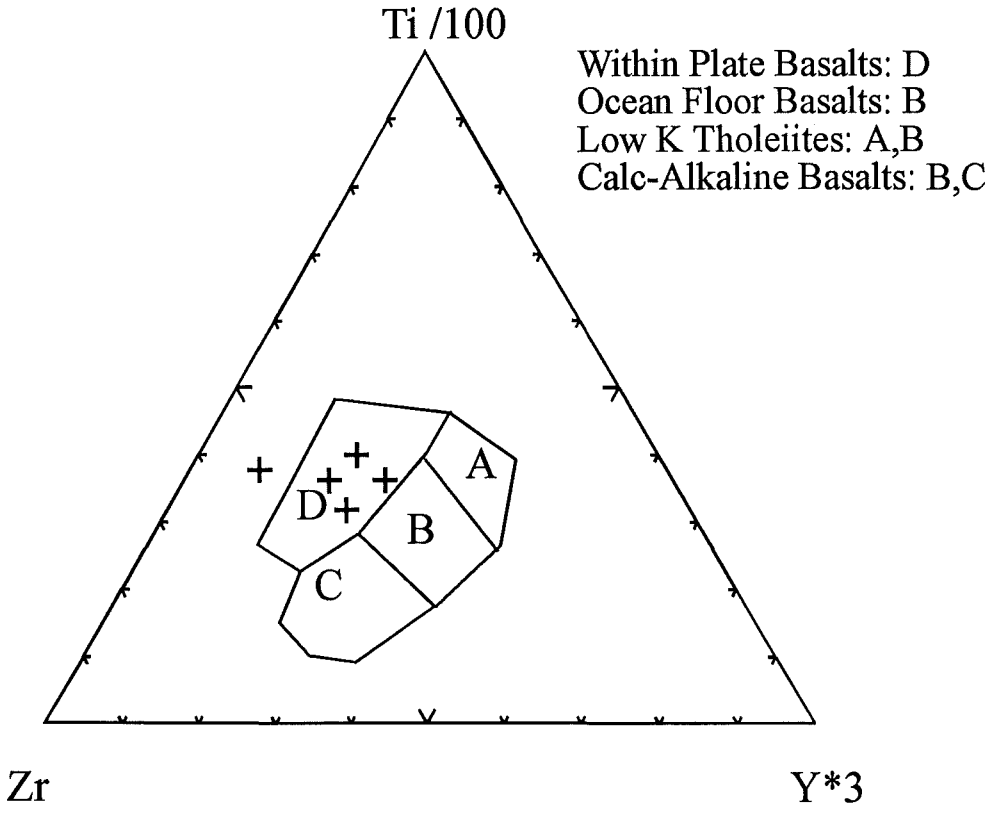

Figure 4.20 Tectonic discrimination diagram of Pearce and Cann (1973), showing that the Rotoroa lamprophyre dikes have within plate characterisrics.

CHAPTER FIVE: REGIONAL SYNTHESIS

5.1 Introduction

The Rotoroa Complex in NW Nelson has been correlated with the Darran Complex in Fiordland by a number of workers. Blattner (1980), suggested the Rotoroa Complex as an alternative when comparing the Riwaka Complex to the Darran Complex based on chlorine and fluorine ~~isotopes~~ analyses, Kimbrough *et al* (1993) suggest similarities based on age, composition and structural position, and Wellman (1973), based his comparison on similar magnetic anomalies. Suggate *et al* (1978), and Bradshaw (1993), have also suggested that they are related.

5.2 Rock types

Various rock types described within the Darran Complex are similar to those described in the Rotoroa Complex (Challis *et al in prep.*). They are all generally dioritic in composition. Williams and Harper (1978) included the Darran Complex as part of the McKay Intrusives. In view of problems regarding the age of the McKay Intrusives, which now appear to be older than the Darran Complex (Dr. R. J. Muir pers. comm.), this comparison is restricted to the Darran Complex. Williams and Harper (1978) describe a range of plutonic suites from gabbros to diorites to leucogranites. Pirajno (1981) describes the Darran Complex as consisting of a range of rocks of broadly dioritic aspect. The western belt is essentially leucogabbro and hornblende diorite, while the eastern belt is described by Blattner (1978) as consisting of leuco-quartz-diorites. Blattner (1991), and McCulloch *et al* (1987), describe in detail the biotite bearing leuco-gabbros of the Darran Complex and its altered equivalent, a hornblende diorite.

5.3 Age

Up to now the age of the Darran Complex has not been well constrained. The ages assigned to the complex range from 208 - 69 Ma (Pirajno 1981). Adams (1975), dated pegmatites in the leucogabbro exposed at the Homer Tunnel at 149 - 140 Ma and Williams and Harper (1978), have K/Ar dated leucocratic gabbroic to dioritic rocks in the upper Hollyford area at between 136 - 130 Ma. Bradshaw (1993) gives a 135 Ma age to the Darran Complex, similar to recent U/Pb SHRIMP dating of gabbroic and dioritic rocks from the Darran Complex, which has yielded ages between 140 - 160 Ma. (Dr S.D. Weaver pers. comm.). These ages are consistent with the 156 U/Pb crystallisation age and $^{40}Ar/^{39}Ar$ 140 - 130 Ma emplacement, cooling or metamorphic resetting ages assigned to the Rotoroa Complex by Kimbrough *et al* (1993).

5.4 Magnetic similarities

The magnetic and gravitational anomalies to the north of the Rotoroa Complex (Wellman 1973), and Tulloch (1992), are suggested as its northward extension by Kimbrough *et al* (1993). These are particularly strong over the gabbro (Kidd 1972), which is relatively rich in magnetite **(Table # 3.1)**. There is also a pronounced magnetic anomaly over the Darran Mountains which is thought to be related to locally abundant magnetite (Pirajno 1981).

5.5 Geochemistry

To my knowledge no one has compared the whole-rock geochemistry of the Rotoroa Complex and Darran Complex, although geochemical analyses of the Darran Complex are described in Williams and Harper (1978), Williams and Smith (1983), McCulloch, Bradshaw and Taylor (1987) and Blattner (1991). Williams and Smith (1978) included the Darran Complex as part the McKay Intrusives. Only their analyses from the Darran Complex were used. All of the analyses presented by the authors on the Darren Complex have major elements oxides. Unfortunately the number of trace elements analyses provided is variable, as a result the number of data points from plot to plot varies. Selected major oxides and useful trace elements are plotted against SiO_2 and are presented in **Figures 5.1 and 5.2**.

5.5.1 Major and Trace element Comparisons

Clearly the Darran Complex major elements all share similar trends, and plot very well within the field defined by the Rotoroa Complex analyses **(Figures 5.1 and 5.2)**. Bradshaw (1986) states that "*although analyses of gabbros, diorites, and granites from various unrelated calc-alkalic provinces will plot on a similar trend, the existence of such a trend in no way implies that these rocks are products of the same magma.*" The trends apparent in the four trace elements common to all authors are essentially consistent with those of the Rotoroa Complex.

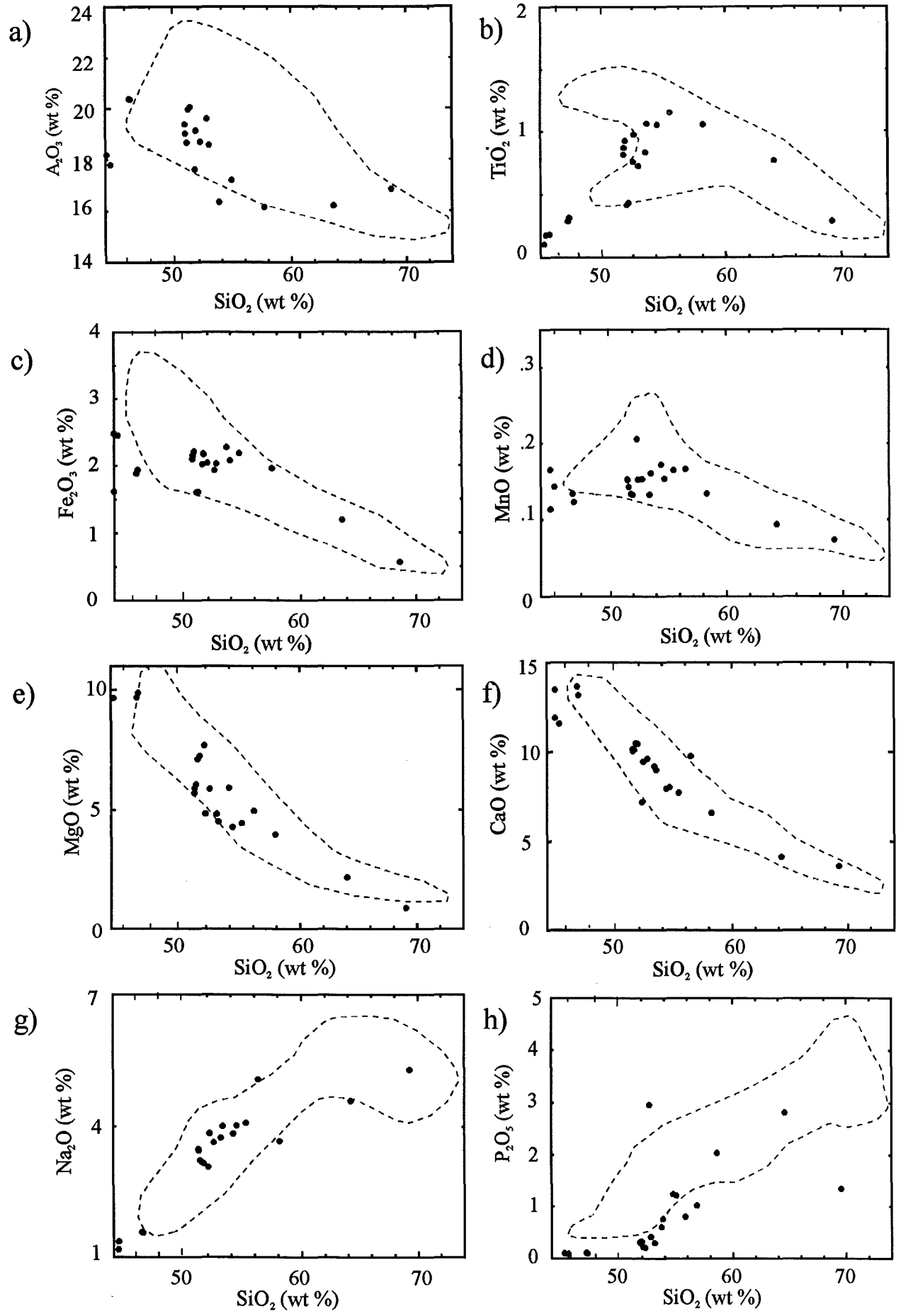

Figure 5.1 Major element oxide trends of Darran Complex rocks plotted as filled circles compared to those of the Rotoroa Complex, represented by the dashed field.

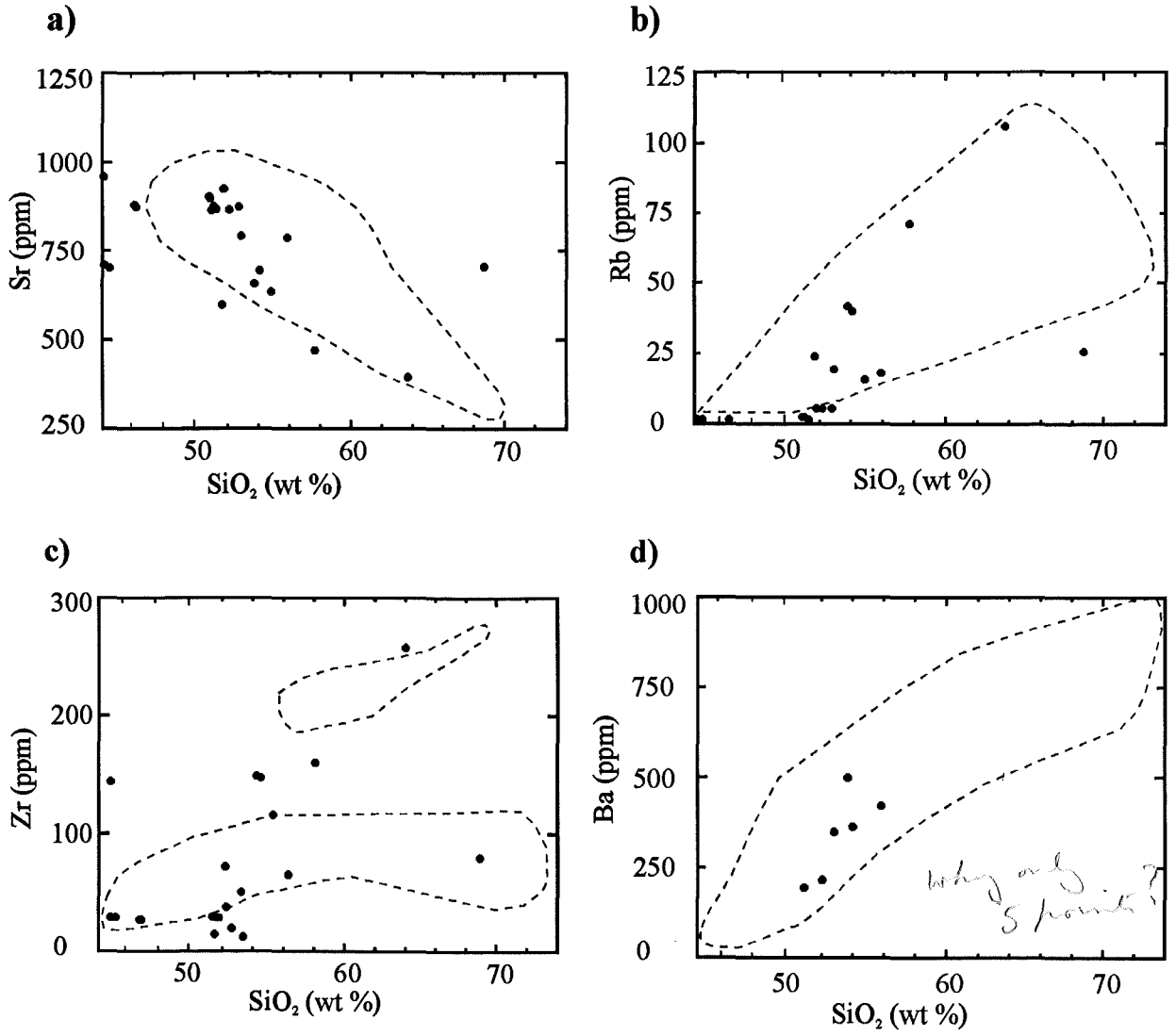

Figure 5.2 Selected trace elements of Darran Complex rocks plotted as filled circles compared to those of the Rotoroa Complex, represented by the dashed field.

5.5.2 Classification

The Darran Complex is metaluminous in nature like the Rotoroa Complex. In the mesonormative Q-A-P diagram of Le Maitre *et al* (1989),**(Figure 5.3)**, it follows the same trend as the Rotoroa Complex and ranges from gabbro to diorite. Geochemically the Darran Complex ranges from sub-basaltic to dacite-rhyolitic rocks, which vary from low K in some cases through to high K in the more SiO_2 rich samples **(Figure 5.4)**. They are subalkaline with a calc-alkaline trend **(Figures 5.5 and 5.6 respectively)**. In terms of their geochemical compositions and fractionation trends, the Darran Complex is clearly very similar to the Rotoroa Complex.

5.5.3 Tectonic Discrimination

In the Rb versus Y + Nb granitoid discrimination diagram of Pearce *et al* (1984), the various samples plot within the VAG (Volcanic Arc Granite) field **(Figure 5.7)**. A second diagram devised by Pearce *et al* (1977), determines the tectonic environment for rocks with between 51 - 56 % SiO_2. The samples plotted all fall in the orogenic field as does the Rotoroa Complex **(Figure 5.8)**.

In the two diagrams of Pearce and Cann (1973), which use Ti, Zr, and Y or Sr for unaltered basic volcanic rocks, the Darran Complex samples plot slightly differently from the Rotoroa Complex. In both **Figure 5.9** and **Figure 5.10** the Fiordland samples plot along a calc-alkaline trend. In **Figure 4.12** the Rotoroa Complex plot into the Within Plate Basalts field. This was attributed to an anomalously low Y. With this exception the trend of the two complexes would be similar. The trend of the Fiordland rocks in the Ti-Zr-Sr plot **(Figure 5.10),** is consistent with that of the Rotoroa Complex.

By using the tectonic discrimination diagrams listed above for comparison, it seems that overall, the samples of the Rotoroa Complex, and the samples obtained by various authors from the Darran Complex, indicate a similar tectonic environment.

5.6 Comparison

Based on geochemical comparison, classification and tectonic discrimination, it could be argued that the Rotoroa Complex is the northward extension of the Darran Complex of Fiordland, offset along the Alpine Fault **(Figure 1.1a)**. Further detailed geochemical comparison involving isotopes, REE's and a wide variety of trace elements is desirable to confirm this.

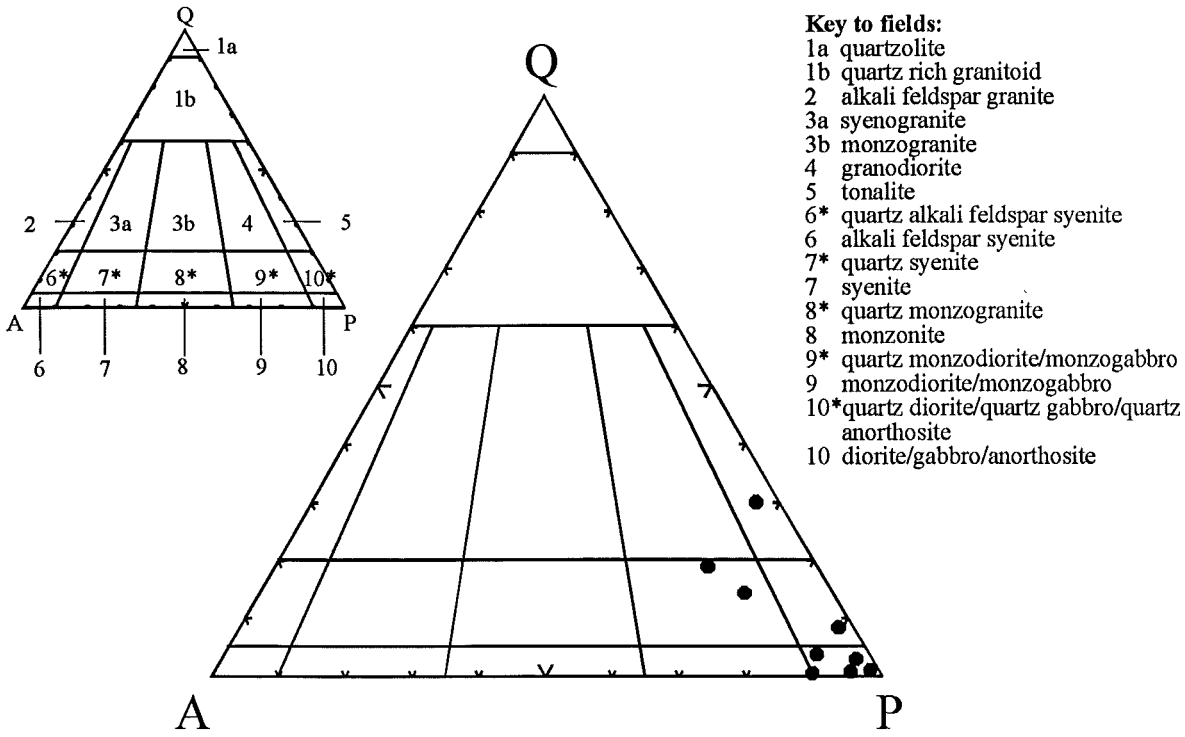

Figure 5.3 Mesonormative Q-A-P classification of the Darran Complex (after Le Maitre *et al* 1989).

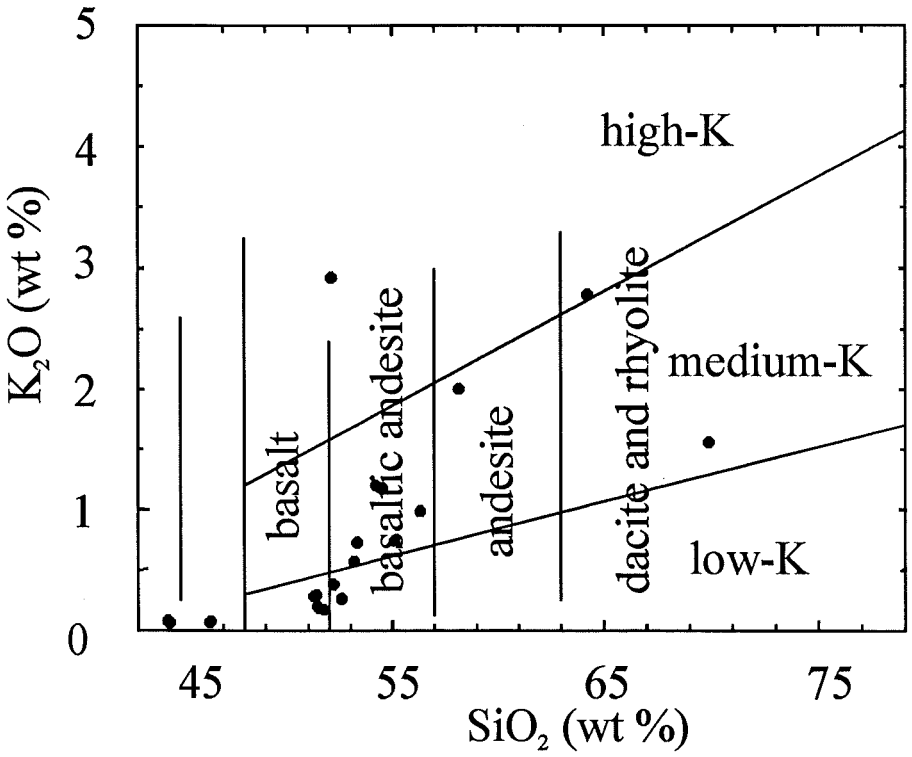

Figure 5.4 Geochemical classification of the Darran Complex (after Le Maitre *et al* 1989).

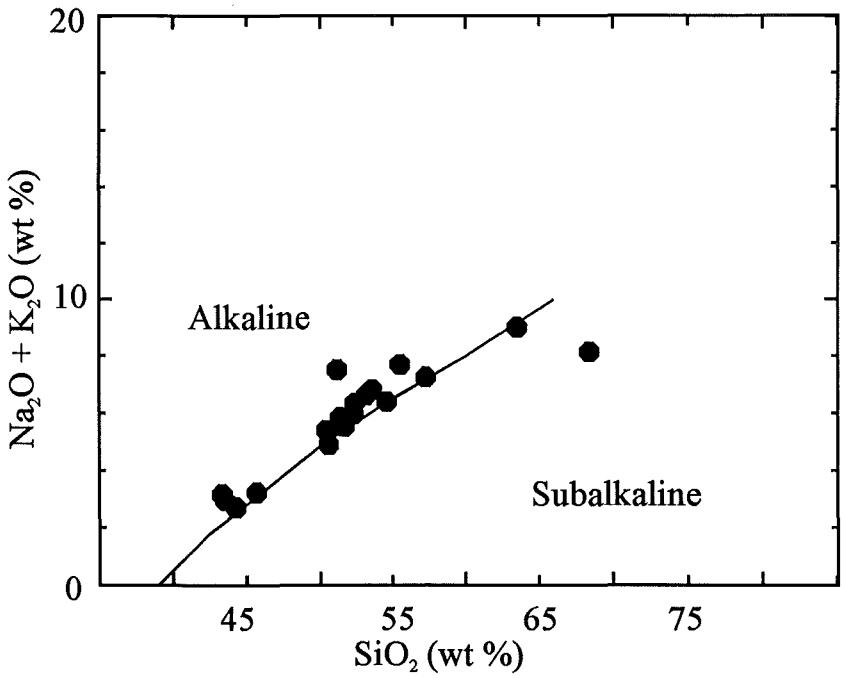

Figure 5.5 The plot of Irvine and Barager (1971) showing the subalkaline character of the Darran Complex .

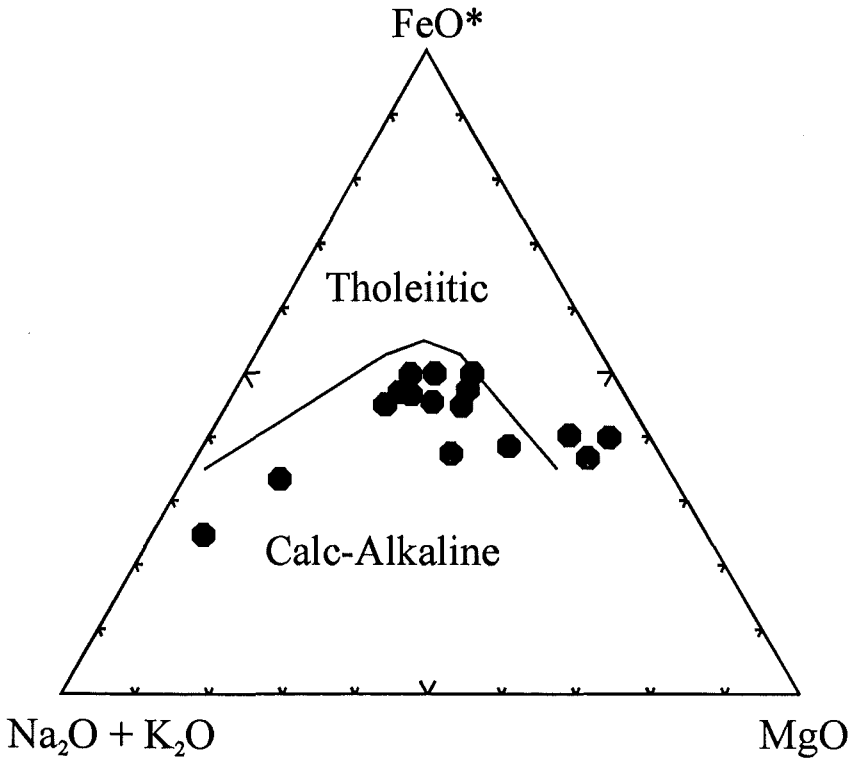

Figure 5.6 A-F-M diagram illustrating the calc-alkaline trend of the Darran Complex (after Irvine and Barager 1971).

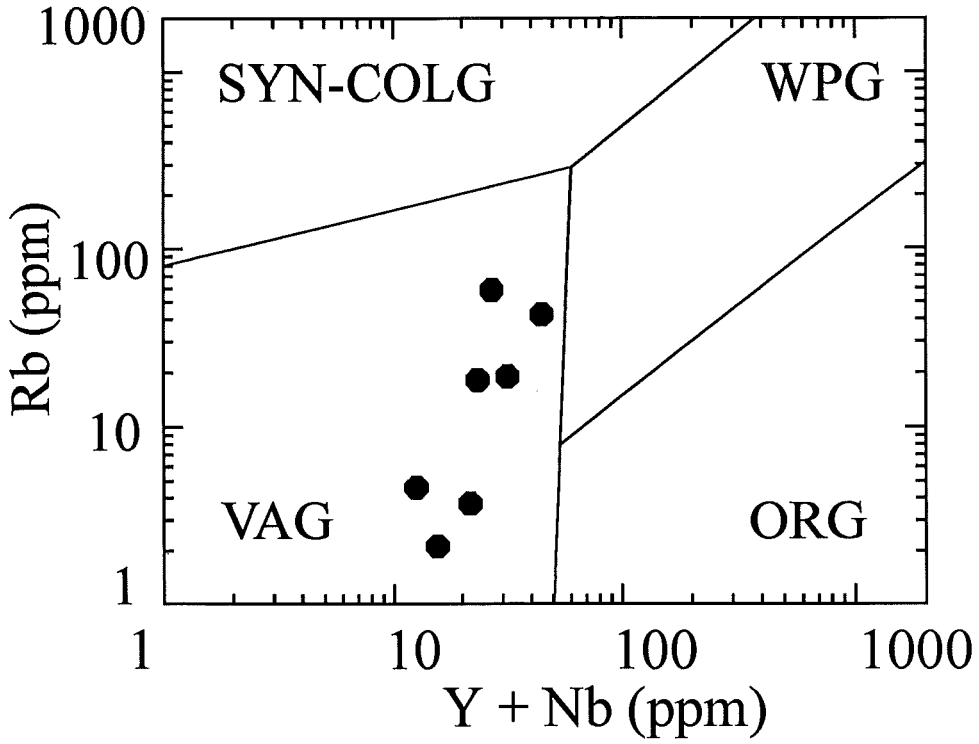

Figure 5.7 The tectonic discrimination diagram of Pearce *et al* (1984) which shows that the Darran Complex has a Volcanic Arc Granite affinity.

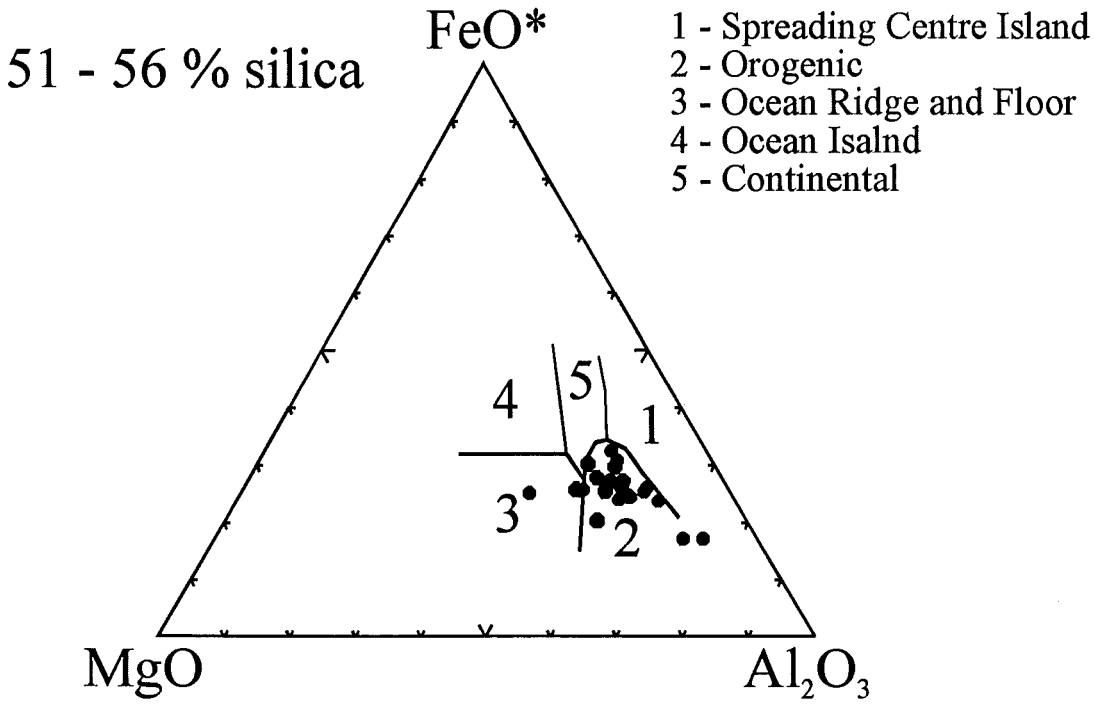

Figure 5.8 Tectonic discrimination plot of Pearce *et al* (1977), in which the samples of the Darran Complex plot in the orogenic field, as do the Rotoroa Complex.**(Figure 4.10)**

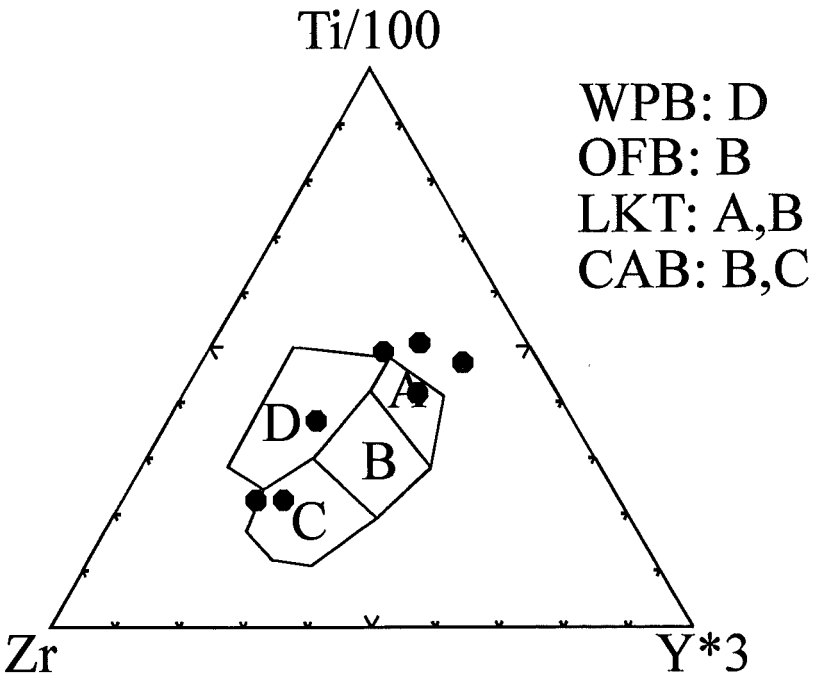

Figure 5.9 A tectonic discrimination diagram by Pearce and Cann (1973). This shows that the Darran Complex plots in the fields typical of calc-alkaline basalts.

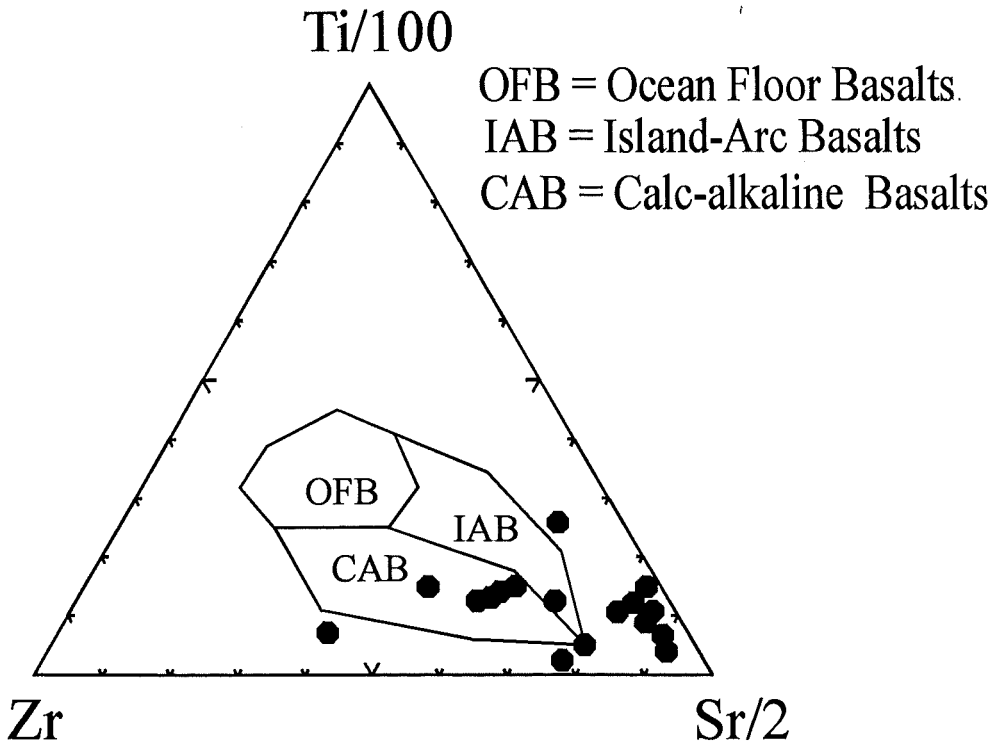

Figure 5.10 A second tectonic discrimination plot by Pearce and Cann (1973), suggesting that the Darran Complex rocks represent an island-arc /calc-alkaline basalt forming environment.

CHAPTER SIX: DISCUSSION

6.1 Introduction

The following chapter is a brief overview of the data obtained from my study of the western margin of Lake Rotoroa.

6.2 Age of the Rotoroa Complex

Rocks of the Rotoroa Complex have been dated by Aronson (1968) and Harrison and McDougall (1980). Many of these earlier ages obtained were ~ 114 Ma, and were either on pegmatites of the Separation Point Granite, or were metamorphic ages associated with its Cretaceous emplacement. Kimbrough *et al* (1993) have dated the Rotoroa Complex rocks using zircon U/Pb and 40Ar/39Ar methods. The zircon U/Pb method gave a 156 Ma age which the authors interpret as an igneous crystallisation age. The hornblende biotite 40Ar/39Ar technique gave a 140 -130 Ma age, which is interpreted to represent emplacement ages, cooling ages or a metamorphic resetting event. The Separation Point Granite has been dated at ~ 118 Ma by Muir *et al* (1994).

6.3 Petrogenesis of the Rotoroa Complex

Because an intrusive contact with the Rotoroa Complex has not been identified in rocks of the Eastern or Western provinces, the Rotoroa Complex cannot be labelled as part of either. The Takaka Terrane has been stitched to the Rotoroa Complex by the Early Cretaceous Separation Point Batholith, however the Rotoroa Complex should be identified as a separate terrane (Bradshaw 1993). The Median Tectonic Zone as defined by Kimbrough *et al* (1993), includes the Rotoroa Complex as part of a "*series of - dismembered Mesozoic volcanic-plutonic arc associations ... which lack a clear affinity to the Western or Eastern Province terranes which enclose them*". Muir *et al* (in press.), believe that the volcanic-plutonic assemblages of the MTZ represent a long-lived island arc system related to west-facing subduction, probably along the line of the Dun Mountain ophiolite - Livingstone Fault suture.

The location of the subduction zone and its polarity are the subject of much debate. Assuming subduction was west-facing, the Rotoroa Complex would have been separated from the trench by the components of the Eastern Province. The full width of the Eastern Province, including the vast-Torlesse accretionary prism, results in an arc-trench distance of >600 km, and a subduction angle that is unacceptably shallow. It is more reasonable therefore suppose that the subduction zone-trench complex related to the MTZ arc is actually within the Eastern Province. The Livingstone Fault is a logical location, however

the absence of a recognisable accretionary fore-arc complex linked to the MTZ arc suggests that crust has removed by strike-slip faulting. The Rotoroa Complex may represent a remnant fragment of such a system. The close proximity of the intra-oceanic Brook Street Terrane (of the MTZ), and the continental Western Province suggest considerable telescoping or tectonic excision has occurred (Bradshaw 1993).

A petrogenetic model for the Rotoroa Complex is based on melting of supra-subduction lithosphere. This is supported by the spidergram in **Figure 4.8a,** which is characterised by a Sr peak and low incompatible element content. This suggests a source where plagioclase is unstable and breaking down to garnet at depths of ~ 80 - 100 km (e.g., the plag-peridotite - garnet- peridotite transition) Wilson (1989). The low Y content of the Rotoroa Complex also supports a garnet bearing protolith source, and implies a similar depth of origin. Partial melting of the mantle wedge in response to subduction produced hydrous calk-alkaline magmas which were parental to the Rotoroa Complex and other plutonic bodies of the Median Tectonic Zone.

6.4 Relationship of the Rotoroa Complex to the Separation Point Granite.

The 1:50 000 geological map, sheet M29 BD "Lake Rotoroa" (Challis *et al in prep.),* which is to be released this year shows the Rotoroa Complex cut by a series of NE trending sheets of Separation Point Suite affinity **(Figure 1.3)**. The petrological and geochemical data obtained from analysis of samples in the thesis area, show that there appears to be only one sample with true Separation Point characteristics.

Based on geochemical and petrological evidence it would appear that lithologies with Separation Point Suite affinity are uncommon in the Rotoroa Complex. There is good evidence from both major and trace elements that the range of igneous rocks in the Rotoroa Complex follow a primary magmatic fractionation trend from the most mafic hornblendite through to the most siliceous quartz diorite. Challis *et al* (in prep.) note the possibility in **Petrogenesis and Origin of the Rotoroa Complex** that ..."*the gabbro, gabbronorites, hornblende gabbros, anorthosites and metagabbros, form the lowest exposed portion of a layered intrusion, possibly representing a level transition between the critical and main zones as defined for the Bushveld intrusion. Apart from rare lens of hornblendite, ultramafic rocks are not found in the mapped area, but might be expected to underlie the gabbros. The major and trace element composition of some diorites, quartz diorites and trondhjemites follow a calc-alkaline trondhjemitic differentiation trend, and the volume of quartz diorite and trondhjemite is not too great to rule out derivation by crystal fractionation, involving the removal of olivine, pyroxene, hornblende and plagioclase, from gabbroic magma*".

While the areas mapped as Separation Point by Challis *et al* (in prep.), are petrographically distinct as quartz-rich, biotite-bearing diorites, only one sample, AC7A appears to have consistent Separation Point mineralogy and geochemistry. This was also the only example of Separation Point Granite recognised during field work. This may in part be due to its poor resistance to weathering, and failure to form outcrop. However it seems likely that Separation Point Suite lithologies are present only as rare apophyses and minor sheets intruded into the Rotoroa Complex.

This work suggests that the area mapped as the Rotoroa Complex by Challis *et al* (in prep.) is appropriately identified as such. The quartz diorites previously identified as Separation Point Suite should be included within the Braeburn Diorite as the Braeburn Quartz Diorite or Granodiorite of the Rotoroa Complex. It should be recorded that minor intrusions of Separation Point Suite do occur within the Rotoroa Complex. These are not as spatially significant as was originally thought.

6.5 Regional Correlation.

The geological similarities between the Rotoroa Complex and the Darran Complex of Fiordland suggest that there is a good basis for correlation with a fair degree of confidence. Recent U/Pb SHRIMP dating of the Darran Complex at between 140 - 160 Ma. (Dr S. D. Weaver pers. comm.) adds support to this. Further comparison, particularly of selected REE's and isotopic data would help to test this correlation.

7. CONCLUSIONS

- The Rotoroa Complex of NW Nelson is a lithologically variable unit of plutonic rocks dominated by diorite, and is of Late Jurassic age. The complex forms part of a series of dismembered Mesozoic volcano-plutonic arc associations which make up the Median Tectonic Zone (MTZ).

- The Rotoroa Complex is a metaluminous, calc-alkaline suite which has the typical features of an island-arc/calc-alkaline subduction-related plutonic complex.

- The rock types of the Rotoroa Complex range from hornblendite through gabbros, to diorites and quartz diorites. These are probably geochemically related by a primary magmatic fractionation trend.

- There are small apophyses or sheets of Separation Point Suite affinity intruded into the Rotoroa Complex. These are much less extensive than those mapped by Challis *et al* (in prep.). Quartz diorites previously identified as Separation Point lithologies are part of the Rotoroa Complex, and may be included within the Braeburn Diorite or Braeburn Quartz Diorite. The metamorphic and metasomatic effects of the emplacement of the Separation Point Batholith are widespread throughout the complex.

- At least one generation of lamprophyre dikes at Lake Rotoroa, predates the emplacement of the Separation Point Batholith.

- Brittle deformation features on a range of scales are ubiquitous in the Rotoroa Complex and may be linked to Cenozoic movement on the Alpine Fault.

8. FUTURE WORK:

- Further mapping and sample collection elsewhere in the Rotoroa Complex in order to support and expand on the findings made from this study.

- REE and isotopic characterisation of the Rotoroa Complex.

- A well constrained geochemical comparison of the Rotoroa Complex and the Darran Complex involving major element, trace element, REE's, and isotopic data.

- Dating of aplite dikes to confirm that they are related to the emplacement of the Separation Point Batholith.

- Petrological, geochemical description and of mafic - intermediate dikes from the Darran Complex of Fiordland for comparison. Age determination of the mafic - intermediate dikes from the Rotoroa Complex and the Darran Complex of Fiordland.

9. REFERENCES:

ADAMS, C. J. D. (1975) New Zealand potassium argon age list 2. N.Z.J.G.G. **18** 443 - 467.

ARONSON, J.L. (1968) Regional Geochronologyof New Zealand. Geochimica et Cosmochima Acta. **32** 669-697.

BLATTNER, P. (1978) Geology of the crystalline basement between Milford Sound and the Hollyford Valley, New Zealand,NZJGG **21** 33 - 47

BLATTNER, P. (1980) Chlorine-Enriched Leucogabbro in Nelson and Fiordland, New Zealand. Contrib. Mineral. Petrol. **72** 291-296.

BLATTNER, P. (1991) The North Fiordland transcurrent convergence. N.Z.J.G.G. **34** 533 - 542.

BOWEN, F.E. (1964) Sheet 15 "Buller" 1st Ed. Geological Map of New Zealand 1:250 000. DSIR, Wellington, New Zealand.

BRADSHAW, J.D. (1993) A review of the Median Tectonic Zone: Terrane boundaries and Terrane amalgamation near the Median Tectonic Line. N.Z.J.G.G. **36** 117 - 125

BRADSHAW, J.Y. (1986) Letters to the editor, Comment on "Geochemistry and mineralisation of the southern part of the Darran Complex, Fiordland, New Zealand." N.Z.J.G.G. **26** 127 - 128.

CHALLIS, G.A., JOHNSTON, M.R., LAUDER, W.R., SUGGATE, R.P.,(in prep., to be published this year) Geology of the Lake Rotoroa area, Nelson. Scale 1:50 000. Institute of Geological & Nuclear Sciences geological map 8.1 + 32p. Institute of Geological Sciences Ltd, Lower Hutt, New Zealand

COOPER, A.F., BARREIRO, B.A., KIMBROUGH, D.L. and MATTINSON, J.M. (1987) Lamprophye dike intrusion and the age of the Alpine Fault, New Zealand. Geology **15** 941-944

FYFE, H.E. (1928) Murchison Subdivision. N.Z.G.S. Annual Report 22.

FYFE, H.E. (1968) Geology of the Murchison Subdivision. N.Z.G.S. Bull **36** 18-23.

GILL, J.B. (1981) Orogenic andesites and plate tectonics. Springer-Verlag Berlin.

HARRISON, T.M. and McDOUGAL, I. (1980) Investigations of an intrusive contact Northwest Nelson, New Zealand. Thermal, chronological and isotopic constraints. Geochimica et Cosmochima Acta. **44** 1985 - 2003.

IRVINE, T.N. and BARAGER, W.R.A. (1971) A guide to chemical classification of the common volcanic rocks. Canadian Journal of Earth Sciences **8** 523 - 548.

KIDD, C.H. (1972) An acidic-basic igneous association near Lake Rotoroa, Southeast Nelson, and its bearing on the nature of the Rotoroa Complex. Unpublished BSc. Honours Thesis University of Canterbury.

KIMBROUGH, D.L., TULLOCH, A.J., GEARY, E.,COOMBS, D.S. and LANDIS, C.A. (1993) Isotopic ages from the Nelson region of the South Island of New Zealand: crustal structure and definition of the Median Tectonic Zone.Tectonophysics **225** 433 - 448.

LANDIS, C.A. and COOMBS, D.S. (1967) Metamorphic belts and orogenesis in southern New Zealand. Tectonophysics **4** 501 -518.

LEMAITRE, R.W. (editor), BATEMAN,P., DUDEK,A., KELLER, J., LAMEYRE, J., LE BAS, M,J., SABINE, P.A., SCHMID, R., SORENSON, H., STRECKEISEN, A., WOOLEY, A.R., and ZANETTIN, B. (1989) A classification of igneous rocks and glossary of terms: Recommendations of the International Union of Geological Sciences Subcommission on the Systematics of Igneous Rocks. Blackwell Scientific Publications, Oxford.

MANIAR, P.D. and PICCOLI, P.M. (1989) Tectonic discrimination of granitoids. Geological Society of America Bulletin **101** 635 - 643.

MARRE, J. (1986) The structural analysis of granitic rocks.(English translation). North Oxford Academic Publishers Ltd.

McCULLOCH, M.T., BRADSHAW, J.Y. and TAYLOR, S.R. (1987) Sm-Nd and Rb-Sr isotopic and geochemical systematics in phanerozoic granulites from Fiordland, Southwest New Zealand. Contrib. mineral. Petrol. **97** 183 - 195.

McDONOUGH, W.F., SUN, S., RINGWOOD, A.E., JAGOUTZ, E. and HOFMANN, A.W. (1992) K, Rb and Cs in the earth and moon and the evolution of the earths mantle. Geochimica et Cosmochimica Acta. Ross Taylor symposium volume **56** 1001 - 1012.

MUIR, R.J., IRELAND, T.R., WEAVER, S.D. and BRADSHAW, J.D. (1994) Ion microprobe U-Pb geochronology of granitic magmatism in the Western Province of the South Island, New Zealand. Chemical Geology **113** 171 - 189.

MUIR, R.J., WEAVER, S.D., BRADSHAW, J.D., EBY, G.N. and EVANS, J.A.,(in press) Geochemistry of the Cretaceous Separation Point Batholith, New Zealand: granitoid magmas formed by the melting of mafic lithosphere. Journal of the Geological Society of London **152**

NORRISH, K. and HUTTON, J.T. (1969) An accurate X-ray spectrographic method for the analysis of a wide range of geologic samples. Geochima Cosmochima Acta. **33** 431-453.

PEARCE, J.A. and CANN, J. R. (1973) Tectonic setting of basic volcanic rocks using trace element analysis. Earth Planet. Sci. Lett. **19** 290 - 300.

PEARCE, J.A., HARRIS, N.B. and TINDLE, A.G. (1984) Trace element discrimination diagrams for the tectonic interpretation of granitic rocks. Journal of Petrology **25** 956 - 983.

PEARCE, T.H., GORMAN, B.E., and BIRKETT, T.C. (1977) The relationship between major element chemistry and tectonic environment of basic and intermediate volcanic rocks. Earth and Science Planetary Letters **36** 121 - 132

PEACOCK, M.A. (1931) Classification of Igneous rock series. Journal of Geology **39** 54 - 67.

PITCHER, W. (1982) Granite type and tectonic environment in **HSU, K.J. (ed.)** (1982) Mountain building processes. Academic press.

PIRAJNO, F. (1981) Geochemistry and mineralisation of the southern part of the Darran Complex, Fiordland, New Zealand. N.Z.J.G.G. **24** 491 - 513.

PIRAJNO, F. (1982) Lamprophyre dikes in the Victoria Range sector of the Karamea Batholith, New Zealand. New Zealand Journal of Geology and Geophysics **25** 499-502.

REED, J.J. (1968) Plutonic and Metasedimentary rocks in: **FYFE, H.E.** (1968) Geology of the Murchison Subdivision. N.Z.G.S. Bulletin **36**

ROCK, N. M. S. (1991) Lamprophyres. Blackie & Son Ltd Glasgow.

SHELLEY, D.S. (1985) Optical Mineralogy. 2nd Ed. Elsevier New york

SHELLEY, D.S. (1993) Igneous and metamorphic rocks under the microscope. Chapman and Hall, London.

SUGGATE, R.P., STEVENS, G.R. and TE PUNGA, M.T. (1978) Geology of New Zealand Vol. 1 Government Printer, Wellington.

SUGGATE, R.P. (1984) Sheet M29AC "Mangles Valley" Geological Map of New Zealand 1:50 000 Map and notes. Wellington, New Zealand. DSIR.

SUN, S. and McDONOUGH, W.F. (1989) Chemical and isotopic systematics of oceanic basalts: implications for mantle composition and processes. In **SAUNDERS, A.D., and NORRY, M.J. (eds)** (1989) Magmatism in the Ocean Basins. Geological Society Special Publication **42** 313 - 345.

THORNTON, J. (1985) Field guide to New Zealand geology. Reed Methuen, Auckland.

TULLOCH, A.J. (1979) Plutonic and metamorphic rocks in the Victoria Range segment of the Karamea Batholith, South-West Nelson, New Zealand. Unpublished PhD. Thesis, Otago University

TULLOCH, A.J. (1983) Granitoid rocks of New Zealand- a brief review. Geological Society of America Memoir **159** 5-19.

TULLOCH, A.J. (1988) Batholiths, plutons, and suites: nomenclature for granitoid rocks of Westland-Nelson, New Zealand. N.Z.J.G.G. **31** 505-509.

TULLOCH, A.J. (1992) Magnetic Susceptibilities, Westland rocks. N.Z.J.G.G. **32** 197 - 203.

TULLOCH, A.J. and KIMBROUGH, D.L. (1989) The Paparoa Metamorphic Core Complex, New Zealand: Cretaceous extension associated with fragmentation of the Pacific-Margin of Gondwana. Tectonics **8** No. **6**, 1217 - 1234.

WEAVER, S.D., GIBSON, I.L., HOUGHTON, B.F. and WILSON, C.J.N. (1990) Mobility of rare earth elements and other elements during recrystallisation of peralkaline silicic lavas. Journal of Volcanology and Geothermal Research **43** 57 - 70.

WELLMAN, H.W. and WILLET, R.W. (1942) The geology of the West Coast from Abut Head to Milford Sound.- Part 1: Royal Society of New Zealand Transactions **14** 34 - 350.

WELLMAN, H.W. (1973) The Stokes magnetic anomaly. Geological Magazine **110(5)** 419 - 429.

WILLIAMS, J.G. AND HARPER, C.T. (1978) Age and status of the McKay Intrusives in the Eglinton-upper Hollyford area. N.Z.J.G.G. **6** 733 - 42.

WILLIAMS, J.G. and SMITH, I.E.M. (1983) The Hollyford Gabbronorite-a calc-alkaline cumulate. N.Z.J.G.G. **26** 345 - 357.

WILSON, M. (1989) Igneous Petrogenesis Harper-Collins London.

10. APPENDICES:

Appendix # 1. Sample description and location

(with corresponding University of Canterbury rock store numbers)

Sample	Location	Description	University of Canterbury No:
AC1A	796204	Siliceous volcanogenic sediment	14524
AC1B	795202	Altered basaltic rock	14525
AC3A	807229	Lamprophyre dike	14526
AC3B	806231	Howard Metagabbro	14527
AC3G	807249	Braeburn Diorite	14528
AC3E	808237	Howard Gabbro	14529
AC3F	809242	Howard Metagabbro	14530
AC5G	799257	Lamprophyre dike	14531
AC5I	797256	Braeburn Quartz Diorite	14532
AC5J	799251	Braeburn Quartz Diorite	14533
AC6A	802225	Howard Gabbro	14534
AC7A	808225	Separation Point Granite	14535
AC7E	775212	Braeburn Quartz Diorite	14536
AC8B	774310	Braeburn Dioirte	14537
AC8C	774310	Braeburn Quartz Diorite	14538
AC8D	770302	Rotoroa Hornblendite	14539
AC8E	774305	Braeburn Quartz Diorite	14540
AC9A	799263	Braeburn Quartz Diorite	14541
AC9B	792282	Braeburn Diorite	14542
AC9C	782282	Howard Metagabbro	14543
AC10B	808229	Braeburn Quartz Diorite	14544
AC10C	808229	Braeburn Quartz Diorite	14545
AC10D	809225	Braeburn Diorite	14546
AC10E	808232	Braeburn Quartz Diorite	14547
AC10F	809236	Howard Gabbro	14548
AC11B	782289	Braeburn Diorite	14549
AC11E	779289	Braeburn Diorite	14550
AC12B	806225	Howard Metagabbro	14551
AC12C	804229	Howard Gabbro	14552
AC12E	799231	Howard Gabbro	14553
AC14A	797256	Braeburn Quartz Diorite	14554
AC14B	796255	Braeburn Quartz Diorite	14555
AC15B	805242	Lamprophyre dike	14556
AC16A	772330	Braeburn Quartz Diorite	14557
AC16B	772330	Braeburn Diorite	14558
AC16D	764329	Braeburn Quartz Diorite	14559
AC16G	764328	Braeburn Diorite	14560
AC16I	765232	Braeburn Diorite	14561
AC16K	766231	Braeburn Diorite	14562
AC16N	766322	Braeburn Quartz Diorite	14563
AC17A	802253	Braeburn Diorite	14564
AC17E	795249	Braeburn Diorite	14565
AC17F	795249	Braeburn Quartz Diorite	14566
AC18C	796267	Braeburn Quartz Diorite	14567
AC18E	795266	Howard Metagabbro	14568

Sample	Location	Description	University of Canterbury No:
AC18H	792265	Braeburn Diorite	14569
AC19A	794278	Howard Metagabbro	14570
AC19B	793278	Braeburn Diorite	14571
AC19E	784274	Braeburn Diorite	14572
AC20A	809233	Howard Gabbro	14573
AC20C	809234	Howard Metagabbro	14574
AC20G	807246	Howard Metagabbro	14575
AC20J	807246	Howard Gabbro	14576
AC20L	807247	Braeburn Diorite	14577
AC20M	808246	Braeburn Quartz Diorite	14578
AC21A	775315	Braeburn Quartz Diorite	14579
AC21C	774314	Howard Metagabbro	14580
AC22A	823216	Torlesse mylonite	14581
AC22C	798215	Braeburn Quartz Diorite	14582
AC22E	797215	Howard Gabbro	14583
AC23B	799225	Howard Gabbro	14584
AC23E	789222	Howard Gabbro	14585
AC23G	787222	Howard Gabbro	14586
AC23H	788221	Howard Gabbro	14587
AC23L	787210	Braeburn Quartz Diorite	14588
AC24A	803256	Lamprophyre dike	14589
AC24C	798210	Pegmatite dike	14590
AC24D	797211	Pegmatite dike	14591
AC24F	794213	Braeburn Quartz Diorite	14592
AC24G	793214	Braeburn Quartz Diorite	14593
AC25A	785309	Lamprophyre dike	14594
AC25B	785255	lamprophyre dike	14595
AC25D	777241	Pegmatite dike	14596
AC25E	774231	Pegmatite dike	14597
AC25F	762225	Braeburn Quartz Diorite	14598
AC26A	775309	Aplite dike	14599
AC26B	775309	Braeburn Quartz Diorite	14600
AC26C	771302	Lamprophyre dike	14601
AC26D	770303	Aplite dike	14602
AC27A	719335	Howard Gabbro	14603
AC27E	773323	Rotoroa Hornblendite	14604
AC27F	733321	Braeburn Diorite	14605
AC27H	748334	Pegmatite dike	14606

Appendix # 2. Point Count Results.

Sample No:	AC3B	AC3G	AC3E	AC3F	AC5G	AC5I	AC5J
Quartz	12.0	8.7	0.9	-	0.8	31.3	28.3
Plagioclase	51.2	63.7	64.5	56.5	47.3	33.5	24.8
K-feldspar	5.3	1.7	3.6	1.9	1.8	22.9	24.6
Pyroxene	-	-	15.7	1.0	-	-	-
Biotite	-	12.7	10.7	-	2.7	5	3.2
Muscovite	-	-	-	1.5	-	-	-
Hornblende	41.1	10.3	-	38.3	41.5	6.4	17.6
Magnetite	1.2	2.9	4.6	0.8	-	0.9	1.5
Titanite	-	-	-	-	-	<1.0	<1.0
Epidote	-	-	-	-	-	-	-
Total	100.0	100.0	100.0	100.0	100.0	100.0	100.0

Sample No:	AC6A	AC7A	AC8C	AC8D	AC8E	AC9B	AC9C
Quartz	5.3	23.7	34.7	-	12.8	8.1	0.8
Plagioclase	74.7	47.7	18.9	10.4	45.4	59.3	52.9
K-feldspar	3.8	24.1	18.1	1.9	10.4	4.2	1.2
Pyroxene	-	-	-	11.7	-	-	-
Biotite	5.1	3.4	24.4	-	9.6	8.5	2.2
Muscovite	-	0.7	2.3	-	1.3	0.2	-
Hornblende	7.5	-	1.2	76.0	19.3	19.1	40.9
Magnetite	3.6	0.4	0.4	-	1.2	0.6	2.0
Titanite	<1.0	<1.0	<1.0	<1.0	<1.0	<1.0	-
epidote	-	-	-	-	-	-	-
Total	100.0	100.0	100.0	100.0	100.0	100.0	100.0

Sample No:	AC10C	AC10F	AC11B	AC12B	AC12E	AC15B	AC16A
Quartz	8.0	0.6	8.8	3.6	-	-	26.7
Plagioclase	23.0	65.7	54.6	48.7	69.8	48.0	24.1
K-feldspar	10.5	1.2	4.2	1.7	2.7	1.0	21.6
Pyroxene	-	15.2	-	10.0	24.0	-	-
Biotite	0.3	13.1	6.4	-	1.7	8.1	22.3
Muscovite	-	-	-	-	-	-	2.9
Hornblende	11.6	-	24.4	32.5	-	41.3	-
Magnetite	0.1	4.2	1.6	3.5	1.8	1.6	2.4
Titanite	<1.0	<1.0	<1.0	-	-	-	<1.0
epidote	46.5	-	-	-	-	-	-
Total	100.0	100.0	100.0	100.0	100.0	100.0	100.0

Sample No:	AC16D	AC16K	AC16N	AC17A	AC17E	AC18C	AC18E
Quartz	46.8	0.8	25.6	9.3	12.0	45.6	10.8
Plagioclase	18.5	34.2	44.1	49.6	27.9	46.4	52.6
K-feldspar	20.0	5.6	1.8	6.5	13.4	3.7	4.3
Pyroxene	-	-	-	-	-	-	-
Biotite	9.6	15.0	23.8	10.6	4.8	3.8	-
Muscovite	4.9	4.7	1.8	0.5	0.2	-	-
Hornblende	-	36.6	<1.0	21.9	35.4	-	25.5
Magnetite	0.2	3.1	2.9	1.6	6.3	0.5	6.8
Titanite	<1.0	<1.0	<1.0	<1.0	<1.0	<1.0	<1.0
epidote	-	-	-	-	-	-	-
Total	100.0	100.0	100.0	100.0	100.0	100.0	100.0

Sample No:	AC18H	AC19A	AC19E	AC20A	AC20C	AC20G	AC20J
Quartz	10.7	12.6	14.1	8.4	3.8	12.5	0.8
Plagioclase	50.1	55.1	13.4	52.4	50.8	35.4	51.3
K-feldspar	4.6	4.2	17.9	-	4.6	8.9	3.2
Pyroxene	-	-	-	-	1.6	-	4.2
Biotite	17.0	-	34.4	2.6	-	-	-
Muscovite	-	-	2.0	0.8	-	5.5	-
Hornblende	16.9	27.6	29.0	33.8	35.4	36.5	34.2
Magnetite	0.7	0.5	0.2	2.0	3.8	1.2	6.3
Titanite	<1.0	-	<1.0	<1.0	<1.0	<1.0	-
epidote	-	-	-	-	-	-	-
Total	100.0	100.0	100.0	100.0	100.0	100.0	100.0

Sample No:	AC20M	AC21A	AC21C	AC22C	AC22E	AC23B	AC23L
Quartz	36.7	44.6	0.6	30.8	1.4	1.6	2.2
Plagioclase	28.2	14.8	42.8	32.9	60.6	56.0	38.6
K-feldspar	27.1	22.6	3.1	19.1	7.4	7.8	5.3
Pyroxene	-	-	-	-	14.2	2.7	-
Biotite	2.6	13.0	0.7	4.6	14.0	-	-
Muscovite	-	-	1.6	-	0.6	0.8	1.2
Hornblende	4.6	-	47.1	-	-	22.3	0.5
Magnetite	0.8	0.2	2.1	17.0	1.8	8.8	0.5
Titanite	<1.0	<1.0	<1.0	-	<1.0	<1.0	<1.0
epidote	-	4.8	-	12.6	-	-	-
Total	100.0	100.0	100.0	100.0	100.0	100.0	100.0

Appendix # 3. Whole rock Major and Trace element geochemistry.

The major elements are initially presented in their raw form with LOI (loss on ignition) included. Major element data from Newpet92 as presented in this thesis, is expressed on an anhydrous basis recalculated from the LOI to 100 %. Recalculated major element abundances are presented at the bottom of each table.

The ratio Fe_2O_3 = .3 FeO was assumed in all cases.

Analytical precision and detection limits for XRF and Primative Mantle normalisation values used in this research are also given.

Rotoroa Complex

SAMPLE	AC3G	AC3F	AC5I	AC7E	AC8B	AC9A	AC9B	AC10B	AC10C	AC10E
SiO_2	54.42	47.19	67.00	67.24	50.67	58.29	52.55	51.19	53.49	51.67
TiO_2	1.13	0.39	0.48	0.49	1.24	0.74	0.90	1.08	0.51	0.78
Al_2O_3	17.87	20.73	15.68	15.29	17.93	17.93	17.87	18.07	20.72	14.13
Fe_2O_3	8.44	6.42	2.16	4.09	9.62	6.35	9.86	9.23	5.33	8.97
MnO	0.15	.012	0.03	0.07	0.14	0.10	0.18	0.21	0.09	0.16
MgO	3.52	7.85	0.66	1.46	5.91	2.78	5.51	5.07	2.27	9.76
CaO	6.18	13.89	2.24	3.27	7.99	6.17	8.05	5.65	9.19	7.49
Na_2O	4.46	1.54	4.14	3.91	3.94	4.51	3.74	3.35	1.84	2.86
K_2O	1.47	.56	4.38	3.31	1.47	1.26	0.57	2.30	4.32	1.52
P_2O_5	0.25	.07	.09	0.14	0.31	0.2	0.09	0.19	0.14	0.18
LOI	0.65	1.69	2.21	1.63	0.32	1.09	1.13	3.66	2.08	2.27
TOTAL	98.54	100.45	99.07	99.90	99.54	99.42	100.45	100.00	99.98	99.13
ASI	0.81	0.73	1.00	0.96	0.79	0.90	0.83	0.99	0.85	0.71
Cr	34	134	4	11	111	15	82	41	59	28
Ni	15	71	6	8	48	10	44	18	22	10
V	201	139	40	81	257	153	158	324	108	260
Pb	11	13	20	21	11	13	12	18	53	20
Zn	102	61	25	45	106	72	101	82	44	108
K	12549	4731	37603	27767	12394	10691	4801	19966	36786	9736
Rb	46	17	96	87	39	30	11	62	134	37
Ba	315	108	912	696	511	398	224	414	892	432
Sr	600	787	308	370	965	737	648	691	758	674
Ga	22	18	18	17	19	21	23	19	22	22
Nb	57	2	6	5	3	5	2	4	4	5
Zr	77	26	274	114	56	100	62	87	108	90
Ti	6966	2379	2976	2969	7733	4543	5475	6771	3136	8071
Y	24	4	10	15	14	15	10	18	10	22
Th	4	2	6	7	1	4	4	6	6	5
La	16	5	14	13	11	14	5	14	5	15
Ce	44	5	24	30	46	32	10	30	30	38
Nd	27	14	10	17	21	20	10	10	10	21
SiO_2	55.96	48.02	69.29	67.95	51.59	59.58	53.32	53.53	54.87	53.66
TiO_2	1.16	0.40	.50	0.50	1.29	0.76	0.91	1.13	0.52	1.35
Al_2O_3	18.38	21.10	16.22	15.45	17.94	18.33	18.13	18.90	21.25	16.94
Fe_2O_3	2.00	1.51	0.52	0.95	2.28	1.50	2.31	2.23	1.26	2.45
FeO	6.01	4.52	1.55	2.86	6.83	4.49	6.392	6.68	3.78	7.35
MnO	0.15	0.12	0.03	0.07	0.14	0.10	0.18	0.22	0.09	0.19
MgO	3.62	7.99	0.68	1.48	6.00	2.84	5.59	5.30	2.33	4.43
CaO	6.36	14.14	2.32	3.30	8.11	6.31	8.17	5.91	9.43	8.10
Na_2O	4.51	1.57	4.28	3.95	4.00	4.61	3.79	3.50	1.89	4.07
K_2O	1.59	0.57	4.53	3.34	1.49	1.29	0.58	5.91	4.43	1.17
P_2O_5	0.26	.07	0.09	0.14	0.31	0.20	0.09	3.50	0.14	0.30
Total	100.00	100.00	100.00	100.00	100.00	100.00	100.00	100.00	100.00	100.00
q	2.63	0.00	20.42	21.68	0.00	8.83	0.99	0.00	3.19	0.00
or	8.95	3.37	26.81	19.80	8.84	7.62	3.42	14.24	26.24	9.30
ab	38.81	13.26	36.23	33.43	33.86	39.00	32.11	29.64	15.97	24.99
an	25.13	48.88	11.24	14.60	26.63	25.57	30.77	28.38	36.50	21.94
c	0.00	0.00	0.17	0.00	0.00	0.00	0.00	0.15	0.00	0.00
z	0.04	0.01	0.06	0.02	0.01	0.01	0.00	0.02	0.02	0.02
di	4.14	16.91	0.00	0.99	9.82	3.92	7.73	0.00	8.13	12.40
hy	14.72	4.71	3.35	6.96	2.70	11.10	19.78	21.10	7.01	21.91
ol	0.00	9.86	0.00	0.00	11.83	0.00	0.00	0.78	0.00	4.43
mt	2.90	2.19	0.75	1.38	3.30	2.17	3.35	3.23	1.83	3.10
cm	0.01	0.03	0.00	0.00	0.02	0.00	0.02	0.01	0.01	0.22
il	2.21	0.75	0.94	0.94	2.45	1.44	1.73	2.14	0.99	1.53
ap	0.61	0.19	0.22	0.34	0.75	0.49	0.22	0.47	0.34	0.44

Rotoroa Complex

SAMPLE	AC10D	AC10E	AC10F	AC11E	AC12C	AC12E	AC14A	AC14B	AC15B	AC16A
SiO_2	42.77	52.61	55.67	59.73	59.54	46.86	70.81	61.03	50.62	61.28
TiO_2	0.98	1.32	1.16	0.88	1.04	0.39	0.26	0.97	0.91	0.41
Al_2O_3	15.42	16.61	17.39	18.41	17.90	20.41	15.55	17.22	16.48	19.84
Fe_2O_3	7.70	10.41	7.52	5.25	6.03	7.35	1.96	6.18	9.07	4.85
MnO	0.17	0.19	0.14	0.08	0.12	0.11	0.06	0.13	0.15	0.09
MgO	4.25	4.34	3.02	2.64	2.21	8.97	0.50	2.29	6.95	0.93
CaO	4.72	7.94	5.54	5.33	4.92	13.25	2.29	5.12	6.89	4.32
Na_2O	2.87	3.99	4.61	5.28	5.50	1.74	4.90	4.55	3.77	6.13
K_2O	1.91	1.15	2.31	1.34	1.51	0.28	2.37	2.07	1.77	1.44
P_2O_5	0.16	0.29	0.38	0.27	0.31	0.08	0.09	0.25	0.20	0.18
LOI	18.21	1.14	1.18	1.25	0.56	0.59	0.44	0.65	2.07	0.76
TOTAL	99.16	99.99	98.92	100.46	99.64	100.03	99.23	100.46	98.88	100.23
ASI	1.00	0.75	0.75	0.93	0.91	0.75	1.05	0.90	0.80	1.02
Cr	63	28	17	23	9	146	3	24	53	4
Ni	26	10	15	20	10	64	4	17	27	7
V	331	260	149	129	126	111	23	131	275	28
Pb	22	20	20	14	16	4	21	18	10	23
Zn	58	108	78	73	71	55	42	90	83	51
K	19731	9736	19736	11258	12711	2350	19945	17299	9770	12063
Rb	50	37	72	28	46	7	62	61	22	28
Ba	205	432	689	586	464	134	644	470	419	826
Sr	912	674	656	1068	644	914	460	458	803	694
Ga	21	22	20	25	15	19	19	21	18	18
Nb	4	5	7	4	9	3	5	6	4.1	4
Zr	72	90	190	76	217	26	118	199	88	235
Ti	7311	8071	7157	5340	6323	2365	1581	5854	7847	2480
Y	11	22	23	7	19	3	5	20	16	13
Th	5	5	7	1	10	1	4	5	4	10
La	6	15	24	9	29	5	8	18	12	24
Ce	15	38	54	29	56	5	30	44	31	58
Nd	12	21	19	11	35	10	14	21	11	18
SiO_2	53.23	53.66	57.30	60.45	60.38	47.39	71.79	61.44	52.67	61.84
TiO_2	1.22	1.35	1.19	0.89	1.05	0.39	0.26	0.98	0.95	0.41
Al_2O_3	19.19	16.94	17.90	18.63	18.15	20.64	15.76	17.34	17.15	20.02
Fe_2O_3	2.21	2.45	1.79	1.23	1.41	1.72	0.46	1.11	2.18	1.13
FeO	6.63	7.35	5.36	3.68	4.23	5.15	1.38	4.31	6.53	3.39
MnO	0.21	0.19	0.14	0.08	0.12	0.11	0.06	0.13	0.16	0.09
MgO	5.29	4.43	3.11	2.67	2.24	9.07	0.51	2.31	7.23	0.94
CaO	5.87	8.10	5.70	5.39	4.99	13.40	3.32	5.15	7.17	4.36
Na_2O	3.57	4.07	4.74	5.34	5.58	1.76	4.97	4.58	3.92	6.19
K_2O	2.38	1.17	2.38	1.36	1.53	0.28	2.40	2.08	1.84	1.45
P_2O_5	0.20	0.30	0.39	0.27	0.31	0.08	0.09	0.25	0.21	0.18
Total	100.00	100.00	100.00	100.00	100.00	100.00	100.00	100.00	100.00	100.00
q	0.00	0.90	5.85	2.84	7.11	0.00	27.25	13.65	0.00	13.80
or	14.07	6.95	14.02	14.08	9.07	1.68	14.22	12.30	10.91	21.40
ab	30.22	34.43	39.98	40.14	47.19	14.89	42.03	38.63	33.19	42.01
an	28.23	24.53	20.49	20.57	20.02	47.64	11.27	20.56	23.79	11.78
c	0.42	0.00	0.00	0.00	0.00	0.00	0.89	0.00	0.00	0.00
z	0.01	0.02	0.04	0.02	0.04	0.01	0.02	0.04	0.01	0.05
di	0.00	11.60	4.33	4.60	2.50	14.99	0.00	2.79	8.80	1.31
hy	19.35	14.92	5.71	12.14	9.44	3.45	3.09	4.43	12.08	6.22
Ol	1.86	0.00	0.00	0.00	0.00	14.05	0.00	0.00	12.22	0.00
mt	3.21	3.55	2.17	2.59	2.05	2.49	0.66	1.74	3.16	1.45
cm	0.01	0.01	0.00	0.00	0.01	0.03	0.00	0.01	0.04	0.00
il	2.32	2.56	2.26	2.27	2.00	0.75	0.50	1.85	1.80	1.55
ap	0.47	0.70	0.93	0.93	0.75	0.19	0.22	0.60	0.50	0.61

Rotoroa Complex

SAMPLE	AC16B	AC16G	AC16I	AC17F	AC20G	AC20J	AC20L	AC21C	AC23G	AC23H
SiO_2	50.14	59.04	50.56	64.96	51.22	43.11	58.92	48.45	72.26	54.45
TiO_2	1.29	0.54	1.32	0.81	0.68	1.19	0.94	1.47	0.12	0.9
Al_2O_3	17.99	20.72	17.04	16.23	21.88	18.69	16.95	19.11	15.37	19.28
Fe_2O_3	10.44	4.56	11.58	4.30	5.88	12.91	6.70	9.44	0.94	.79
MnO	0.15	0.07	0.24	0.10	0.11	0.12	0.13	0.14	0.02	0.15
MgO	5.07	1.42	4.62	1.33	3.43	7.08	2.73	5.13	0.24	3.48
CaO	8.83	5.65	6.92	2.93	9.36	13.54	5.34	8.70	1.99	7.96
Na_2O	3.95	5.44	3.86	4.92	3.33	1.61	4.46	3.98	4.88	3.67
K_2O	1..16	1.36	1.63	3.58	1.47	0.18	2.68	1.40	2.80	1.06
P_2O_5	0.35	0.20	0.29	0.25	0.15	0.06	0.28	0.41	0.05	0.20
LOI	0.92	0.95	0.89	0.56	2.61	1.04	0.56	1.84	1.65	0.79
TOTAL	100.29	99..95	98.95	99.97	100.12	99.53	99.69	100.07	100.32	99.84
ASI	0.75	1.00	0.96	0.94	0.91	0.85	0.85	0.80	1.47	0.89
Cr	53	8	10	3	67	71	26	64	3	17
Ni	27	7	16	6	24	50	16	39	4	16
V	275	55	240	67	157	586	134	233	19	217
Pb	10	10	8	28	25	16	19	11	30	10
Zn	83	51	116	58	60	80	74	97	24	88
K	9770	11445	13925	29995	12573	1532	22560	11920	23575	8938
Rb	22	21	37	113	52	2	78	31	52	19
Ba	419	478	516	711	305	42	717	469	989	469
Sr	8.3	906	807	397	765	666	565	1296	573	910
Ga	18	19	15	19	15	21	16	21	19	23
Nb	4	5	10	7	5	2	6	3	3	3
Zr	88	214	37	248	87	24	239	87	59	59
Ti	7874	3281	8144	4901	4201	7317	5714	9039	729	5481
Y	16	10	19	24	11	4	23	12	2	11
Th	4	1	2	18	5	1	12	1	4	1
La	12	14	24	23	6	5	21	6	7	5
Ce	31	31	55	56	22	5	51	27	17	16
Nd	11	21	29	26	11	10	24	12	10	14
SiO_2	50.87	59.03	52.03	65.56	52.77	44.22	59.75	49.69	73.29	55.31
TiO_2	1.31	1.36	1.36	0.82	0.70	1.22	0.95	1.51	0.12	0.91
Al_2O_3	18.25	17.54	17.54	16.38	22.54	19.17	17.19	19.60	15.59	19.59
Fe_2O_3	2.44	2.75	2.75	1.00	1.40	3.06	1.57	2.23	0.22	1.85
FeO	7.33	8.25	8.25	3.00	4.19	9.17	43.70	6.70	0.66	5.55
MnO	0.15	0.25	0.25	0.10	0.11	0.12	0.13	0.14	0.02	0.15
MgO	5.14	4.75	4.75	1.34	3.53	7.26	2.77	5.26	0.24	3.54
CaO	8.96	7.12	7.12	2.96	9.64	13.89	5.42	8.92	2.02	8.09
Na_2O	4.01	3.97	3.97	4.97	3.43	1.65	4.52	4.08	4.95	3.73
K_2O	1.18	1.68	1.68	3.61	1.51	0.18	2.72	1.44	2.84	1.08
P_2O_5	0.36	0.30	0.30	0.25	0.15	0.06	0.28	0.42	0.05	0.20
Total	100.00	100.00	100.00	100.00	100.00	100.00	100.00	100.00	100.00	100.00
q	0.00	6.54	0.00	13.80	0.01	0.00	6.66	0.00	28.51	5.14
or	6.96	8.16	9.93	21.40	8.97	1.09	16.09	8.50	16.80	6.37
ab	33.91	46.06	33.61	42.01	29.03	10.89	38.27	29.49	41.88	31.54
an	28.39	27.55	25.12	11.78	41.69	44.38	18.62	30.99	10.16	33.60
c	0.00	0.37	0.00	0.00	0.00	0.00	0.00	0.00	0.68	0.00
z	0.02	0.04	0.01	0.05	0.02	0.00	0.05	0.02	0.01	0.01
di	11.60	0.00	7.18	1.31	4.50	19.93	5.60	9.08	0.00	4.66
hy	0.80	7.81	10.53	6.22	12.21	4.77	10.16	0.00	1.47	13.96
ol	11.62	0.00	1.51	0.00	0.00	15.23	0.00	12.33	0.00	0.00
mt	3.54	1.55	3.99	1.45	2.03	4.43	2.27	3.24	0.32	2.69
cm	0.01	0.00	0.00	0.00	0.01	0.02	0.01	0.01	0.00	0.00
il	2.49	1.04	2.58	1.55	1.81	2.23	1.81	2.86	0.23	1.74
ap	0.84	0.48	0.71	0.61	0.68	0.15	0.68	1.00	0.12	0.48

Rotoroa Complex

SAMPLE	AC23E	AC2F	AC24G	AC25F	AC26B	AC27A	AC27E	AC27F
SiO_2	50.88	58.46	58.27	63.94	57.78	70.02	45.55	48.75
TiO_2	1.00	1.07	0.88	0.11	0.57	0.38	3..94	0.52
Al_2O_3	20.25	16.60	16.92	14.32	21.12	15.78	8.76	23.02
Fe_2O_3	9.31	6.9	7.75	0.93	3.86	2.63	15.22	6.19
MnO	0.16	0.13	0.14	0.05	0.05	0.04	0.30	0.10
MgO	4.29	3.65	5.07	0.20	1.50	1.13	10.62	6.62
CaO	11.29	5.38	8.53	6.10	5.53	2.81	13.73	9.03
Na_2O	2.12	4.64	3.46	5.91	6.14	4.58	1.15	3.22
K_2O	0.22	1.86	1.61	3.40	1.25	2.40	0.28	0.96
P_2O_5	0.17	0.28	0.24	0.03	0.20	0.12	0.40	0.11
LOI	1.43	1.18	0.20	4.61	0.86	3.06	1.12	2.69
TOTAL	101.12	100.15	100.07	99.60	98.86	102.95	101.07	101.21
ASI	0.70	0.85	0.74	0.58	0.98	1.04	0.32	1.01
Cr	26	85	121	5	9	9	154	291
Ni	23	34	38	4	14	9	62	71
V	283	132	187	32	106	61	417	78
Pb	11	19	16	14	17	22	6	8
Zn	75	75	87	14	59	41	138	61
K	1845	15685	13463	29725	10621	19985	2353	8128
Rb	4	85	59	70	28	44	6	24
Ba	94	502	350	232	660	1617	20	188
Sr	517	616	592	431	1556	862	340	855
Ga	25	20	14	15	24	11	15	18
Nb	5	8	6	4	4	3	7	3
Zr	54	456	113	54	107	38	68	33
Ti	6057	6517	5315	694	3497	2285	23912	3179
Y	11	22	16	6	1	1	26	2
Th	2	11	5	26	2	1	1	1
La	7	21	13	13	5	5	5	5
Ce	18	57	32	24	17	11	13	12
Nd	20	29	19	19	10	10	23	10
SiO_2	51.41	59.39	55.67	67.36	59.14	70.24	46.11	49.72
TiO_2	1.00	1.09	0.89	0.12	0.58	0.38	3.99	0.53
Al_2O_3	20.46	16.86	17.04	15.09	21.62	15.83	8.87	23.48
Fe_2O_3	2.17	1.62	1.80	0.23	0.91	0.61	3.56	1.46
FeO	6.51	4.85	5.40	0.68	2.73	1.83	10.66	4.37
MnO	0.16	0.13	0.14	0.05	0.05	0.04	0.30	0.10
MgO	4.33	3.71	5.11	0.21	1.54	1.13	10.75	6.75
CaO	11..41	5.47	8.59	6.43	5.66	2.82	13.90	9.21
Na_2O	2.14	4.71	3.49	6.23	6.28	4.59	1.16	3.28
K_2O	0.22	1.89	1.62	3.58	1.28	2.41	0.28	0.98
P_2O_5	0.17	0.28	0.24	0.03	0.20	0.12	0.40	0.11
Total	100.00	100.00	100.00	100.00	100.00	100.00	100.00	100.00
q	5.77	6.74	3.72	9.21	2.10	25.59	0.00	0.00
or	1.32	11.20	9.61	21.20	7.75	14.25	1.68	5.80
ab	18.12	39.88	29.49	52.68	53.17	38.87	9.85	27.79
an	45.59	19.32	26.10	2.64	27.12	13.95	18.41	45.33
c	0.00	0.00	0.00	0.00	0.00	0.61	0.00	0.43
z	0.01	0.09	0.02	0.01	0.02	0.01	0.01	0.01
di	8.30	5.15	12.41	2.95	0.31	0.00	38.87	0.00
wo	0.00	0.00	0.00	10.78	0.00	0.00	0.00	0.00
hy	15.51	12.75	13.92	0.00	7.07	5.12	15.56	3.16
ol	0.00	0.00	0.00	0.00	0.00	0.00	2.26	14.23
mt	3.15	2.35	2.61	0.33	1.32	0.80	5.16	2.11
cm	0.01	0.02	0.03	0.00	0.00	0.00	0.03	0.06
il	1.92	2.06	1.68	0.22	1.11	0.72	7.57	1.01
ap	0.41	0.68	0.57	0.08	0.49	0.29	0.27	0.27

	Granite	Pegmatite dikes					Aplite dikes	
SAMPLE	AC7A	AC24C	AC24D	AC25D	AC25E	AC27H	AC26A	AC26D
SiO_2	72.77	75.94	70.32	75.21	70.06	75.96	68.13	73.14
TiO_2	0.20	0.13	0.45	0.06	0.48	0.13	0.35	0.08
Al_2O_3	15.04	12.62	14.52	12.76	15.08	11.76	17.15	15.82
Fe_2O_3	1.16	1.08	2.47	1.38	2.68	0.65	2.38	0.77
MnO	0.02	0.01	0.03	0.01	0.05	0.01	0.03	0.01
MgO	0.37	0.16	0.35	0.05	0.68	0.15	0.61	0.18
CaO	1.41	0.71	1.00	0.66	1.59	0.30	3.24	2.70
Na_2O	4.82	3.16	5.08	3.34	4.32	3.01	5.44	6.21
K_2O	3.51	5.21	4.77	5.29	4.79	5.33	1.98	0.38
P_2O_5	0.06	0.03	0.08	0.03	0.12	0.02	0.13	0.03
LOI	0.32	0.71	0.01	-0.25	0.65	0.59	0.43	0.74
TOTAL	99.68	99.63	99.08	98.54	100.50	97.91	99.87	100.06
ASI	1.05	1.04	0.95	1.03	0.99	1.04	1.01	1.04
Cr.	3	3	3	3	4	3	4	3
Ni	5	4	4	3	5	3	5	3
V	28	24	11	27	34	12	47	27
Pb	17	23	17	70	26	15	18	20
Zn	36	16	31	10	35	8	40	19
K	29352	43702	40046	44500	39905	45488	16560	3177
Rb	59	112	99	41	109	71	32	8
Ba	771	1375	762	115	606	478	1077	420
Sr	666	237	90	41	194	33	1038	732
Ga	18	9	19	17	19	19	21	16
Nb	2	4	14	9	9	9	4	3
Zr	54	84	446	74	298	81	133	42
Ti	1208	787	2729	365	2888	801	2114	484
Y	17	3	33	10	23	26	3	1
Th	6	17	17	25	18	9	8	3
La	5	5	27	16	22	34	20	5
Ce	15	10	59	33	45	68	48	10
Nd	10	10	30	18	28	31	15	10
SiO_2	73.30	76.73	71.12	76.21	70.31	78.09	68.64	73.68
TiO_2	0.20	0.13	0.46	0.06	0.48	0.13	0.35	0.08
Al_2O_3	15.15	12.75	14.68	12.93	15.13	12.09	17.28	15.94
Fe_2O_3	0.27	0.25	0.58	0.32	0.62	0.15	0.55	0.18
FeO	0.81	0.76	1.73	0.97	1.86	0.46	1.66	0.54
MnO	0.02	0.01	0.03	0.01	0.05	0.01	0.03	0.01
MgO	0.37	0.16	0.35	0.05	0.68	0.15	0.61	0.18
CaO	1.42	0.72	1.01	0.67	1.60	0.31	3.26	2.72
Na_2O	4.86	3.19	5.14	3.38	4.34	3.09	5.48	6.26
K_2O	3.54	5.26	4.82	5.36	4.81	5.48	1.99	0.38
P_2O_5	0.06	0.03	0.08	0.03	0.12	0.02	0.13	0.03
Total	100.00	100.00	100.00	100.00	100.00	100.00	100.00	100.00
q	27.48	35.69	19.68	33.90	21.47	37.98	20.39	2.29
or	20.92	31.16	28.55	31.70	28.45	32.41	11.80	10.21
ab	41.08	27.02	43.47	28.64	36.68	26.18	46.37	39.00
an	7.11	3.82	2.78	3.17	7.36	1.54	16.01	23.00
c	0.76	0.43	0.00	0.40	0.11	0.51	0.28	0.00
z	0.01	0.01	0.09	0.01	0.06	0.02	0.03	0.02
di	0.00	0.00	1.66	0.00	0.00	0.00	0.00	5.21
hy	1.90	1.38	2.05	1.56	3.90	0.90	3.60	14.77
ol	0.00	0.00	0.00	0.00	0.00	0.00	0.00	0.00
mt	0.39	0.37	0.84	0.47	0.90	0.22	0.80	2.49
cm	0.00	0.00	0.00	0.00	0.00	0.00	0.00	0.02
il	0.38	0.25	0.86	0.12	0.91	0.25	0.67	2.45
ap	0.15	0.08	0.20	0.07	0.29	0.05	0.32	0.87

Mafic - intermediate dikes

SAMPLE	AC3A	AC24A	AC25A	AC25B	AC26C
SiO_2	48.88	50.09	50.36	48.86	55.62
TiO_2	0.99	1.18	0.91	0.98	1.27
Al_2O_3	18.30	18.32	19.37	18.95	17.58
Fe_2O_3	9.19	9.22	9.11	9.70	7.34
MnO	0.16	0.19	0.16	0.13	0.10
MgO	6.97	5.92	5.11	4.25	4.42
CaO	9.30	9.84	7.21	8.51	6.16
Na_2O	2.37	3.54	3.97	3.83	4.54
K_2O	1.61	1.01	1.82	0.64	1.70
P_2O_5	0.26	0.21	0.20	0.19	0.34
LOI	2.46	0.78	0.63	3.06	1.27
TOTAL	98.54	98.92	98.85	99.10	100.34
ASI	0.94	0.74	0.89	0.84	0.86
Cr.	69	115	45	29	90
Ni	98	39	44	18	53
V	230	264	235	276	192
Pb	23	8	9	3	11
Zn	94	98	97	68	85
K	13733	8485	15493	5575	14326
Rb	63	20	63	21	27
Ba	304	189	349	186	729
Sr	718	653	748	874	1209
Ga	22	16	27	21	21
Nb	5	4	5	4	5
Zr	79	71	64	61	106
Ti	6098	7159	5594	6165	7730
Y	14	13	10	14	7
Th	4	3	1	1	2
La	5	5	5	5	9
Ce	26	17	21	21	27
Nd	12	10	21	15	16
SiO_2	50.23	50.69	51.64	51.27	54.46
TiO_2	1.02	1.19	0.93	1.03	1.29
Al_2O_3	18.80	18.54	19.86	19.89	17.85
Fe_2O_3	2.18	2.15	2.16	2.35	1.72
FeO	6.54	6.46	6.47	7.05	5.16
MnO	0.16	0.19	0.16	0.14	0.10
MgO	7.16	5.99	5.24	4.46	4.49
CaO	9.56	9.96	7.39	8.93	6.25
Na_2O	2.44	3.58	4.07	4.02	4.61
K_2O	1.65	1.02	1.87	0.67	1.73
P_2O_5	0.27	0.21	0.21	0.20	0.35
Total	100.00	100.00	100.00	100.00	100.00
q	0.00	0.00	0.00	0.00	29.35
or	9.80	6.05	11.05	3.98	2.27
ab	20.60	30.31	34.44	34.01	52.93
an	35.58	31.52	30.06	34.29	13.68
c	0.00	0.00	0.00	0.00	0.24
z	0.02	0.01	0.01	0.01	0.01
di	8.49	13.65	4.29	7.49	0.00
hy	13.22	1.85	0.17	7.84	1.18
ol	3.77	10.83	14.34	6.71	0.00
mt	3.16	3.12	3.13	3.41	1.26
cm	0.04	0.02	0.01	0.01	0.00
il	1.93	2.27	1.77	1.95	0.15
ap	0..63	0.50	0.49	0.47	0.07

XRF PRECISION AND DETECTION LIMITS
(from Weaver *et al* 1990)

Oxide (wt%) Element (ppm)	Standard Deviation	XRF Detection Limit
SiO_2	0.210	0.20
TiO_2	0.004	0.01
Al_2O_3	0.078	0.20
Fe_2O_3	0.036	0.01
MnO	0.018	0.01
MgO	0.020	0.05
CaO	0.005	0.01
Na_2O	0.074	0.10
K_2O	0.033	0.01
P_2O_5	0.007	0.01
LOI	0.105	-
V	1.1	3
Cr	0.8	3
Ni	1.1	3
Zn	4.7	3
Ga	0.9	2
Rb	1.6	1
Sr	0.5	1
Y	2.7	1
Zr	10	1
Nb	1.0	2
Ba	20	20
La	2.5	5
Ce	4.0	5
Nd	4.0	10
Pb	1.7	1
Th	2.5	1

NORMALISATION VALUES

Primordial Mantle normalisation values (all ppm unless stated): from McDonough *et al* (1992), a revision of the values of Sun and McDonough (1989).

Pb	0.071
Rb	0.635
Ba	6.990
Th	0.084
U	0.021
K	240.0
Nb	0.713
La	0.708
Ce	1.833
Sr	21.10
Nd	1.366
P_2O_5 (wt%)	0.019
Zr	11.20
Ti	1280
Y	4.550

Appendix # 4. Geochemical analysis of a dike from the Victoria Range

SAMPLE	4533OU S38/4211146
SiO_2	44.31
TiO_2	3.06
Al_2O_3	15.21
Fe_2O_3	4.20
FeO	8.20
MnO	0.21
MgO	6.68
CaO	10.45
Na_2O	3.56
K_2O	1.37
P_2O_5	0.65
LOI	1.68
TOTAL	99.58
Cr	183
Ni	87
V	26
Pb	6
Zn	111
K	-
Rb	58
Ba	515
Sr	724
Ga	71
Nb	73
Zr	220
Ti	-
Y	32
Th	6
La	61
Ce	109
Nd	-

Dike analysis from the Victoria range supplied by Dr. A.J. Tulloch (1979).

Igneous Geology of Lake Rotoroa

Geological Key:

- Fault
- Exposure
- Intense pegmatisation

Cultural Symbols:

- Power pylons
- Swampy area
- Bush edge
- Walking track
- 700 Contours(in 100m intervals)
- Creek
- Hut

Geological Legend:

Tertiary

- Brunner Coal Measures
- Unconformable contact

Separation Point Granite

- Leucocratic monzogranite
- Intrusivecontact

Rotoroa Complex

- Braeburn Quartz Diorite
- Braeburn Diorite
- Howard Gabbro
- Rotoroa Hornblendite
- **Fault contact**

Brook Street Volcanics

- Intercalated volcanic sediments and altered mafic igneous rock
- **Alpine Fault**

Torlesse Supergroup

- Sandstone and mudstone

Rotoroa
Jetty
Braeburn Track
Boulder Stream
Johansen Stream
Maori Stream
Lake depth 145 m
Lake Rotoroa
Lake level - 450 m
Area of enlargement
South Island of New Zealand
N
G - M angle
Grid North
Magnetic North
Magnetic North on this map is 22° East of Grid North in 1994
Mt Hutton
1200
Tiraumea Hut
Tiraumea River
Tiraumea Saddle
D'Urville Hut
Jetty
DSIR Hut
D'Urville River
Alpine Fault
Jetty
Sabine Hut
Sabine River
Nelson Lakes National Park
0 1 2 km
1000 900 800 700 600 500
1100 1000 900 800 700 600 500

59 35000 N
34
33
32
31
59 30000 N
29
28
27
26
59 25000 N
24
23
22
21
59 20000 N
76 77 78 79 24 80000 N 81 82 83 84